THREE DIMENSIONAL THERMAL MODELLING OF HIGH TEMPERATURE PROTON EXCHANGE MEMBRANE FUEL CELLS IN A SERPENTINE DESIGN

LYNNDLE CAROLINE MAASDORP

A thesis submitted in partial fulfilment of the requirements for the degree of Magister Scientiae in the Department of Physics, University of the Western Cape.

November 2010

Supervisor: Prof. Dirk Knoesen (Physical Science Department)

Co-supervisor: Dr. Øystein Ulleberg (HySA, SAIAMC)

ABSTRACT

THREE DIMENSIONAL THERMAL MODELLING OF HIGH TEMPERATURE PROTON EXCHANGE MEMBRANE FUEL CELLS IN A SERPENTINE DESIGN

L. C. Maasdorp

MSc Thesis, Department of Physics, University of the Western Cape

In this thesis, I explore the subjects of fluid dynamics and high temperature proton exchange membrane fuel cells, PEMFC. Fuel cells have been found to be at the forefront of providing the world with its much needed alternative energy resource. Despite the already existing applications, a full scale distribution, as to other alternative energy resources, still faces many challenges. Among these challenges is the thermal management of the fuel cell. Unmanaged temperature distribution of a fuel cell affects the cells mechanical stability and durability.
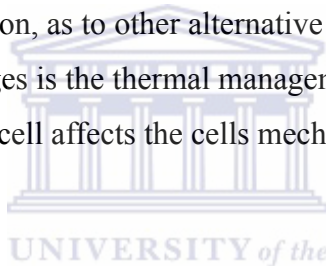
 The aim of my work is to model a segment of a unit cell of a fuel cell stack using numerical methods which is classified as computational fluid dynamics and implementing the work in a commercial computational fluid dynamics package, FLUENT. The focus of my work is to study the thermal distribution within this segment. The results of the work aid in a better understanding of the fuel cell operation in this temperature range.

At the time of my investigation experimental results were unavailable for validation and therefore my results are compared to previously published results published. The outcome of the results corresponds to this, where the current flux density increases with the increasing of operating temperature and fixed operating voltage and the temperature variation across the fuel cell at varying operating voltages. It is in the anticipation of determining actual and or unique material input parameters that this work is done and at which point this studies results

would contribute to the understanding high temperature PEM fuel cell thermal behaviour, significantly.

November 2010

THREE DIMENSIONAL THERMAL MODELLING OF HIGH TEMPERATURE PROTON EXCHANGE MEMBRANE FUEL CELLS IN A SERPENTINE DESIGN

Lynndle Maasdorp

KEYWORDS

Fuel Cell

Proton Exchange Membrane

3D Thermal modelling

Computational fluid dynamics

Hydrogen economy

High temperature

Catalysis

Thermal management

Fluid flow design

Membrane assembly

DECLARATION

I declare that *Three dimensional thermal modelling of high temperature proton exchange membrane fuel cells in a serpentine design* is my own work, that it has not been submitted before for any degree or examination in any other university, and that all the sources I have used or quoted have been indicated and acknowledged as complete references.

Lynndle Caroline Maasdorp   November 2010

Signed: . . . .

Acknowledgements

I would like to firstly and above all thank God, Our Lord Jesus Christ who through the Holy Spirit has guided me in every step way. For it is only through Him, I have victory, Isaiah 26, through Him, I walk with humility, Romans 12: 1-4 and " But whatever I am now, it is all because God poured out His special favour on me--and not without results. For I have worked harder than any of the other apostles; yet it was not I but God who was working through me by His grace" (1 Corinthians 15:10). Therefore let every earthly glory return unto Him.

I would like to thank my grandmother, Martha van Rooyen, my mother, Kathleen Maasdorp, sisters, Candice and Taryn and my brother Renoir for their continuous love, emotional and financial support. I would like to thank my friends, Celeste, Carmen, Teffo, Hilton, my classmates, Natasha, Valentino, Zwelinthini and Blaine, Jenny and the ladies at connect group and my boyfriend George for guidance and love and perspective.

I would also like to thank the staff of the physics department at UWC for the willingness to go the extra mile for me, academic support and for a successful MANUS/MATSCI program. I would like to especially thank Mr. Ian Schroeder, my supervisors Prof. D Knoesen and Dr. Ø. Ulleberg for their assistance. I appreciate the technical assistance from Dr. de Kock from ANSYS and the financial support from Hydrogen South Africa (HySA), South African Institute of Applied Materials Chemistry (SAIAMC) and the Department of Science and Technology (DST).

Nomenclature

F — Faraday's constant 96 485 C/mol

R — Ideal gas constant 8.314 J/mol K

T — Temperature

Q — Heat

W — Work

E — Energy

ΔS — Entropy

h — Enthalpy

V — Volume

P — Pressure

m — Mass

M — Molecular weight

n — Number of moles

c_p — Specific heat

c_v — Specific volume

q — Charge

U — Potential difference

e — Electron

H_2 — Hydrogen

O_2 — Oxygen

α — Activity of species

$\tilde{\eta}$ — Efficiency

j — Current Density

i — Current

r — Resistance

v — Voltage

A — Area

A_{cell} — Active area

v_d — Drift velocity

dt — Change in time

κ — Conductivity

$\bar{\sigma}$ — Thermal conductivity

σ — Stefan Boltzmann constant

δ_{thick} — Thickness of electrolyte

$\tilde{\tau}$ — Mean free time

τ — Stress Tensor

λ — Viscosity for volumetric deformation

m_e — Mass of an electron

z_e — Charge number (valence electrons)

c_e — Number of moles of charge carriers per unit volume

C — Concentration

k — Rate Coefficients

$\breve{J}$ — Flux

J_k — Diffusive mass flux

Y_k — Mass fraction

D_k — Diffusion coefficient

T_{ref} — Reference temperature [298.15 K]

η — Over-potential

ψ — Electrical potential

R_e	Reynolds Number	$\tilde{L}$	Scan length	l	Liquid phase
ρ	Density	CFD	Computational Fluid Dynamics	$elec$	Electrical
μ	Fluid viscosity	PEM	Proton Exchange Membrane	$ionic$	Ionic
K	Hydraulic permeability	HTPEMFC	High Temperature PEM Fuel Cells	k	Species
u	velocity	LTPEMFC	Low Temperature PEM Fuel Cells	act	Activation
u_e	Mobility of free electrons	Pe	Peclet Number	$ohmic$	Ohmic
S	Source terms	Γ	Diffusion conductance	$irrev$	Irreversible
$\bar{S}$	Stoichiometric ratio	H	Mass flux per unit area	rev	Reversible
Ψ	Relative humidity	$\tilde{\zeta}$	Water content	0	Initial
$\dot{m}$	Mass flow rate	s	Liquid water volume fraction	sol	Solid
j	Transfer current	r_s	Pore Blockage	GDL	Gas diffusion layer
ε	Convection heat transfer coefficient	d_{ch}	Flow channel diameter	GCL	Gas catalyst layer
$\epsilon^{1.5}$	Coefficient to take into account tortuosity	$\tilde{E}$	Electric field	**Superscripts**	
$\tilde{K}$	Geometric constant	**Subscripts**		eff	Effective
$\tilde{g}$	Topothesy of surface profile	$anode$	Anode	ref	Reference
ζ	Specific active area	cat	Cathode	f	Forward
$\tilde{\varepsilon}$	Porosity	mem	Membrane	B	Backwards
$\breve{S}$	Shape factor	g	Gas phase	Ox	Oxidised
				Rd	Reduced
				β	Transfer coefficient
				γ	Pressure coefficient

$\tilde{\Psi}$ Concentration
    dependence

CONTENTS

Chapter 1: Introduction

A fuel cell by definition is an electrochemical device which changes chemical energy into electrical energy [9]. If hydrogen is used as the fuel then the by-products are heat and water. Dependent on the operating temperature the water produced is either in vaporous or liquid form or a combination thereof. Fuel cells are expected to provide the worlds much needed clean and efficient practical form of power generation. Applications of fuels cells have already seen the transportation, portable power and stationary arenas [34, 36]. Its broad application is due to their high energy efficiency [36].

The electricity supplied by the fuel cell is available continuously as long as the fuel is provided [9, 21]. The proton exchange membranes fuel cells, (PEMFC) respective constituents is illustrated in Figure 1.
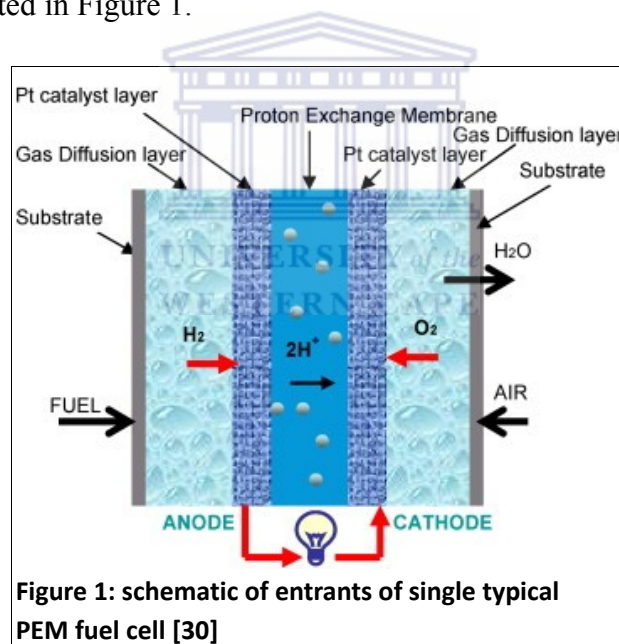
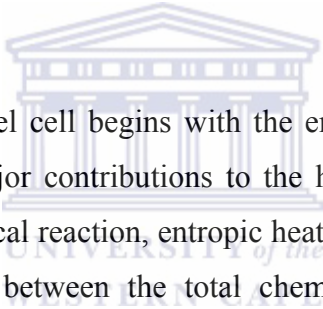**Figure 1: schematic of entrants of single typical PEM fuel cell [30]**

A hydrogen fuel cell operates as follows, the hydrogen flows with respect to its channels, meets the electrode layer where it diffuses in the gas diffusion layer. At the anode end the hydrogen is separated into protons and electrons. The electrons travel to the carbon cloth, flow field plate, to the contact, and then to the load. The protons travel through the polymer exchange membrane to the cathode. At the cathode catalyst layer, oxygen combines with the protons to form water and absorbing the electron [21].

High temperature proton exchange membranes fuel cells, (HTPEMFC) are a subset of proton exchange membranes fuel cells, (PEMFC), which operate above 120°C. The advantages of operating at a higher temperature are that there is an improvement of cathode kinetics, in the catalysts' tolerance to contaminants, in water management, gas transportation and heat rejection due to the difference in temperature between itself and its environment [72]. In HTPEMFC, since water is in its vapor form an improvement in the overall stability and durability of the fuel cell system exists and there is no longer a need to undertake complex shutdown procedures previously required in the low temperature proton exchange membrane fuel cells (LTPEMFC) [72].

The challenges with regards to operating PEMFCs at high temperatures are membrane dehydration and conductivity, degradation of the gas diffusion electrode, relative humidity and humidification issues, degradation of engineering material, mechanical failure and difficulties in heating strategies. The degradation of material is a result of the exposure to water and oxygen at elevated temperatures. These materials that are exposed to oxidation processes and include not only the membrane electrode assembly, MEA but also the seals, gaskets and bipolar plates [72].

For HTPEM fuel cell systems, fast start-up times are problematic due to the high temperatures and the amount of work needed, if these fuel cells are to be used in systems with fast start-up requirements [2, 72]. When H_2 and O_2 combine exothermically on Pt catalyst it generates local hot spots that lead to pinholes. It then in turn accelerates gas crossover—initiating a destructive cycle of increased crossover and membrane degradation. All of which contribute to a loss of mechanical stability with increasing temperature in the fuel cell [72]. A second contribution of pinhole development is the insufficient cooling of the fuel cell, as this leads to the membrane dehydrating in areas. The lack of moisture may cause the membrane to contract or even rupture. From a theoretical perspective, temperature influences the kinetics of the electrochemical reactions occurring within the fuel cell. Thermal management has therefore a vital impact on the durability, reliability and performance of the fuel cell [34, 38].

The majority of the required experimental investigations of fuel cells are expensive and or can only be carried out on a small scale, with a few designs and with difficulties of measurement. A broadly used alternative hereof is numerical modeling [31, 36]. In order to model the flow of gas within the PEMFC one needs to consider a complete set of conservation equations. The set of conservation equations includes the conservation of mass, momentum, energy, species and charge. Over and above the set of conservation equations, one would have to take into consideration the electrochemical kinetics involved [46]. The equations contain non-linearities which are intricately coupled [64]. A method to solve problems associated with non-linearities and pressure- velocities linkages is through the application of a numerical method. Two such methods are the SIMPLE and SIMPLER algorithms which are iterative solution strategies [64]. The SIMPLE algorithm is implemented in this study.

Thermal modelling of a PEM fuel cell begins with the energy equation that balances heat generation and removal. The major contributions to the heat in the fuel cell is due to the irreversibility of the electrochemical reaction, entropic heat of reactions as well as Joule heat. Entropic heat is the difference between the total chemical energy of reactant and the maximum usable work according to the second law of thermodynamics [38]. Joule heating is caused by the set of resistances contributed by the various components within the fuel cell. The irreversible heat results from the irreversibility of the electrochemical reactions [3, 34]. Therefore local temperature distribution of the fuel cell directly influences its performance and it is exactly the study hereof that this investigation aims to achieve.

The study produces three dimensional numerical simulation of gas transport and distribution in a HTPEMFC utilizing a commercial Computational Fluid Dynamics (CFD) computer package, FLUENT. The objective of this study is to investigate the influence of temperature variation within a HTPEMFC channel at varying operating parameters. Material and fuel cell properties was still under experimental validation at the time of this study and therefore this study aims to reproduce, or as close as possible reproduce work done by Peng et al [46]. Exact duplication was limited as all the parameters required for the investigation is not

available in the literature and in those cases default attributes found within FLUENT were used.

Chapter 2: Fuel Cell Fundamentals

2.1 Introduction

The flow of a fluid can be illustrated algebraically and is classified as fluid dynamics/ mechanics. The equations are subject to a few main physical phenomena and in order to model any scenario one would need to understand the mechanisms behind it. In the following investigation where a fuel cell is modelled, the topics that one takes into account and the conservation laws they encompass are the following:

1. Fuel Cell Thermodynamics

2. Fuel Cell Heat Transfer – Conservation of Energy

3. Fuel Cell Electrochemistry and Charge Transport - Conservation of Charge

4. Fuel Cell Mass Transfer – Conservation of Mass, Conservation of Species and Conservation of Momentum
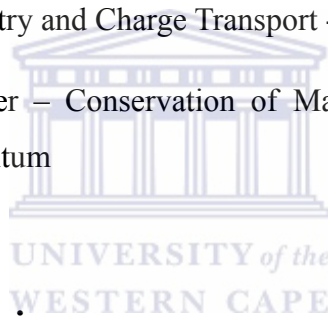
2.2 Fuel Cell Thermodynamics

Thermodynamics is defined as the study of energy changing from one state to another. In these processes of changing from one state to another, energy, E is transferred as heat, Q and or as work, W [27]. Heat is defined as a transfer of energy due to a difference in temperature, where work is defined as the transfer of energy due to processes other than those due to temperature change [69]. Understanding the thermodynamic behaviour of fuel cells is essential for modelling the fuel cell performance [52]. The need hereof is due to underlying phenomena that fuel cells transform chemical energy into electrical energy [63].

The first law of thermodynamics, deduced from the conservation of energy, states that the change in the internal energy, ΔE_i of a thermal system in going from one state to another is the negative of the work, W that the system does on its surroundings, plus the heat flow, Q into the system [23]. This is given algebraically as:

$$\Delta E_i = Q - W \quad .$$

(2.1)

From the second law of thermodynamics, heat flows naturally from a hot object to a colder object and that heat would not spontaneously transfer from a cold to a warmer object [69]. The following concepts of entropy, specific heat, absolute enthalpy and Gibbs free energy fall under the umbrella of fuel cell analysis. Entropy, ΔS is known as a function of state of a system and in some texts it is referred to as the quantitative measure of disorder [69]. Nonetheless entropy is viewed as the measure of the quantity of heat that shows the possibility of conversion into work [27, 69]. Entropy for an isothermal scenario is given as:

$$\Delta S = S_2 - S_1 = \frac{Q}{T} \; ;$$

(2.2)

In Peng et al [46] a good approximation for the change in entropy for the temperature range 373K to 1137K is given empirically as:

$$\Delta S = 33.64 + 4.52564 \times 10^{-2} T - 2.988397 \times 10^{-5} T^2 + 3.40625 \times 10^{-9} T^3 - 2.60417 \times 10^{-12} T^4$$

(2.3)

The link between heat flow and temperature is heat capacity, $\tilde{C}$ and the relationship is given as [26, 69]:

$$dQ = \tilde{C} \, dT$$

(2.4)

17

The value of the heat capacity depends on the particular material and is proportional to the amount of the material [23]. To eliminate the material dependence of the heat capacity, specific heat is defined. Specific heat, c is defined as the heat capacity of $1g$ of the material. Molar heat capacity , c' is defined as the heat capacity of $1mol$ of the material. If the mass in grams m of a thermal system consisting of n moles then the relation to heat capacity is given as:

$$\tilde{C} = mc = nc'$$
(2.5)

Heat capacity depends on how the temperature change is made and on the values of the thermodynamic variables, pressure P , volume V and temperature. The heat capacity can therefore be written as $C = C(P,T)$ or $C = C(V,T)$ [23]. Generally there are two cases of interest and they are when the volume is kept constant and the second is when the pressure is kept constant. This is written algebraically as the following:

$$dQ = \tilde{C}_V \, dT \quad \text{for constant volume and}$$
(2.6)

$$dQ = \tilde{C}_P \, dT \quad \text{for constant pressure}$$
(2.7)

The work done, dW by a gas at constant pressure is:

$$dW = PdV$$
(2.8)

where $dV \equiv \Delta V$ symbolises the change in volume

From the ideal gas relation one has:

$$PV = nRT$$
(2.9)

18

where R is the ideal gas constant. Therefore when the pressure is constant the volume is directly proportional to the change in temperature and one arrives at the following equation [26, 69]:

$$dW = PdV = nRdT \tag{2.10}$$

From the first law of thermodynamics one has for internal energy:

$$dE_i = dQ_V = \tilde{C}_V dT \quad \text{for constant volume} \tag{2.11}$$

and

$$dE_i = -dW_P + dQ_P = -PdV + \tilde{C}_P dT \quad \text{for constant pressure} \tag{2.12}$$

For an ideal gas, because the energy shift dE_i is independent of whether the infinitesimal transformation is made at constant volume or pressure, equations (2.11) and (2.12) can be equated.

$$\tilde{C}_V dT = -nRdT + \tilde{C}_P dT \quad \text{which reduces to} \tag{2.13}$$

$$\tilde{C}_P = \tilde{C}_V + nR \tag{2.14}$$

This relation is known as the molar heat capacities of an ideal gas [69]. There are several alternative specific heat equations that are available in the literature. One that is easy to integrate is in the form of a polynomial.

$$\frac{\tilde{C}_P}{R} = \grave{\alpha} + \grave{\beta} T + \grave{\gamma} T^2 + \grave{\delta} T^3 + \grave{\epsilon} T^4 \tag{2.15}$$

The values for $\grave{\alpha}, \grave{\beta}, \grave{\gamma}, \grave{\delta}$ and $\grave{\epsilon}$ are listed in many thermodynamics texts, and can be found on the NIST website [52, 31].

For this particular investigation we look at an isothermal scenario, which implies that the temperature, T is a constant therefore $Q=0$ and $\Delta E=-W$ [23]. Under constant temperature conditions the work done by an ideal gas is given as [23]:

$$W=\int_{V_1}^{V_2} PdV =nRT_0 \ln\left(\frac{V_2}{V_1}\right)$$

(2.16)

Absolute enthalpy incorporates the enthalpy derived from chemical and sensible thermal energy. Chemical energy, which is also known as the enthalpy of formation is associated with the energy of the chemical bonds, and sensible thermal energy is the enthalpy difference between the given and reference state [52]. Enthalpy, h is given by the following equation [26]:

$$h=E_i+\frac{P}{\rho}$$

(2.17)

where ρ is the density of the substance. Gibbs free energy represents the amount of useful, external work that can be obtained from an isothermal, isobaric system when the system changes from one set of steady-state conditions to another [69]. In a fuel cell the external work involves moving electrons about an external circuit [9]. When considering electrochemical conversion within the fuel cell, one looks at the conversion of the change in free energy associated with a chemical reaction, directly into electrical energy. Gibbs free energy G, by definition is a direct measurement of the maximum electrical work, W_{elec} a system can perform at a constant temperature and pressure from the reaction [52]. This is expressed as:

$$W_{elec} = -\Delta G \quad .$$

(2.18)

20

The change in free energy or the maximum useful work can be obtained when ideal fuel cell operating irreversibly is dependent upon temperature and therefore, W_{elec}, the electrical power output is [52]:

$$W_{elec} = -\Delta G = \Delta h - T \Delta S \qquad (2.19)$$

The ability for a system to do electrical work by a charge q (coulombs), through an electrical potential difference, U in volts, is [52]:

$$W_{elec} = Uq \quad \text{where} \qquad (2.20)$$

$$q = nF \qquad (2.21)$$

Where F is the Faraday constant. This is when the charge is assumed to be carried out by electrons. From the above one arrives at the maximum reversible voltage provided by the cell to be given as follows:

$$\Delta G = -nFU_{rev} \qquad (2.22)$$

where U_{rev} in the equation is the standard reversible potential [52]. When one analyses any electrochemical reaction, there will be a change in the Gibbs energy of formation due to energy release [9].

For any chemical reaction one has the following:

$$\grave{j}\,\acute{A} + \grave{k}\,\grave{B} \Rightarrow \dot{m}\,\acute{C} + \grave{n}\,\acute{D} \qquad (2.23)$$

$\acute{A}$ and $\grave{B}$ are two reactants which produce as a result of a chemical reaction the products $\acute{C}$ and $\dot{D}$. Coefficients $\grave{j}, \grave{k}, \grave{m}$ and $\grave{n}$ are integers dependent on the balancing of the reaction. The change in Gibbs free energy between the product and reactant is [22]:

$$\Delta G = \dot{m} G_{\acute{C}} + \grave{n} G_{\dot{D}} + \grave{j} G_{\acute{A}} + \grave{k} G_{\grave{B}} \qquad (2.24)$$

In the case of a hydrogen-oxygen fuel cell, under standard state conditions for low temperature operation where the resultant product is in liquid form, the enthalpy $\Delta h = -285.8 \, kJ/mol$ and the Gibbs free energy $\Delta G = 237.3 \text{kJ}/mol$ [9, 52]. This is represented as:

$$H_{2(g)} + 1/2 \, O_{2(g)} \Rightarrow H_2 O_{(l)} \qquad (2.25)$$

For high temperature operation however one has $\Delta h = -241.8 \, kJ/mol$ and $\Delta G = 228.6 \, kJ/mol$ and the resultant product is in vapour form, the representation hereof is [9, 52]:

$$H_{2(g)} + 1/2 \, O_{2(g)} \Rightarrow H_2 O_{(g)} \qquad (2.26)$$

The potential for each class of operation is, $U_{H_2/O_2(l)} = 1.229\text{V}$ for low temperature operation and $U_{H_2/O_2(g)} = 1.185\text{V}$ for high temperature operation. This value is interpreted as the theoretical/ ideal electrical potential for a hydrogen/oxygen fuel cell is 1.229V and 1.185V at standard temperature [9, 52]. To determine the theoretical electrical potential of fuels operating at values other than standard conditions one utilises what is better known as the Nernst equation. Incorporating the Nernst equation the above takes on two forms:

$$U = U_{rev} - \frac{RT}{2F} \ln \left(\frac{\alpha_{H_2O}}{\alpha_{H_2} \alpha_{O_2}^{0.5}} \right) \tag{2.27}$$

Where α_k is the activity of species k [52] and in Shah et al [9] the Nernst equation is given in terms of partial pressures and is as follows:

$$U = U_{rev} - \frac{RT}{2F} \ln \left(\frac{P_{H_2} P_{O_2}^{0.5}}{P_{H_2O}} \right) \tag{2.28}$$

Utilising the first Nernst equation in terms of specie activity and at standard temperature and pressure, the theoretical potential of a low temperature hydrogen-air fuel cell can be calculated and is according to Spiegel [52] 1.219V. The implication hereof is that at standard conditions, with no current flowing, the potential between the oxygen cathode, where the reduction occurs and the hydrogen anode, where the oxidation occurs will be 1.219V [52].

The hydrogen fuel cell system has an efficiency much greater than the most complex heat engines such a steam engines or internal combustion [52]. The thermal efficiency of a fuel conversion device is determined by the Gibbs free energy and the enthalpy of formation. Alternatively, said as the amount of useful energy produced relative to the change in enthalpy between the product and reactants [65, 21]. The relation is given as [52]:

$$\tilde{\eta} = \frac{\Delta G}{\Delta h} \tag{2.29}$$

For low temperature where liquid water is a by product the efficiency is 83% and for in the high temperature scenario the efficiency is approximately 95%. From U.S department of energy handbook, [22] the efficiency of an actual fuel cell is often expressed in terms of the ratio between the operating cell voltage to the ideal cell voltage. As discussed in sections to follow, the actual cell voltage is less than the ideal, due to losses associated with cell polarization and ohmic losses [52]. Therefore the thermal efficiency for high temperature operation written in terms of actual cell voltage is given as follows [22]:

$$\tilde{\eta} = \frac{Useful\ Energy}{\Delta h} \tag{2.30}$$

$$\tilde{\eta} = \frac{Useful\ POWER}{\Delta G / 0.945} \tag{2.31}$$

$$\tilde{\eta} = \frac{Volts_{actual} \times Current}{Volts_{ideal} \times Current / 0.945} \tag{2.32}$$

$$\tilde{\eta} = \frac{0.945 \times Volts_{actual}}{U_{ideal}} \tag{2.33}$$

Where U_{ideal}, as previously mentioned, for low temperature operation

$U_{ideal} = U_{H_2/O_2(l)} = 1.229V$ and $U_{ideal} = U_{H_2/O_2(g)} = 1.185V$ for high temperature

operation. Therefore for a high temperature fuel cell the thermal efficiency of an actual fuel

cell operating at a voltage of $Volts_{actual}$, based on the higher heating value of hydrogen is

given by

$$\tilde{\eta} = \frac{0.945}{1.185} \times Volts_{actual} = 0.794 \times Volts_{actual} \tag{2.34}$$

When a fuel cell operates under thermodynamically reversible conditions both maximum
electrical energy output and the potential difference between the cathode and anode, is
achieved [52]. The net voltage of a fuel cell at a certain current density j is the reversible
cell voltage, which is the potential minus the irreversible voltage.

$$v(j) = v_{rev} - v_{irrev} \quad \text{where} \tag{2.35}$$

$$v_{rev} = U_{rev} \quad . \tag{2.36}$$

Where this is defined above as the maximum (reversible) voltage of the fuel cell and V_{irrev} is the irreversible voltage loss also known as the over potential. The maximum possible cell potential is the reversible cell potential. Deviation from the maximum, reversible voltage is due to the irreversible voltages and is illustrated in Figure 2. From this a deduction that the actual work done in the fuel cell is less than the maximum useful work. This is due to the irreversible processes. The irreversible processes that occur within a fuel cell include those of the activation potential (V_{act}), ohmic overpotential (V_{ohmic}), and concentration overpotential (V_{conc}).

Activation losses are associated with the process of charge transfer [35] and stems from the activation energy of the electrochemical reactions at the electrodes [22]. Losses are dependent on the reactions, the electro-catalyst material and microstructure, reactant activities and weakly on the current density [22]. The least intricate losses to understand is the voltage drop due to the internal resistance found within the cell itself. From Janardhanan [35] the major contribution to ohmic overpotential is due to the ionic resistance of the electrolyte material. The losses that arise from the concentration overpotential is due to the mass transport limitations within the porous electrode structure. The maximum potential a fuel cell can achieve depends on the partial pressures of the electrochemically active reactant species and the product of electrochemical charge transfer reaction at the reaction site [35].

To summarise the voltage irreversible processes are given as follows:

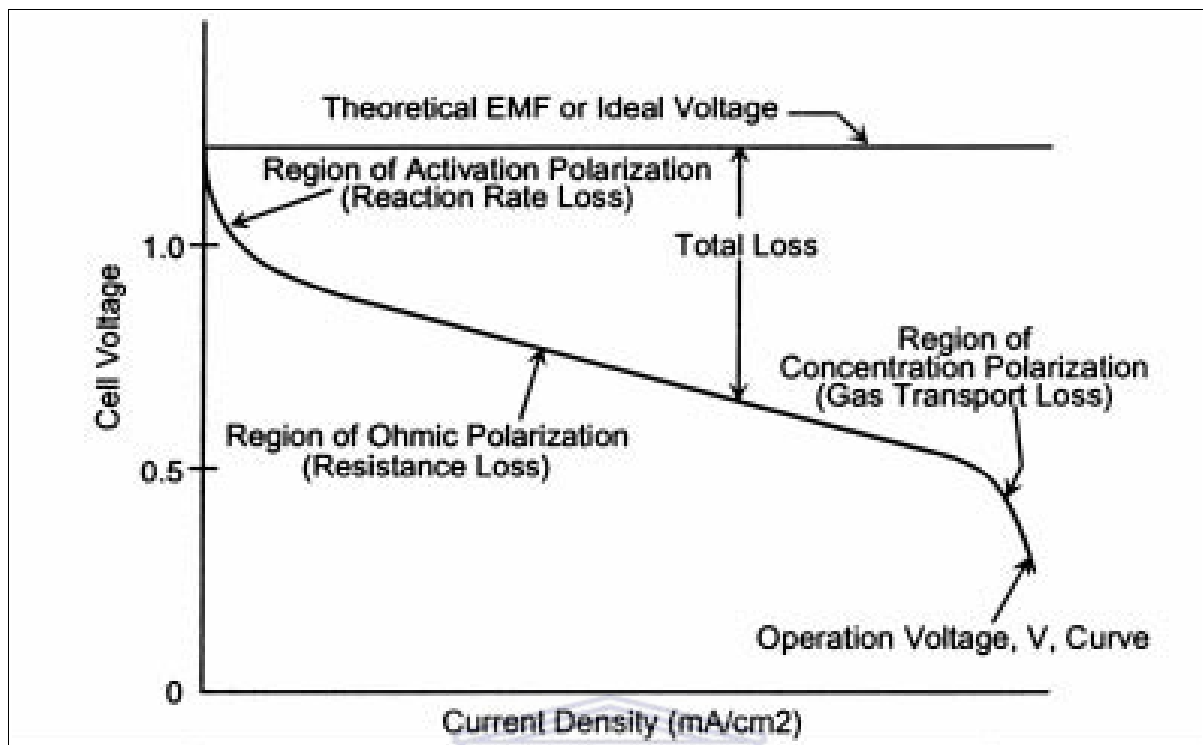$$V_{irrev} = V_{act} + V_{ohmic} + V_{conc} \tag{2.37}$$

Figure 2: Hydrogen - Oxygen Fuel Cell performance curve - [22]

1.3 Fuel Cell Heat Transfer

Heat transfer is a study that seeks to predict the energy transfer which takes place between material bodies as a result of a temperature difference [31]. Thermodynamics however, deals with systems in equilibrium. Heat transfer does not only merely seek to explain how energy is transferred but also to determine how under specified conditions, the rate at which it is done [61]. When a temperature gradient exists in a body a transfer of energy occurs from the higher temperature to lower temperature [61].The transfer of energy from more energetic particles to less energetic particles due to the interaction between the particles is defined as conduction. The process of heat transfer is defined in terms of rate equations and known as Fourier's law. The rate of heat transfer in the x-direction through a finite cross sectional area, A is expressed as [31]:

$$\frac{dQ}{dx} = -\kappa \frac{\partial T}{\partial x}$$

(2.38)

where the rate of heat transfer is $\frac{dQ}{dx}$ and $\frac{\partial T}{\partial x}$ is the temperature gradient which is in the direction of the heat flow. κ, a positive constant, is the thermal conductivity of a material.

It is considered to be a transportation property which gives an indication of the rate at which energy is transferred through the diffusion process and is dependent on the atomic and molecular structure of the substance. The minus sign ensures that the second principle of thermodynamics is satisfied [31, 61]. Under linear steady-state condition the heat transfer temperature gradient may be expressed as follows:

$$\frac{dQ}{dx} = \kappa \frac{T_1 - T_2}{L}$$

(2.39)

where L is considered to be the length along a particular direction.
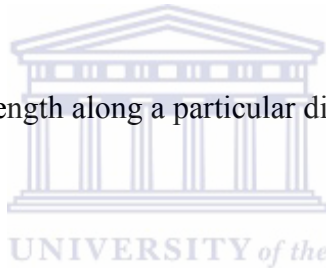
Within a fuel cell, despite a constant mass flow rate in the channel, temperature distribution is not uniform. There are many reasons for this, some of which are for example, the air convection or heat produced by the catalyst layer. To predict the temperature-dependent parameters the, rate of reactions, rate species transport and the heat distribution throughout the fuel cell stack need to be determined accurately [61]. To determine the heat distribution in a fuel cell one has to perform energy balances on the system. Energy balance in a fuel cell takes into account the power produced, the fuel cell reactions and losses in terms of heat. Between the solid surface and the gas streams convective heat transfer occurs and in the solid and or the porous structures conductive heat transfer [61].

From Spiegel [61] the general energy balance states that the enthalpy of the reactants entering the cell equals the enthalpy of the products leaving the cell plus the sum of the heat generated by the power output, and the rate of heat loss to the surroundings. This is given as:

$$\sum (h_i)_{into} = W_{elec} + \sum (h_i)_{out} + Q \quad . \tag{2.40}$$

The enthalpy inputs, $(h_i)_{into}$ are those of the fuel, the oxidant and water vapor. The enthalpy outputs are those of the products leaving, $(h_i)_{out}$. The additional terms on the right hand side are those of the the electric power produced W_{elec} and the heat leaving the fuel cell Q. Heat leaving the fuel takes place through the coolant of the fuel cell, conduction, convection, or radiation. The heat leaving the fuel cell through conduction and convection is given as depicted below and their corresponding thermal resistances are $r_{conduction}$ and $r_{convection}$ respectively. One dimensional flow is illustrated as:

$$Q_{conduction} = -\kappa A \frac{dT}{dx} \tag{2.41}$$

$$r_{conduction} = \frac{T_1 - T_2}{Q_{conduction}} = \frac{1}{\kappa A} \tag{2.42}$$

$$Q_{convection} = \xi A (T_2 - T_1) \tag{2.43}$$

$$r_{convection} = \frac{(T_2 - T_1)}{Q_{convection}} = \frac{1}{\xi A} \tag{2.44}$$

Where the overall effect of convection is taken from Newton's law of cooling and ξ is called the convective heat transfer coefficient in units of $W/m^2 K$ [31, 61]. The resistance, since the conduction and convection resistances are in series, is summed as follows:

$$r_{tot} = \frac{1}{\xi_1 A} + \frac{1}{\kappa A} + \frac{1}{\xi_2 A} \tag{2.45}$$

A fuel cell consists of many layers and the composition of each differs. The temperature drop between materials can be significant and is classified as the thermal contact resistance [61]. Thermal contact resistance is expressed as:

$$r_{tc} = \frac{\Delta T}{Q} \ .$$

(2.46)

The thermal resistance, $r_{thermal}$ is defined as:

$$r_{thermal} = \frac{1}{\frac{1}{r_{convective}} + \frac{1}{r_R}}$$

(2.47)

where $r_{convective}$ is the thermal resistance and the heat leaving the fuel cell through radiation is known as the radiative thermal resistance r_R and is given as:

$$r_R = \frac{1}{\sigma \, \breve{s} \, A_s (T_s + T_0)(T_s^2 + T_0^2)}$$

(2.48)

where σ is known as the Stefan Boltzmann' constant, $\breve{s}$ is termed as the shape factor, A_s is the exposed surface area, T_s and T_0 refer to temperatures of the surrounding and initially. The shape factor is dependent on the geometry of body through which heat is being conducted [62].

The internal heat generation can be described by the Poisson equation [61]:

$$\frac{d^2 T}{dx^2} + \frac{Q_{internal}}{\kappa} = 0$$

(2.49)

where $Q_{internal}$ is the rate of heat generation per unit volume.

29

In a nutshell in a fuel cell, one has the fuel, hydrogen entering at the anode end of the cell at a temperature $T_{H_{2(g)}}$, pressure $P_{H_{2(g)}}$, mole fraction x_{H_2} and mass flow rate $(\dot{m})_{H_2}$. Oxygen enters the fuel cell at its respective temperature, $T_{O_{2(g)}}$, pressure $P_{O_{2(g)}}$, mole fraction x_{O_2} and mass flow rate $(\dot{m})_{O_2}$ at the cathode end of the fuel cell. The hydrogen and oxygen react completely to produce water which exits the cell at temperature $T_{H_2O(g)}$, pressure $P_{H_2O(g)}$, mole fraction x_{H_2O} and a mass flow rate $(\dot{m})_{H_2O}$. Therefore from the generic energy balance, equation (1.41) ,one has the following entering on the left hand side of the equation and leaving on the right hand side [61]:

$$h_{H_2}+\frac{1}{2}h_{O_2}=W_{elec}+Q+h_{H_2O} \qquad (2.50)$$
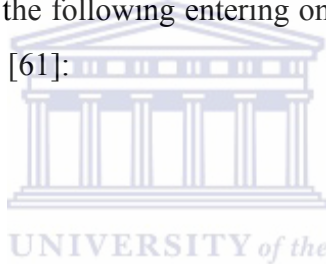
Where the enthalpy for each dry gas or mixture of dry gases is [61]:

$$h=(\dot{m})\tilde{C}T \qquad (2.51)$$

If the gas has a high heating value HHV, (combustible) as in the case with water vapour, the enthalpy is given as [61]:

$$h=(\dot{m})(\tilde{C}T+h^0_{HHV}) \qquad (2.52)$$

Values of the higher heating values are generally reported for values that correspond to 25°C. The energy balance of a fuel cell system is given schematically Figure 3.
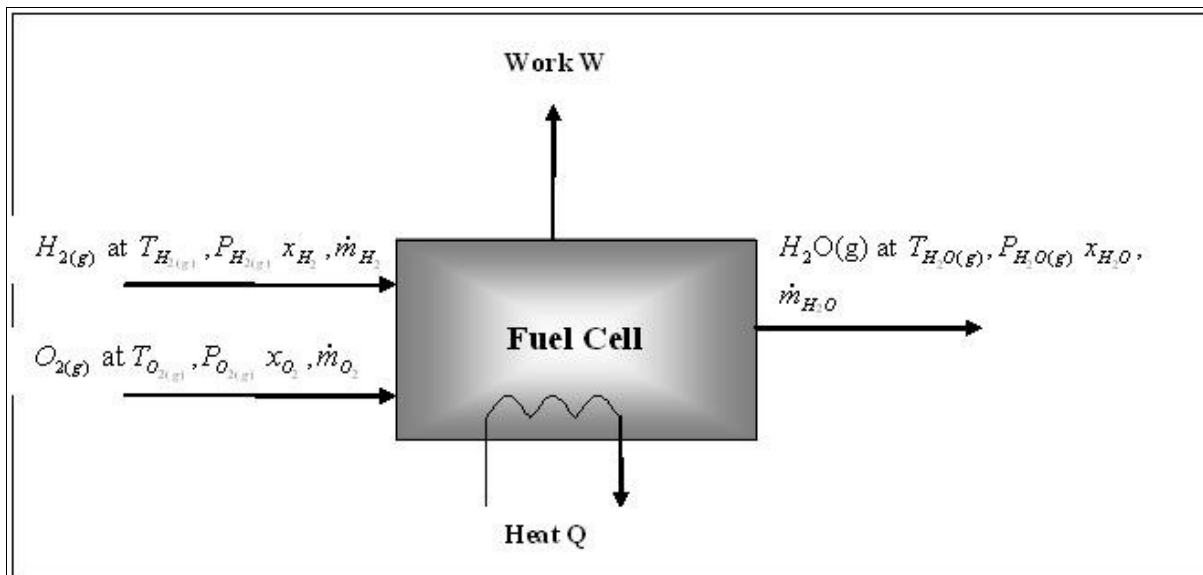
Figure 3: Fuel Cell Energy Balance [60]

The generic heat balance for a fuel cell stack is then given by:

$$\sum Q_{into} - \sum Q_{out} = W_{el} + Q_{dis} + Q_c \qquad (2.53)$$

where Q_{into} is the heat of the reactant gases coming into the system, Q_{out} the heat of the unused reactants, W_{el} is the electricity generated, Q_{dis} is the heat dissipated to the environment and Q_c is the heat removed to the active cooling of the fuel cell [61]. In the thermodynamics section of this chapter the first law of thermodynamics is derived from the conservation of energy and in order to model the fuel cell thermally one considers the energy equation which serves as the transport equation for temperature [34, 63]. The energy of a system is such that the following principles hold [63]:

Rate of change in Energy of a fluid particle	=	Net rate of heat added to a fluid particle	+	Net rate of work done on a fluid particle	+	Net rate of increase in energy due to sources

Where the effects due to potential energy changes are taken into account by the source term [63].

The conservation of energy is given as [46]:

$$\nabla \cdot (\vec{u}(\rho E + P)) = \nabla \cdot \left(\kappa^{eff} \nabla T - \sum h_k J_k + (\tau_{eff} \cdot \vec{u}) \right) + S_h \tag{2.54}$$

where for any variable, Φ

$$\nabla \cdot \Phi = \frac{\partial \Phi_x}{\partial x} + \frac{\partial \Phi_y}{\partial y} + \frac{\partial \Phi_z}{\partial z} \quad , \tag{2.55}$$

$\vec{u} = (u, v, w)$ (2.56) denotes the superficial velocity vector in the porous media and ρ the density of the gas mixture.

$$\rho = \frac{1}{\sum_k (Y_k / \rho_k)} \tag{2.57}$$

Where Y_k is the mass fraction of species k and ρ_k the density thereof. ρ_k is determined by the ideal gas relation of:

$$\rho_k = \frac{P M_k}{RT} \quad . \tag{2.58}$$

M_k refers to the molecular weight of the gas and P, R and T are as previously mentioned pressure, ideal gas constant and temperature respectively. Further on the right hand side of equation (2.54) one has, κ^{eff} which is defined as the thermal conductivity in a porous material consisting of the electrode solid matrix and gas and from Peng et al [46] the equation hereof is given below:

$$\kappa^{eff} = \tilde{\varepsilon} \kappa_f + (1 - \tilde{\varepsilon}) \kappa_{sol} \tag{2.59}$$

32

where $\tilde{\varepsilon}$ is the porosity, κ_f is the thermal conductivity of the gas and κ_{sol} the thermal

conductivity of the electrode solid matrix. ∇T is defined as:

$$\nabla T = \frac{\partial T}{\partial x}\hat{i} + \frac{\partial T}{\partial y}\hat{j} + \frac{\partial T}{\partial z}\hat{k}$$

(2.60)

Continuing with equation (2.54) one has h_k and J_k which are the which is the enthalpy

and the flux of species k respectively. J_k is defined by the following equation:

$$J_k = -\sum_{k=1} \rho D_k \nabla Y_k$$

(2.61)

where D_k is the diffusion coefficient of species k. τ_{eff} is the effective stress tensor,

which based on the assumption that the flow of gases for the fuel cell is laminar, it can be

ignored. This is primarily due to the low velocity of gas flow [46]. Motivation for the choice

of flow is explained in the sections to follow. S_h In equation (2.54) is the net rate of

increase in energy due to sources which is zero in all areas except in the cathode catalyst and

membrane where:

$$S_h = \frac{|j_{cat}|}{2F} T |\Delta S| + |j_{cat}\eta_{cat}| \quad \text{for the cathode catalyst}$$

(2.62)

and in the membrane

$$S_h = \frac{i^2}{\kappa_{mem}}$$

(2.63)

i is defined as current, j_{cat} the transfer current in the cathode and η_{cat} the

overpotential in the cathode, all of which is discussed in greater detail in the following

section, "Fuel cell Electrochemistry and Charge transport". ΔS is the entropy as defined in equation (2.2) and (2.3) and κ_{mem} the membrane conductivity.

In the computational fluid dynamics package FLUENT and PEM fuel cell model S_h is the total source that goes to the thermal energy equation and is given as [3]:

$$S_h = h_{react} - j_{anode/cat} \eta_{anode/cat} + i^2 r_{ohmic} + h_L \qquad (2.64)$$

where h_{react} is the net enthalpy due to the electrochemical reactions, r_{ohmic} the ohmic resistance and h_L is the enthalpy change due to condensation/ vaporization of water [3].

1.4 Fuel Cell Electrochemistry and Charge Transportation

Electrochemistry is the study concerned with the transference of electrical charges across interfaces through a solution [17, 48]. Within the fuel cell it is the transfer of electrons between the interfaces of the electrode and the chemical species found with in the electrolyte. In a fuel cell there exists two types of charges, electrons and ions and the transportation hereof induces what is called electronic and ionic losses respectively [54, 55]. Collectively these losses are known as the Ohmic loss. Where ohmic resistance is given algebraically as:

$$r_{ohmic} = r_{ionic} + r_{elec} \qquad (2.65)$$

Each charge, electronic or ionic experiences a resistance unique to the material. Each of theses resistances in turn contributes to the reduction in voltage. Ohmic polarization is known as the materials' natural resistance to the flow of charge which results in a loss in the cell voltage. During this process a change in Gibbs free energy arises [54].

The relation between the voltage drop and resistance is given as:

$$v_{ohmic} = i r_{ohmic}$$
(2.66)

where v_{ohmic} refers to the ohmic voltage, i is the current and r_{ohmic} the ohmic resistance. This relation is also known as Ohms law.

According to Spiegel [54] ionic transport is far more difficult to model and predict. The region in which the ionic losses occur is that of the fuel cell membrane and where the $H^{'+'}$ ions travel through the electrolyte [55] . The net flow of charge dq is given as:

$$dq = q(nAv_d \, dt)$$
(2.67)

where q is the charge of a particle, n the concentration of particles, v_d the drift velocity and dt the duration. Current, i is a direct measure of the electrochemical reaction rate, which in turn is the rate at which electrons are created or consumed [55] and is given by the following equation:

$$i = \frac{dq}{dt} = qnAv_d$$
(2.68)

The current density also referred to as the current per unit cross-section area, j

$$j = \frac{i}{A} = qnv_d = \kappa_{elec} \tilde{E}$$
(2.69)

κ_{elec} is the electrical conductivity of a material and $\tilde{E}$ is the electric field.

$$\kappa_{elec} = \frac{i}{r_{ohmic}} = nq \frac{v_d}{\tilde{E}} = nq\, u_e \qquad (2.70)$$

where u_e is often termed as the mobility [54, 40].

To improve the performance of a fuel cell, the resistance would have to be decreased. To reduce the resistance either the conductivity of the electrolyte can be improved and or the membrane thickness can be reduced. Where the relation between resistance and the membrane thickness is given by the following equation [54]:

$$r_{ohmic} = \frac{\delta_{thick}}{\kappa\, A_{cell}} \qquad (2.71)$$

where A_{cell} is the active area and δ_{thick} is the thickness of the electrolyte layer and therefore equation (2.66) can be rewritten as:

$$v_{ohmic} = i r_{ohmic} = j A_{cell} \frac{\delta_{thick}}{\kappa_{elec}\, A_{cell}} = j\, \frac{\delta_{thick}}{\kappa_{elec}}. \qquad (2.72)$$

Furthermore, the fuel cells total resistance is the summation of the resistance of each layer, therefore v_{ohmic} is the current multiplied by the total resistance r_{ohmic}.

The mobility of free electrons, u_e in a metal conductor is given as:

$$u_e = \frac{q\tilde{\tau}}{m_e} \qquad (2.73)$$

36

where $q = 1.60 \times 10^{-19} C$ and is the elementary electron charge in Coulombs, $\tilde{\tau}$ is the mean free time between scattering events and $m_e = 9.11 \times 10^{-31} kg$ is the mass of an electron [54]. It follows that equation for conductivity becomes:

$$\kappa = \frac{|z_e| F c_e q \tilde{\tau}}{m_e} \tag{2.74}$$

where z_e is the charge number (valence electrons) for the carrier, F is Faraday' constant and c_e is the number of moles of charge carriers per unit volume.

The conductivity of ions follows a different relationship and for the membrane its conductivity can be accurately described by the Arrhenius equation [46, 38, 3]:

$$\kappa_{mem} = \kappa_0 e^{\frac{-E_{A,\kappa}}{R}\left(\frac{1}{T} - \frac{1}{303}\right)} \tag{2.75}$$

where κ_0 is the membranes conductivity at standard conditions. From Ju et al [38] the effective conductivity of the anode and cathode catalyst layers follows that of the membrane however with the Bruggmann correlation and is given as:

$$\kappa_{sol} = \kappa_{cat}^{eff} = \kappa_{anode}^{eff} = \varepsilon_{mc}^{1.5} \kappa_{mem} \tag{2.76}$$

where κ_{sol} accounts for the constituents of the electrode solid conductive matrix, $\varepsilon_{mc}^{1.5}$ is the volume fraction of ionomer in the anode and cathode catalyst layers [46].

To continue the discussion on the electrochemistry and charge transport within a fuel cell one considers the reactions that occur within it. Along the anode, the hydrogen gas reaches the

electrode and the first step it undergoes is absorption and dissociation into H atoms [55]. This reaction is given as:

$$H_{2(g)} \to H \times H \qquad (2.77)$$

A second step follows of further dissociation at the electrode, takes on the following form:

$$H \to H^{'+'} + \acute{e} \qquad (2.78)$$

where $H^{'+'}$ is referred to as the oxidized form of the chemical species H and is the reduced form of the chemical species. $\acute{e}$ refers to an electron. If one denotes the change in concentration of the oxidized form as the forward reaction and change in concentration of the reduced form as the backward reaction then the flux, (rate of the reaction) is given as follows [55]:

$$\breve{J}_f = k_f C_{Ox} \quad \text{and} \qquad (2.79)$$

$$\breve{J}_B = k_B C_{Rd} \qquad (2.80)$$

k_f and k_B are the rate coefficients. C_{Ox} and C_{Rd} are the surface concentrations of the reactant species. Essentially these reactions either consume or release electrons and net current is the difference [55]:

$$i = nF(k_f C_{Ox} - k_B C_{Rd}) \; . \qquad (2.81)$$

From the Butler-Volmer model of electrode kinetics, the above equation is further refined to give the following for the forward and backward oxidation reaction rate coefficients [55]:

$$k_f = k_{0,f} e^{\frac{\beta_{Rd} FU}{RT}} \quad \text{and} \qquad (2.82)$$

$$k_b = k_{0,b} \, e^{\frac{\beta_{Ox} F U}{RT}}$$

(2.83)

where β is the transfer coefficient, F Faraday's constant and U is the potential. The transfer coefficient is found to be a measure of symmetry of the energy barrier and its value in the absence of actual measurements is usually approximated by 0.5 [55]. Backward oxidation is alternatively known as reduction. The net current is therefore then given by:

$$i = nF \left\{ k_{0,f} C_{Ox} \, e^{\frac{\beta_{Rd} F U}{RT}} - k_{0,b} C_{Rd} \, e^{\frac{\beta_{Ox} F U}{RT}} \right\}$$

(2.84)

Further the transfer current at the anode and cathode and is given by the Butler-Volmer equations as [46]:

$$j_{0,anode} = j_{anode}^{ref} \left(\frac{P_{H_2}}{P_{H_2}^0} \right)^{\breve{\alpha}} \left[e^{\left(\frac{\beta_{anode} F \eta_{anode}}{RT} \right)} - e^{\left(\frac{-\beta_{cat} F \eta_{anode}}{RT} \right)} \right] \quad \text{and}$$

(2.85)

$$j_{0,cat} = j_{cat}^{ref} \left(\frac{P_{O_2}}{P_{O_2}^0} \right)^{\breve{\alpha}_1} \left(\frac{P_{H_2O}}{P_{H_2O}^0} \right)^{\breve{\alpha}_2} \left[e^{\left(\frac{-\beta_{cat} F \eta_{cat}}{RT} \right)} - e^{\left(\frac{\beta_{anode} F \eta_{cat}}{RT} \right)} \right]$$

(2.86)

P_k is the partial pressure of species k and P_k^0 is reference to standard pressure. From Peng et al [46] the values for $\breve{\alpha} = 0.25, \breve{\alpha}_1 = 0.5$ and $\breve{\alpha}_2 = 0.25$ and are determined empirically and are concentration parameters. j_{anode}^{ref} and j_{cat}^{ref} are the anodic and cathodic reference exchange current densities dependent on the local temperature, given in the following equation:

$$j_{anode}^{ref} = j_{anode,0}^{ref} \, e^{\left[\frac{-E_{A,a}}{R} \left(\frac{1}{T} - \frac{1}{353.15} \right) \right]} \quad \text{and}$$

(2.87)

$$j_{cat}^{ref} = j_{cat,0}^{ref} \, e^{\left[\frac{-E_{A,c}}{R} \left(\frac{1}{T} - \frac{1}{353.15} \right) \right]} \quad \text{respectively [38].}$$

(2.88)

Where $E_{A,a}$ and $E_{A,c}$ are the respective activation energies. The driving force for the

kinetics is the local surface overpotential [3]. η_{anode} And η_{cat} are the local overpotentials'

determined by the following equations:

$$\eta_{anode} = \phi_{sol} - \phi_{mem} \quad \text{and} \tag{2.89}$$

$$\eta_{cat} = \phi_{sol} - \phi_{mem} - V_0 \tag{2.90}$$

where ϕ_{sol} and ϕ_{mem} refer to the solid and membrane phase potentials respectively and

V_0 is the open-circuit voltage on the cathode side [3]. In Peng et al, [46] it is defined as the

thermodynamic equilibrium potential which for temperatures greater than 373.15K is

defined by the following equation:

$$V_0 = 1.17 - 2.756 \times 10^{-4}(T - 373.15) + 4.308 \times 10^{-5} \ln\left(\frac{\chi_{H_2}(\chi_{O_2})^{(1/2)}}{\chi_{H_2O}}\right) \tag{2.91}$$

where $\chi_{H_2}, \chi_{O_2}^{1/2}$ and χ_{H_2O} is defined as a ratio between the respective species partial

pressure to standard pressure [46].

In the FLUENT, the computational fluid dynamics package used to model the fuel cell, the
Butler-Volmer equation takes on the following form [3]:

$$j_{0,anode} = \zeta_{anode} j_{anode}^{ref} \left(\frac{[C]}{[C]_{ref}}\right)^{\psi_{anode}} \left[e^{\left(\frac{\beta_{anode} F \eta_{anode}}{RT}\right)} - e^{\left(\frac{\beta_{cat} F \eta_{anode}}{RT}\right)}\right] \quad \text{and} \tag{2.92}$$

$$j_{0,cat} = \zeta_{cat} j_{cat}^{ref} \left(\frac{[C]}{[C]_{ref}}\right)^{\psi_{cat}} \left[e^{\left(\frac{-\beta_{cat} F \eta_{cat}}{RT}\right)} - e^{\left(\frac{\beta_{anode} F \eta_{cat}}{RT}\right)}\right] \tag{2.93}$$

where ζ is the specific active area, $[C]$ local species concentration, $[C]_{ref}$ the reference species concentration and $\tilde{\Psi}$ is the concentration dependence [3].

From the conservation of charge, the below argument holds:

$$\nabla \cdot (\kappa_{sol} \nabla \phi_{sol}) + S_{sol} = 0 \tag{2.94}$$

$$\nabla \cdot (\kappa_{mem} \nabla \phi_{mem}) + S_{mem} = 0 \tag{2.95}$$

The source terms, S_{mem} and S_{sol} in the above equations are non-zero only inside the catalyst layers and are computed as [3, 46, 38]:

- For the solid phase:

  - $S_{sol} = -j_{anode}$ on the anode side and $\tag{2.96}$

  - $S_{sol} = j_{cat}$ on the cathode side. $\tag{2.97}$

- For the membrane phase:

  - $S_{mem} = j_{anode}$ on the anode side and $\tag{2.98}$

  - $S_{mem} = -j_{cat}$ on the cathode side. $\tag{2.99}$

2.5 Fuel Cell Mass Transport

Fuel cell mass transport is viewed as the transportation of the species. As previously mentioned, the three factors contributing to voltage losses within a fuel cell are activation losses, ohmic losses and mass transport limitations. The losses due to mass transport

limitations can be reduced by optimising mass transport in each of the respective layers within a fuel cell [53, 18]. Mass transfer is due to density gradients or hydrodynamic transport and is termed as convection and is further characterised as laminar, turbulent flow or stagnant regions. The criterion which determines whether flow is laminar or turbulent is known as the Reynolds number [18]. In Spiegel [53] for small Reynolds numbers

$R_e < 2300$ flow is laminar, $R_e > 4000$ flow is turbulent and between this range

$2300 < R_e < 4000$ flow is said to be transitional. Reynolds number is defined as the ratio between the inertial forces to viscous forces and is given by the following equation [53]:

$$R_e = \frac{\rho u_m d_{ch}}{\mu} = \frac{u_m d_{ch}}{\nu}$$
(2.100)

where u_m is the characteristic velocity of the flow (m/s), ρ is the fluid density, μ is the fluid viscosity, ν is the kinematic viscosity (m²/s) and d_{ch} is the flow channel diameter or characteristic length (m). The effective Reynold's number for rectangular channels is:

$$R_{e_{rect}} = \frac{\rho \bar{u}_m d_{rect}}{\mu} \quad \text{where}$$
(2.101)

$$d_{rect} = \frac{4 A_c}{\tilde{P}}$$
(2.102)

A_c is the cross-sectional area of channel with width a and length b, $\tilde{P}$ is the perimeter and $\bar{u}_m$ the mass averaged velocity in the channel.

In the fuel cell flow channels the flow is convective and in the fuel cell gas diffusion layers and catalyst regions one finds tiny pores and therefore it is considered to be governed by

diffusion. The flow along the walls of the fuel cell is generally slower and aids in the transition of flow from convective to diffusive [53].

The rate at which mass flows into and out of the fuel cell subsystem, stack, or fuel cell layer, needs to be accounted for and from the continuity equation one has that the sum of all of the mass inputs is equal to the mass outputs. The continuity equation is given as [46]:

$$\nabla \cdot (\rho \vec{u}) = S_m \tag{2.103}$$

In a porous medium $\vec{u}$ denotes the superficial velocity vector and S_m an additional source term and is defined as follows:

$$S_m = \frac{-M_{H_2}}{2F} j_{anode} \quad \text{for the anode side and} \tag{2.104}$$

$$S_m = \frac{-M_{O_2}}{2F} j_{cat} + \frac{M_{H_2O}}{2F} j_{cat} \quad \text{cathode side.} \tag{2.105}$$

M_k is the molecular weight for species k, F Faraday' constant, j_{cat} and j_{anode} is as defined in equation (2.85) and (2.86) the transfer currents. The mass balance of a system and can be expressed as [53]:

$$\sum (m_k)_{into} = \sum (m)_{out} \tag{2.106}$$

Where m_k is the mass of specie k going in and out of the fuel cell. From Spiegel [53] the flow rates at the inlet are proportional to the current and number of cells. The power output for the cell:

$$W_{elec} = n_{cell} V_{cell} i \tag{2.107}$$

43

where n_{cell} is the number of cells and V_{cell} is the cell voltage. All flows, $i\,n_{cell}$ are proportional to the power output and proportional to the cell voltages [53]:

$$i\,n_{cell} = \frac{W_{elec}}{V_{cell}} \tag{2.108}$$

In table 1 and summarised from Spiegel [53], the mass flow rates, $\dot{m}_k$ at the inlet and outlet for each respective specie found within a PEM fuel cell. Where the mass flow rate is defined as:

$$\dot{m}_k = \frac{dm}{dt} \tag{2.109}$$

and is the rate at which mass of a specific specie passes through a specified area.

Table 1: Mass Flow rates (g/s) of species within a PEM fuel cell [53]	
Specie	**Hydrogen (H_2)**
Inlet	$\dfrac{d\,m_{H_{2,into}}}{dt}=\bar{S}_{H_2}\dfrac{M_{H_2}}{2F}\,i\,n_{cell}$ (2.110)
Outlet	$\dfrac{d\,m_{H_{2,out}}}{dt}=(\bar{S}_{H_2}-1)\dfrac{M_{H_2}}{2F}\,i\,n_{cell}$ (2.111)
Specie	**Oxygen (O_2)**
Inlet	$\dfrac{d\,m_{O_{2,into}}}{dt}=\bar{S}_{O_2}\dfrac{M_{O_2}}{4F}\,i\,n_{cell}$ (2.112)
Outlet	$\dfrac{d\,m_{O_{2,into}}}{dt}=(\bar{S}_{O_2}-1)\dfrac{M_{O_2}}{4F}\,i\,n_{cell}$ (2.113)
Specie	**Air**
Inlet	$\dfrac{d\,m_{air_{into}}}{dt}=\dfrac{\bar{S}_{O_2}}{r_{O_2}}\dfrac{M_{O_2}}{4F}\,i\,n_{cell}$ (2.114)
Outlet	$\dfrac{d\,m_{air_{out}}}{dt}=\left[(\bar{S}_{O_2}-1)M_{O_2}+\bar{S}_{O_2}\dfrac{1-r_{O_2}}{r_{O_2}}M_{N_2}\right]\dfrac{i\,n_{cell}}{4F}$ (2.115)
Specie	**Nitrogen (N_2)**
Inlet	$\dfrac{d\,m_{N_2,into}}{dt}=\bar{S}_{O_2}\dfrac{M_{N_2}}{4F}\dfrac{1-r_{O_2,into}}{r_{O_2,into}}\,i\,n_{cell}$ (2.116)
Outlet	$\dfrac{d\,m_{N_2,out}}{dt}=\dfrac{d\,m_{N_2,into}}{dt}=\bar{S}_{O_2}\dfrac{M_{N_2}}{4F}\dfrac{1-r_{O_2,into}}{r_{O_2,into}}\,i\,n_{cell}$ (2.117)
Specie	**Water Vapour in hydrogen, $H_2O(g)$ in H_2**
Inlet	$\dfrac{d\,m_{H_2O,intoH_2,into}}{dt}=\bar{S}_{H_2}\dfrac{M_{H_2O}}{2F}\dfrac{\Psi_{anode}P_{vs(T_{anode},into)}}{P_{anode}-\Psi_{anode}P_{vs(T_{anode},into)}}\,i\,n_{cell}$ (2.118)

	Table 1: Mass Flow rates (g/s) of species within a PEM fuel cell [53]
Outlet	$\dfrac{d\,m_{H_2O,\,intoH_2,out}}{dt}=min\left[(\bar{S}_{H_2}-1)\dfrac{M_{H_2O}}{2F}\dfrac{\Psi_{anode}P_{vs(T_{anode},out)}}{P_{anode}-\Psi_{anode}P_{vs(T_{anode},out)}}\,i\,n_{cell}\dfrac{d\,m_{H_2Ointo,\,H_2Oout}}{dt}\right]$ (2.119)
Specie	**Water Vapour in Oxygen, H₂O(g) in O₂**
Inlet	$\dfrac{d\,m_{H_2O,\,intoO_2,into}}{dt}=\bar{S}_{O_2}\dfrac{M_{H_2O}}{4F}\dfrac{\Psi_{cat}P_{vs(T_{anode},into)}}{P_{cat}-\Psi_{cat}P_{vs(T_{anode},into)}}\,i\,n_{cell}$ (2.120)
Outlet	(2.121) $\dfrac{d\,m_{H_2O_{into},\,H_2out},\,(g)}{dt}=min\left[(\dfrac{\bar{S}_{O_2}-r_{O_2into}}{r_{O_2into}})\dfrac{M_{H_2O}}{4F}\times\dfrac{P_{vs(T_{out,anode})}}{P_{cat}-\Delta P_{cat}-P_{vs(T_{out,anode})}}\,i\,n_{cell},\dfrac{d\,m_{H_2O_{into},\,Air_{out}}}{dt}\right]$
Specie	**Water Vapour in Air, H₂O(g) in Air**
Inlet	(2.122) $\dfrac{d\,m_{H_2O,\,inAir,into}}{dt}=\dfrac{\bar{S}_{O_2}}{r_{O_2}}\dfrac{M_{H_2O}}{4F}\dfrac{\Psi_{cat}P_{vs(T_{anode},into)}}{P_{cat}-\Psi_{cat}P_{vs(T_{anode},into)}}\,i\,n_{cell}$
Outlet	(2.123) $\dfrac{d\,m_{H_2O_{into},\,H_2out},\,(g)}{dt}=min\left[(\dfrac{\bar{S}_{O_2}-r_{O_2into}}{r_{O_2into}})\dfrac{M_{H_2O}}{4F}\times\dfrac{P_{vs(T_{out,anode})}}{P_{cat}-\Delta P_{cat}-P_{vs(T_{out,anode})}}\,i\,n_{cell},\dfrac{d\,m_{H_2O_{into},\,Air_{out}}}{dt}\right]$

$\bar{S}$ is defined as the stoichiometric ratio, M the molecular weight, P_{vs} saturation pressure,

Ψ the relative humidity, n is the number of moles, ΔP_{anode} is the pressure drop on the

anode side, $r_{O_2,into}$ and $r_{O_2,out}$ refers to the volume fraction of a species at the inlet and

outlet respectively.

To be able to deduce the above equations for the outlet, Spiegel [53], from which the above was deduced, makes the following assumptions:

1. To deduce the flow rate of oxygen at the outlet one considers the oxygen supplied at the inlet less the oxygen consumed in the fuel electrochemical reaction.

2. Nitrogen does not participate in the fuel cell reaction therefore the nitrogen flow rate at the exit is the same as the inlet.

3. The depleted air flow rate is a sum of the oxygen and nitrogen flow rates.

4. The water content in the cathode outlet is the summation of the amount of water brought into the cell, the water generated in the cell and the water transported across the membrane [53]. Which is written algebraically as:

$$m_{H_2O\,into,\,Air_{out}} = m_{H_2O\,into,\,Air_{into}} + m_{H_2O\,gen} + m_{H_2O\,ED} + m_{H_2O\,OBD} \tag{2.124}$$

Convective flow exists in the reactant flow channel and diffusive flow through the gas diffusion and catalyst layers. The reactant is supplied to the flow channel at a concentration C_0, and it is transported from the flow channel to the concentration at the electrode surface, C_s, through convection. From Fick's law, the mass transfer by diffusion of the reactants to the catalyst layer can be calculated as follows [18]:

$$\frac{dm}{dt} = -D\frac{dC}{dx} \tag{2.125}$$

Further studies conclude that the one-dimensional mass transfer along the x-axis, also known as the Nernst-Planck equation is given as [18, 53]:

$$\frac{dm_k}{dt} = J_k(x) = -D_k \overbrace{\frac{\partial C_k}{\partial x}}^{diffusion} - \overbrace{\frac{z_k F}{RT} D_k C_k \frac{\partial \Phi(x)}{\partial x}}^{migration} + \overbrace{C_k u(x)}^{convection} \tag{2.126}$$

where $J_k(x)$ is the flux of species k at a distance x form the surface, D_k is the diffusion coefficient, $\frac{\partial C_k(x)}{\partial x}$ is the concentration gradient at distance x, $\frac{\partial \Phi(x)}{\partial x}$ is

the potential gradient, z_k the charges, and $u(x)$ is the velocity with which a volume element in solution moves along the axis [18, 53]. From Peng et al [46] and for the purpose of this study, J_k the diffusive mass flux vector takes on the form:

$$J_k = -\sum_{j=1}^{N-1} \rho D_k \nabla Y_k \qquad (2.127)$$

where Y_k is the mass fraction of species k. The diffusion coefficient in the anode and cathode gas channels is calculated as a function of temperature and pressure. For the porous regions, i.e. the catalyst and diffusion layers the expression for the diffusion coefficient, D_k is modified into the effective species diffusivity, D_k^{eff} using Bruggmann correlation.

$$D_k = D_0 \left(\frac{T}{T_0}\right)^{3/2} \left(\frac{P_0}{P}\right) \qquad \text{for gas channels} \qquad (2.128)$$

$$D_k^{eff} = \varepsilon^{1.5} D_k \quad \text{for porous regions} \qquad (2.129)$$

where $\varepsilon^{1.5}$ is used to model and take into account the effect of tortuosity [3]. Tortuosity is defined as the quality or condition of being tortuous which refers to the materials disjointedness or crookedness [33].

To further the discussion one has from the conservation of species:

$$\nabla \cdot (\rho \vec{u} Y_k) = \nabla \cdot \vec{J}_k + S_k \qquad (2.130)$$

The source term $S_k = 0$ for all regions other than the catalyst layers [46] where in these regions taken from [3]

$$S_{H_2} = \frac{-M_{w,H_2}}{2F} j_{anode} \tag{2.131}$$

$$S_{O_2} = \frac{-M_{w,O_2}}{2F} j_{cat} \tag{2.132}$$

$$S_{H_2O} = \frac{-M_{w,H_2O}}{2F} j_{cat} \tag{2.133}$$

where j_{anode} and j_{cat} is defined in equation (2.85) and (2.86), M_k for species k is the molecular weight and F Faraday' constant. The final conservation law that needs to be taken into account is that of momentum which is as follows:

$$\frac{1}{(\tilde{\varepsilon})^2} \nabla \cdot (\rho \vec{u} \vec{u}) = -\nabla P + \nabla \cdot \tau + S_u \tag{2.134}$$

where $\tilde{\varepsilon}$ takes into account the porosity of a material.

2.6 Overview of Governing Equations

In Summary the main equations governing the fluid flow within a fuel cell are [46, 38]:

1. Mass or Continuity: $\nabla \cdot (\rho \vec{u}) = S_m$

2. Momentum: $\frac{1}{(\tilde{\varepsilon})^2} \nabla \cdot (\rho \vec{u} \vec{u}) = -\nabla P + \nabla \cdot \tau + S_u$

3. Species: $\nabla \cdot (\vec{u} C_k) = \nabla \cdot (D_k^{eff} \nabla C_k) + S_k$

4. Charge: $\nabla \cdot (\kappa^{eff} \nabla \phi_e) + S_\phi = 0$

49

5. Energy: $\nabla \cdot (\vec{u}(\rho E + P)) = \nabla \cdot (\kappa^{eff} \nabla T - \sum h_k J_k + (\tau_{eff} \cdot \vec{u})) + S_h$

The sources terms for each region of the fuel cell is given in the table below

	Gas flow channels	Gas diffusion layer	Catalyst layer		Membrane
			Anode	Cathode	
Continuity	$S_m = 0$	$S_m = 0$	$S_m = \dfrac{-M_{H_2}}{2F} j_{anode}$	$S_m = \dfrac{M_{O_2}}{4F} j_{cat} + \dfrac{M_{H_2O}}{2F} j_{cat}$	-
Momentum	$S_u = 0$	$S_u = -\dfrac{\mu}{K_{GDL}}$	$S_u = -\dfrac{\mu}{K_{GDL}}$		-
Energy	$S_h = 0$	$S_h = 0$	$S_h = 0$	$S_h = \dfrac{\|j_{cat}\|}{2F} T\|\Delta s\| + \|j_{cat} \eta_{cat}\|$	$S_h = \dfrac{i^2}{\kappa_{mem}}$
Species	$S_k = 0$	$S_k = 0$	$S_k = \dfrac{-M_{H_2}}{2F} j_{anode}$ For H$_2$ $S_k = \dfrac{-M_{O_2}}{4F} j_{cat}$ for O$_2$ $S_k = \dfrac{-M_{H_2O}}{2F} j_{anode}$ for H$_2$O		
Charge	$S_{sol} = 0$ $S_{mem} = 0$	$S_{sol} = 0$ $S_{mem} = 0$	$S_{sol} = -j_{anode}$ $S_{mem} = j_{cat}$	$S_{sol} = j_{cat}$ $S_{mem} = -j_{cat}$	$S_{sol} = 0$ $S_{mem} = 0$

Table 2: Source terms for continuity, momentum and energy for the conservation equations governing the various regions found PEM fuel cell given by Peng et al [46]

Chapter 3: Fuel Cell Components

3.1 Introduction

The fuel cell components consist of the bipolar plates, anode and cathode flow channels, anode and cathode gas diffusion layers (GDL), anode and cathode catalyst layers (CL) and a membrane. Numerous unit cells forms a fuel cell stack. Illustration hereof is given in Figure 4.
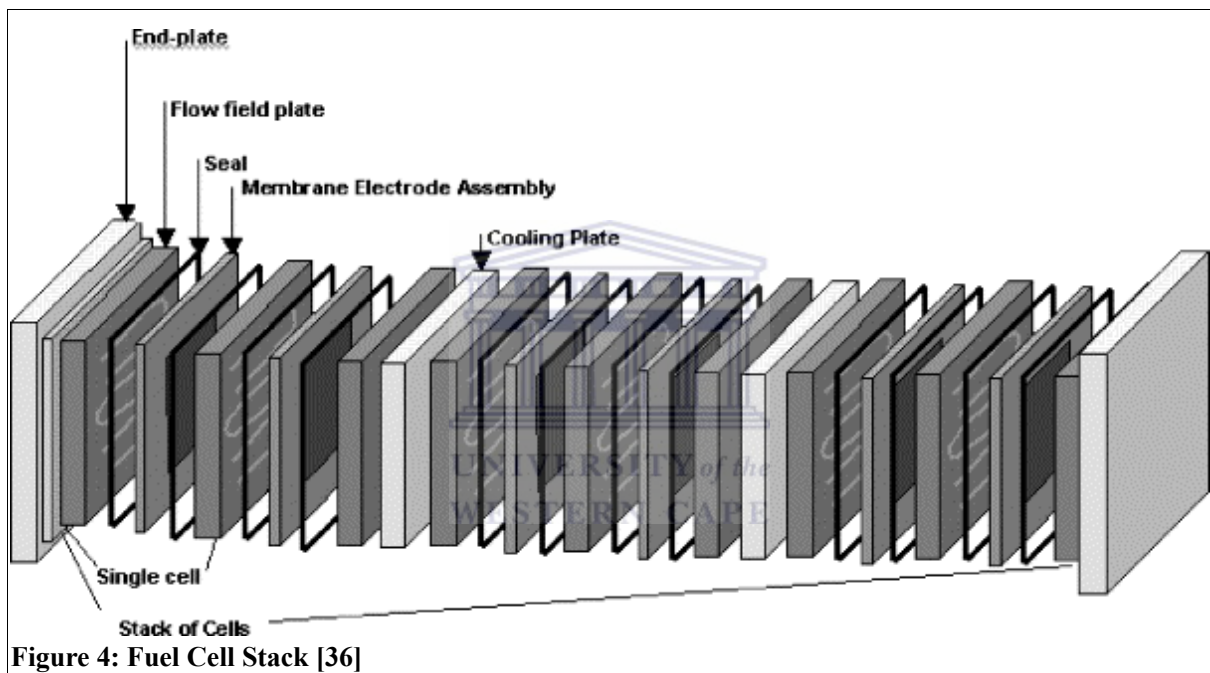

Figure 4: Fuel Cell Stack [36]

The performance of a fuel cell is dependent on two types of parameters, physical and operating. The physical parameters embarks on the actual characteristics of a particular fuel cell including membrane ion conductivity, catalyst distribution and its reaction rate in the catalyst layer, the rate of gas diffusion and the rate of water removal in the GDL [67]. The operating parameters are of the likes of fuel and air fluxes, temperatures, pressures, humidities, cell size and flow channel configuration [67].

As mentioned in the introduction, a hydrogen fuel cell operates as follows, the hydrogen flows with respect to its channels, meets the electrode layer where it diffuses in the gas diffusion layer. At the anode end the hydrogen is separated into protons and electrons. The electrons travel to the carbon cloth, flow field plate, to the contact, and then to the load. The protons travel through the polymer exchange membrane to the cathode. At the cathode catalyst layer, oxygen combines with the protons to form water and absorbing the electron [21]. The fuel cell operation is illustrated in Figure 5.

To follow is the exploration of the composition of each layer of the fuel cell.
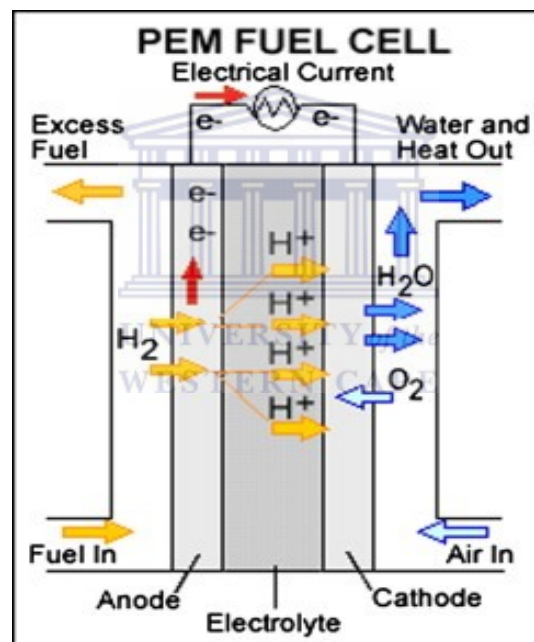
Figure 5: Schematic of PEM fuel cell operation [65]

3.2 Bipolar plates/ Gas Flow Channels

A fuel cell stack consists of numerous cells and separating the cells from one another is what is called the bipolar or flow plates [7]. The bipolar plates separate reactant gases and serve to connect the cells electrically and as a support structure. The flow plates are created in such a manner that on either side, channels exist which direct fluid flow, forming the anode and

cathode compartments of the unit cell. The geometry of these channels affects reactant flow velocities and mass transfer which further ultimately affects the fuel cell performance. The choice of material for a flow plate is based on its chemical compatibility, resistance to corrosion, cost effectiveness, density, electronic conductivity, ease of manufacturing, the stack volume/kW, material strength and thermal conductivity and the gas diffusivity/impermeability [60].

In Jeon et al [37] its concluded that for a fuel cell and in particular for a PEMFC, an ideal flow plate would be able to distribute the uniform gas mole fractions evenly over the entire surface area of the cell. When the gas mole fractions are evenly distributed over the cell it leads to the uniform distribution of current density, temperature and in the case of low temperature PEMFCs, liquid water production. The uniform distribution of the before mentioned parameters, reduce the mechanical stress experienced by the membrane electrode assembly (MEA), which in turn influences the lifetime of the fuel cell positively [37].

When the distribution of reactant along a channel is not uniform and reactants are consumed, the concentration of reactants near the catalyst layer decreases, while the concentration of reaction products increases. Consequently reactants with low concentration near the end of the flow field move slowly to the catalyst surface, which in turn reduces the performance of fuel cells operating at high current density [71]. A factor to take under consideration is that the concentration of products near the catalyst surface can quickly reach saturation. According to Zhang et al [72], the mixing of fluids in channels and increasing reactant concentrations near the catalyst layers is helpful to improve the performance of high temperature fuel cells.
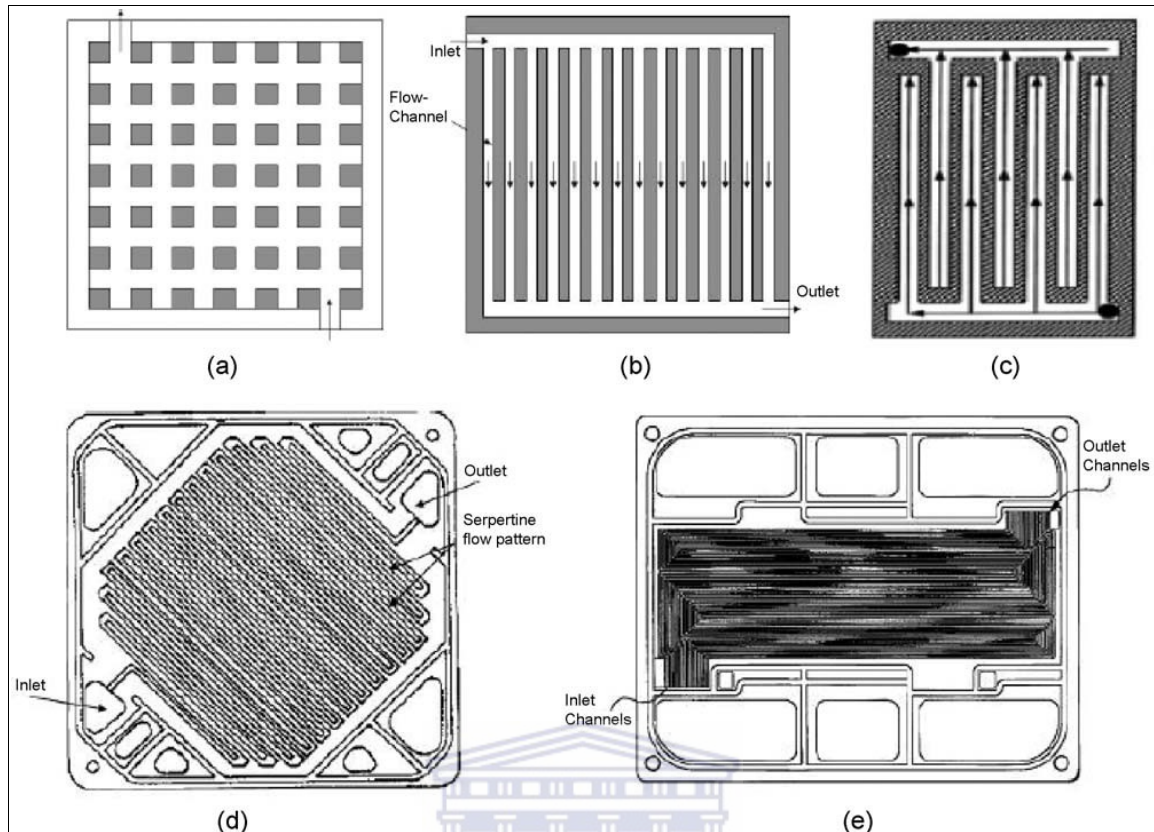
Figure 6: Schematics of flow field designs [71]

As illustrated in Figure 6 designs for flow channels vary and some of the most commonly used on are straight, serpentine (d) and (e), parallel (b), interdigitated (c), or pin-type (a) flow fields [72].

In the current study a selection of channels from the serpentine design is investigated. In previous studies it has been found that in cells with interdigitated and serpentine flow fields a forced convection stream is created which improves reactant transport and liquid water removal [65]. In studies similar to that of Wang et al [65], the performances of cells with interdigitated and serpentine flow designs have been found to be superior to that of parallel flows.

When working with HTPEMFC the designs are simplified in comparison to that of LTPEMFC as there is little or no liquid water present in the fuel cell above 100°C and therefore flow fields may be designed without having to consider two-phase flow [72]. Increasing the width of the channels allow for an increase in the contact of the fuel to the

catalyst layer, the implication hereof is that the pressure drop is less and would allow for a more efficient water removal. However, if the channels are too wide, there will not be enough support for the MEA layer [60].

The advantage of the serpentine flow field is that it is able to force the reactant flow to move and cover the entire active area of electrode. However, this design results in a relatively long reactant flow path, which results in a substantial pressure drop and creates a large concentration gradient from the gas inlet to outlet. In the case of low temperature fuel cells one needs to take into account the increase in the complexity of water removal on the cathode side [60].

In low temperature design one requires a high internal pressure drop to exist to improve the liquid water removal. In high temperature fuel cells however, water is found in vapor form and therefore flow field designs should be focused on decreasing the pressure drop and improving mass transfer by increasing the reactant concentration near MEAs [72].
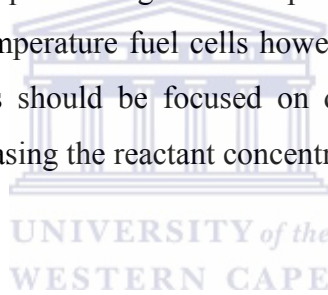
A flow plate with multiple, continuous flow channels, as illustrated in Figure 6 (e), can be used to limit the pressure drop, and reduce the amount of power used for pressurizing the air through a single serpentine channel. Over and above the before mentioned, a design of a flow plate should ensure that it is able to endure tolerances, warping, and the skinning effect. The skinning effect is the accumulation of polymer at the surface of the plate as a result of the molding process [7]. When a multiple serpentine design is implemented the stagnant area formation is alleviated and there is a reduction in the reactant pressure drop, however, according to Zhang et al [72], the reactant pressure drop through each of the serpentine remains relatively high due to the relatively long path of each channel. The implication hereof is that the reactant concentration changes significantly from the flow inlet region to the exit region [72].

When investigating the electrical conductivity of the fuel cell stack one considers the resistance from interfacial contacts between the flow plate and the gas diffusion layer. Testing the losses due to interfacial contact resistance is determined, according to Spiegel [60], by putting a bipolar plate between two gas diffusion layers, and then passing an electrical current through the sandwich and measuring voltage drop. The finding hereof is that the total voltage drop is a strong function of clamping pressure and the bulk resistance for both the bipolar plate and the gas diffusion media is a strong function of the clamping force. The interfacial contact resistance however does not only depend on the clamping pressure, but also on the surface characteristics of the bipolar plate and gas diffusion layer (GDL). From Spiegel, [60], the relationship between the contact resistance and the clamping pressure between the GDL and a bipolar plate is as follows:

$$r_c = \frac{A_a \tilde{K} (\tilde{g})^{(\tilde{d})-1}}{\kappa_{elec}^{eff} L^d} \left[\frac{\tilde{d}}{2 - \tilde{d} P^{'*'}} \right]^{\tilde{d}/2} \tag{3.1}$$

r_c is the contact resistance, A_a is the apparent contact area at the interface, $\tilde{K}$ is the geometric constant, $\tilde{g}$ is the topothesy of a surface profile, $\tilde{d}$ is the fractal dimension of a surface profile, L and is the scan length, $P^{'*}$ is the dimensionless clamping pressure constant which is a ratio of actual clamping pressure and comprehensive modulus of gas diffusion layer and κ_{elec}^{eff} is the effective electrical conductivity of two surfaces [60]. Topothesy is formally defined as the distance along the profile for which the expected angle between two points is one radian [48]. The effective electrical conductivity of two surfaces is as follows:

$$\frac{1}{\kappa_{elec}^{eff}} = \frac{1}{2} \left(\frac{1}{\kappa_1} + \frac{1}{\kappa_2} \right) \tag{3.2}$$

where κ_1 and κ_2 refer to the conductivities of the two surfaces involved. Most flow channels are designed in such a manner that laminar flow in both anode and cathode gas

flows are maintained. As discussed in previous sections, laminar flow conforms to a low Reynolds number, which is defined for a flow channel as:

$$R_e = \frac{Inertial\ force}{Viscosity} = \frac{\rho\, \bar{u}_m d_{rect}}{\mu} \qquad (3.3)$$

where ρ is the density, d_{rect} is the hydraulic diameter of the rectangular channel, μ the viscosity of the gas in the flow channel and $\bar{u}_m$ is the mass averaged velocity in the channel. Where $\bar{u}_M$ is given as [42]:

$$\bar{u}_m = \frac{\dot{m}}{\rho\, A_c} \qquad (3.4)$$

where $\dot{m}$ is the mass flow rate in the channel and d_{rect} is defined as:

$$d_{rect} = \frac{4A_c}{P} \qquad (3.5)$$

where A_c is the cross-sectional area of channel with width a and length b. $\tilde{P}$ is defined as the wetted perimeter and given algebraically as:

$$\tilde{P} = 2(a+b) \qquad (3.6)$$

For laminar flow, Li et al [42] utilizes an accepted correlation for the hydrodynamic entrance length, which is given as:

$$\frac{L_e}{d} \approx 0.06\,\Re \qquad (3.7)$$

From Spiegel, [60] the channel length is given as:

$$L_{chan} = \frac{A_{cell}}{N_{ch}(w_c + w_L)} \qquad (3.8)$$

where A_{cell} is the cell active area, N_{ch} is the number of parallel channels, w_c is the channel width and w_L is the space between channels.

Further one notes that the flow in a channel is driven by a pressure difference between the inlet and outlet and the gas moves with a certain mean velocity. Spiegel [60] states that the pressure can be approximated using the equations for incompressible flow in pipes and is given as follows:

$$\Delta P = f \frac{L_{chan}}{d_{ch}} \rho \frac{(\bar{u})^2}{2} + \sum r_L \rho \frac{(\bar{u})^2}{2} \qquad (3.9)$$

where is the f friction factor, d_{ch} is the hydraulic diameter, ρ is the fluid density, $\bar{u}$ is the average velocity and r_L is the local resistance. The friction factor can be defined as [60]:

$$f = \frac{56}{R_e} \qquad (3.10)$$

The velocity at the fuel cell entrance is:

$$u = \frac{(\dot{m})_{stck}}{N_{cell} N_{ch} A_{ch}} \qquad (3.11)$$

where u is the velocity in the channel (m/s), $(\dot{m})_{stck}$ is the air flow rate at the stack entrance, (m^3/s), N_{cell} is the number of cells in the stack, N_{ch} is the number of parallel channels in each cell, A_{ch} and is the cross-sectional area of the channel, (m^2).

When determining the pressure drop however, for a porous flow field one utilizes Darcy's law which is given by the following:

$$\Delta P = \mu \frac{(\dot{m})_{cell}}{K\,A_c} L_{chan} \tag{3.12}$$

where μ is the viscosity of the fluid , $(\dot{m})_{cell}$ is defined as the geometric flow rate

through the cell and K the permeability [60].

3.3 Gas Diffusion Layers

The gas diffusion layer (GDL) is found between the flow field and catalyst layer, as illustrated in Figure 7. It allows species to diffuse through it in order to reach the catalyst layer. The GDL is generally found to be lower in thermal conductivity and therefore partially insulates the heat generating catalyst [56]. When studying the GDL one needs to incorporate the physics of a porous matrix, the analysis of its equilibrium with the electrolyte and the gas, the thermodynamics and kinetics of the transport process [20]. The porosity of the GDL effects how reactants diffuse to the catalyst layer. A GDL is commercially available and are generally found to be made of carbon paper, or carbon cloth and a thickness ranging from

$100 - 400\,\mu m$ [43] . The function of the carbon paper is that it serves as a structural

support for the electrocatalyst [43].

Figure 7: Composition of a PEM Fuel Cell [8]
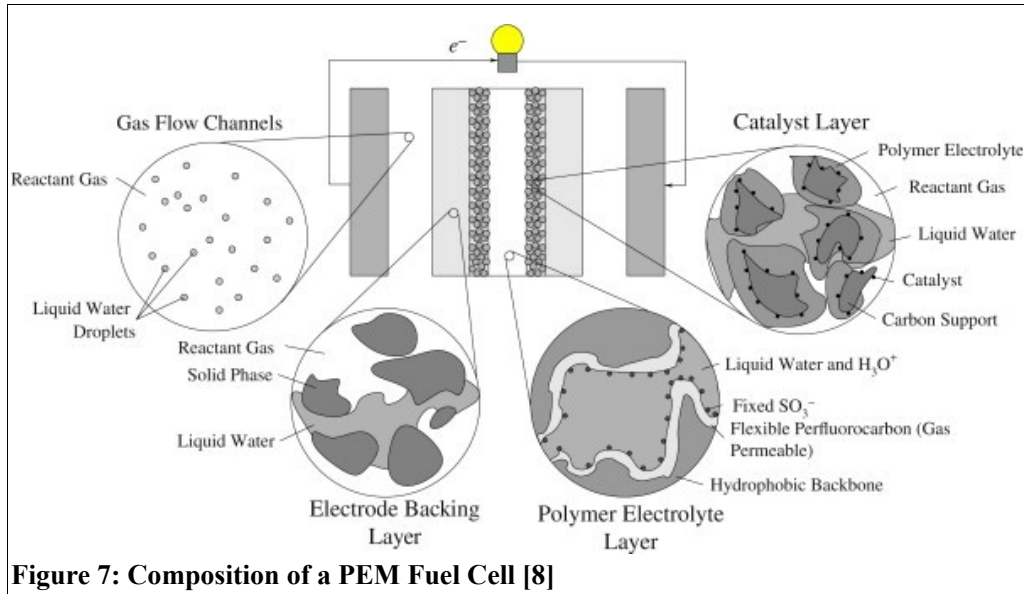
A GDL assists with the water management within the cell as it ensures that the membrane remains hydrated. The water formed should however not choke the pores of the paper or cloth. It is for this primary reason they are, during preparation stages coated with polytetrafluoroethylene (PTFE) commonly known as Teflon [20]. Teflon provides the GDL with a certain degree of hydrophobicity. The Gas diffusion layer serves as a electrical conductor between the carbon supported catalyst and the bipolar plates [9].

The conductivity of the GDL can be determined using Ohm's law [56]:

$$j_1 = -\kappa_0 \epsilon_1^{1.5} \nabla \Phi_1 \tag{3.13}$$

where j_1 is the electronic phase current density, κ_0 the electrical conductivity, $\epsilon_1^{1.5}$ the volume fraction of ionomer and Φ_1 the electronic phase potential. Further in Spiegel [56] there are four main modes of transportation within a porous media and are dependent on the molecule acceleration and environment, namely:

1. **The Free Molecule also known as the Knudsen Flow:** Where the mean free path of the molecule is considered to be very large compared to the pore diameter or the specie density is low. The collisions between molecules are considered negligible in comparison to that of molecules and walls.

60

2. **Viscous Flow:** Where the gas is considered to be a continuum and the collisions between molecules are considered to dominate over those between the molecules and walls.

3. **Ordinary Diffusion:** Movement is driven by the gradients found in temperature, concentrations or any other external forces. Collision between the molecules are considered to dominate.

4. **Surface Flow:** From Spiegel [56] this is defined to be when the molecules move along a solid surface in an adsorbed layer.

Between the Knudsen and ordinary diffusion the choice of model is dependent on the relation between the molecules mean-free-path and its pore radius. If the mean free path is less than 0.01 the pore radius ordinary diffusion dominates, 10 times greater than pore radius, Knudsen diffusion dominates [56].

For gas phase transport in the GDL the Stefan-Maxwell equations can used and is given as the following [56]:

$$\nabla x_k = \frac{\sum_{\bar{k} \neq k} x_k N_{\bar{k}} - x_{\bar{k}} N_k}{C_{Tot} D_{k,\bar{k}}^{eff}} \tag{3.14}$$

where C_{Tot} is the total concentration or the total molar density of all of the gas species,

x_k and $x_{\bar{k}}$ refer to the molar fractions, N_k and $N_{\bar{k}}$ the superficial flux density of

species k and $\bar{k}$ respectively. The interactions between gas species are denoted using a

Stefan-Maxwell binary interaction parameter, however to consider the interaction between the solid one incorporates Knudsen diffusion [66].

The Knudsen diffusion coefficient, D_k for flow in a cylindrical, long straight pores with diffusive scattering is determined as follows:

$$D_k = \left(\frac{2}{3} \tilde{r} \right) \sqrt{\frac{8RT}{\pi M_k}}$$

(3.15)

where $\tilde{r}$ is the radius, R the ideal gas constant, T temperature and M the molecular weight of the gas species k. When geometries other than cylindrical are used, the geometrical parameters can be incorporated into equation (3.15) [57].

The Knudsen and Stefan-Maxwell diffusion can be treated as mass-transport resistances in series yielding the following [56]:

$$\nabla x_k = \frac{-N_k}{C_{Tot} D_{K_k}^{eff}} + \frac{\sum_{\bar{k} \neq k} x_k N_{\bar{k}} - x_{\bar{k}} N_k}{C_{Tot} D_{k,\bar{k}}^{eff}}$$

(3.16)

where $D_{K_i}^{eff}$ is the effective Knudsen diffusion coefficient [62, 66].

3.4 Catalyst Layers

The catalyst layer found in PEMFCs' are situated on either side side of the membrane and are made of platinum, Pt or platinum alloys and carbon, see Figure 7. The noble metals, Pt and Pt- alloys are used as electrocatalysts. The platinum particles found within this layer are nanometer in size and is often supported on high surface area carbon substrate. The carbon supports provide a relatively large surface area for the electrocatalyst and provides good electronic conductivity [72].

The primary function of the catalyst is to be very effective in breaking molecules into protons and electrons and as a requirement to do so one has to have a large enough surface area. The

catalyst region is where the half-cell reactions occur [20]. The challenge in the choice in catalyst is to find one that is effective in breaking the hydrogen into protons and low in cost [58].

Electrochemical energy conversion relies on a high catalytic reactivity [20]. The structure and composition of the surface of the catalyst strongly influences its electrocatalytic reactivity. From Basu et al, [20] the relation between the reactivity and the structure is stated to be obscured by a variety of parameters such as the properties of the carbon support, the preconditioning of the catalyst and the structure of the interface between the electrolyte and the active area.

In the investigation done by Spiegel [58], it was concluded that experimental evidence supports that the electrocatalyst is supported on a carbon agglomerate and covered by a thin layer of membrane. For the catalysis of a reaction the catalytic particles has to be in contact with both protonic and electronic conductors . Pathway for reactants to reach the catalyst sites and for reaction products to leave needs to exist.
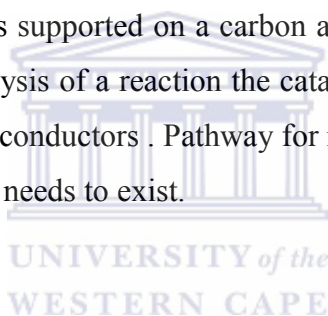
The point of contact or boundary between the reactants, catalyst and electrolyte is also known as the three-phase interface. It is further found that to be able to achieve reaction rates that are acceptable one requires that the active sites within the catalyst layer to be of several orders greater in magnitude than that of the geometric area of the electrode. It is for this reason that one finds the electrode to be made of a porous medium.

Spiegel [58] found that the fuel cell performance remained unchanged as the Pt/C ratio varied from 10%-40% with Pt loading of $0.4mg/cm^2$. Further to this it was concluded that when the ratio was increased beyond 40% the fuels performance actually decreased. From this the deduction that its not the increased Pt loading but Pt utilization that improved the performance of the fuel cell [58].

3.5 Proton Exchange Membrane

The proton exchange membrane is the layer that separates the anode and cathode compartments. High temperature fuel cell operate at temperatures greater than 120ºC and a the membrane most commonly used for this temperature range is a polybenzimidazole (PBI) membrane [15, 70]. The advantages of using PBI is that its light weight and is stable in the temperature range $(150 - 200ºC)$. In comparison to the Nafion membrane, used in most low temperature fuel cells, the PBI membrane is less dependent on water content, has a higher mechanical strength, lower in permeability to hydrogen and methanol resulting in less crossover of fuel at elevated temperatures [15].

The PBI membrane conducts protons through a solid matrix and its conductivity can be improved through doping [70]. In the PBI membrane the $H^{'+'}$ ions are transferred from one another via hydrogen bonds, also known as proton hopping [15]. In the Nafion membrane protons diffuse through the medium that is known as the solvable hydrogen ion species, H_3O^+ [15]. Therefore, the conductivity for the Nafion membrane is observed to be directly related to the rate of carrier diffusion [15].

Further in Cheddie et al [15] an extensive comparison is done between the two membranes. The disadvantage of the PBI based membrane is that its conductivity is significantly lower than the Nafion membrane. Although the proton conductivity of pure PBI is very low, literature by Tang et al [70] speak of remarkable increases in proton conductivity through methods of doping with phosphoric acid or sulfuric acid. Cheddie et al [15] reports the range for the conductivity of doped PBI to be $1-9\,Sm^{-1}$. A significant amount work would need to be done on the doped PBI membrane for it to even match the Nafion membrane where its conductivity is in the region of $17\,Sm^{-1}$ [15].

From Bouchet et al [10] PBI is considered to be made of linear chains whose monomer unit is displayed in Figure 8.
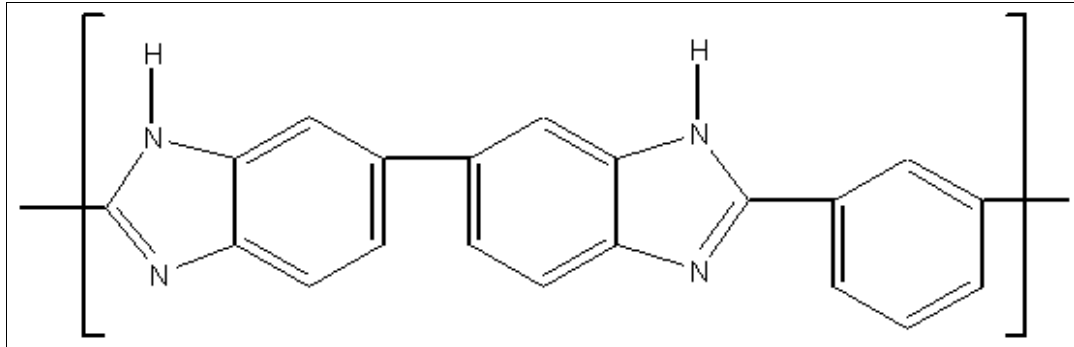

Figure 8: Polybenzimidazol (PBI) monomer unit [10]

Chapter 4: Computational Procedures

The physical aspects of fluid flow are governed by the fundamental principles discussed in chapter 1. These fundamental principles are for the most part governed by partial differential equations. Computational fluid dynamics aids in replacing the partial differential equations with values and advancing these values in space and or time [68]. In theory numerical solutions to problems can be indistinguishable from the exact solution. In many fields modelling has been found to cut costs and the manipulation of the scenario is advantageous.

To model any scenario, certain assumptions pertaining to it are made. When implementing a model one should note that any simulation is only as accurate as its assumptions allow it to be [70, 36]. For this particular investigation the assumptions made are as follows:

• The fuel cell is assumed to operate under steady state and under constant load conditions.

• The gas streams in the flow channel are at low velocities which implies the flows conforms to a low Reynolds number and therefore one can conclude that the flow is laminar.

• The gases utilised by the system are considered to behave as ideal [7, 46].

• From the FLUENT Fuel Cell and Electrolysis Model Theory [3] it is noted that the water activity is defined on the basis of the total water or super-saturated water vapor.

• Pure hydrogen is fed in at the anode and air is paralleled in the cathode gas channel [46].

• All water formed by the electrochemical reaction is assumed to be vaporous phase. This is due to the high operating temperature and therefore single phase flow is assumed [14, 46].

• Water transportation across the membrane is ignored because the water drag coefficient for high temperature membrane is low and therefore is assumed to be negligible and equated to zero [7, 46].

• Dilute solution theory is used to determine the species diffusion [31]

• The membrane is considered to be impermeable to gases. The crossover of reactant gases and product water is neglected [46].

To model the fuel cell thermally one considers the energy equation which serves as the transport equation for temperature [34, 64]. The energy of a system is such that the following principles hold [64];

Rate of change in Energy of a fluid particle	=	Net rate of heat added to a fluid particle	+	Net rate of work done on a fluid particle	+	Net rate of increase in energy due to sources
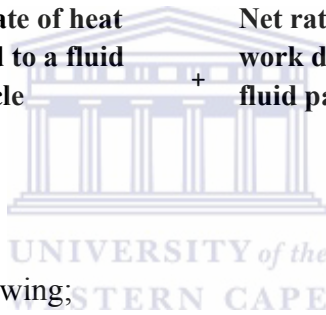
Algebraically denoted as the following;

$$\rho \frac{dE}{dt} = \nabla \cdot (k \nabla T) - \nabla \cdot (P \vec{u})$$
$$+ \left[\frac{\partial u \tau_{xx}}{\partial x} + \frac{\partial u \tau_{yx}}{\partial y} + \frac{\partial u \tau_{zx}}{\partial z} + \frac{\partial v \tau_{xy}}{\partial x} + \frac{\partial v \tau_{yy}}{\partial y} + \frac{\partial v \tau_{zy}}{\partial z} + \frac{\partial w \tau_{xz}}{\partial x} + \frac{\partial w \tau_{yz}}{\partial y} + \frac{\partial w \tau_{zz}}{\partial z} \right]$$
$$+ S_E$$

(4.1)

Energy is denoted by E, density ρ and temperature T. The term $\frac{dE}{dt}$ is known as the

substantive derivative and defined as follows:

$$\frac{dE}{dt} = \frac{\partial E}{\partial t} + \frac{\partial E}{\partial x} \frac{\partial x}{\partial t} + \frac{\partial E}{\partial y} \frac{\partial y}{\partial t} + \frac{\partial E}{\partial z} \frac{\partial z}{\partial t} = \frac{\partial E}{\partial t} + u \cdot \nabla E$$

(4.2)

On the left hand side of one has $\nabla\cdot(k\nabla T)$ which denotes the net rate of heat added to the fluid particle. The work done on a fluid particle for x component alone is given as:

$$\left[\frac{\partial[u(-P+\tau_{xx})]}{\partial x}+\frac{\partial(u\tau_{yx})}{\partial y}+\frac{\partial(u\tau_{zx})}{\partial z}\right]\delta x\,\delta y\,\delta z \quad \text{where} \tag{4.3}$$

$$\vec{u}=(u,v,w) \tag{4.4}$$

which denotes the superficial velocity vector in the porous media and ρ , as mentioned in the sections preceding, the density of the gas mixture.

$$\rho=\frac{1}{\sum_k(Y_k/\rho_k)} \tag{4.5}$$

where Y_k is the mass fraction of species k and ρ_k the density thereof. ρ_k is determined by the ideal gas relation of:

$$\rho_k=\frac{PM_k}{RT} \tag{4.6}$$

where P is the gas pressure and M_k is the molecular weight and R is the universal gas constant [45].

For a Newtonian fluid the rates of deformation are proportional to the viscous stresses [26]. The stresses due to viscosity for compressible flows involves two constants of proportionality: the first relates stresses to linear deformations and the notation hereof is dynamic viscosity, μ and the second viscosity, λ, relates stresses to the volumetric deformation. The nine viscous stress components are as follows [64]:

$$\tau_{xx} = 2\mu\frac{\partial u}{\partial x} + \lambda\nabla \cdot u \tag{4.7}$$

$$\tau_{yy} = 2\mu\frac{\partial v}{\partial y} + \lambda\nabla \cdot u \tag{4.8}$$

$$\tau_{zz} = 2\mu\frac{\partial w}{\partial z} + \lambda\nabla \cdot u \tag{4.9}$$

$$\tau_{xy} = \tau_{yx} = \mu\left(\frac{\partial u}{\partial y} + \frac{\partial v}{\partial x}\right) \tag{4.10}$$

$$\tau_{xz} = \tau_{zx} = \mu\left(\frac{\partial u}{\partial z} + \frac{\partial w}{\partial x}\right) \tag{4.11}$$

$$\tau_{yz} = \tau_{zy} = \mu\left(\frac{\partial v}{\partial z} + \frac{\partial w}{\partial y}\right) \tag{4.12}$$

Energy in the above mentioned equation is the sum of the internal (thermal) energy E_i and

the kinetic energy $\frac{1}{2}(u^2 + v^2 + w^2)$, $E = E_i + \frac{1}{2}(u^2 + v^2 + w^2)$. $\tag{4.13}$

The part of the energy equation attributable to the kinetic energy can be determined by multiplying the above mentioned equation for kinetic energy by the momentum of the fluid particle. The momentum for a system, from Newton's second law states that the rate of change of momentum for a fluid particle is equal to the sum of the forces acting on the particle. From Versteeg et al [64] each momentum component, x, y and z direction is given algebraically and respectively as:

$$\rho\frac{du}{dt} = \frac{\partial\left(-P + \tau_{xx}\right)}{\partial x} + \frac{\partial\left(\tau_{yx}\right)}{\partial y} + \frac{\partial\left(\tau_{zx}\right)}{\partial z} + S_{M_x} \tag{4.14}$$

$$\rho \frac{dv}{dt} = \frac{\partial (\tau_{xy})}{\partial x} + \frac{\partial (-P\tau_{yy})}{\partial y} + \frac{\partial (\tau_{zy})}{\partial z} + S_{M_y} \qquad (4.15)$$

$$\rho \frac{dw}{dt} = \frac{\partial (\tau_{xz})}{\partial x} + \frac{\partial (\tau_{yz})}{\partial y} + \frac{\partial (-P+\tau_{zz})}{\partial z} + S_{M_z} \qquad (4.16)$$

where S_M is rate of increase in momentum due to sources with respect to a specific direction. Therefore for the conservation of kinetic energy one has the following equation [64]:

$$\rho \frac{d[\frac{1}{2}(u^2+v^2+w^2)]}{dt} = -\vec{u} \cdot \nabla P + u\left(\frac{\partial (\tau_{xx})}{\partial x} + \frac{\partial (\tau_{yx})}{\partial y} + \frac{\partial (\tau_{zx})}{\partial z}\right)$$
$$+ v\left(\frac{\partial (\tau_{xy})}{\partial x} + \frac{\partial (\tau_{yy})}{\partial y} + \frac{\partial (\tau_{zy})}{\partial z}\right) + w\left(\frac{\partial (\tau_{xz})}{\partial x} + \frac{\partial (\tau_{yz})}{\partial y} + \frac{\partial (\tau_{zz})}{\partial z}\right) + \vec{u} \cdot S_M \qquad (4.17)$$

Therefore the resultant equation for internal energy is given as [63]:

$$\rho \frac{dE_i}{dt} = -P \nabla \cdot \vec{u} + \nabla \cdot (k \nabla T) + (\tau_{xx} \frac{\partial u}{\partial x} + \tau_{xy} \frac{\partial u}{\partial y} + \tau_{zx} \frac{\partial u}{\partial z})$$
$$+ (\tau_{xy} \frac{\partial v}{\partial x} + \tau_{yy} \frac{\partial v}{\partial y} + \tau_{zy} \frac{\partial v}{\partial z}) + (\tau_{xz} \frac{\partial w}{\partial x} + \tau_{yz} \frac{\partial w}{\partial y} + \tau_{zz} \frac{\partial w}{\partial z}) + S_{E_i} \qquad (4.18)$$

where $S_{E_i} = S_E = \vec{u} \cdot S_M$ \qquad (4.19)

For compressible flows enthalpy is often incorporated and the specific enthalpy, h, and total enthalpy h_0 of a fluid is defined as [64]:

$$h = E_i + \frac{P}{\rho} \quad \text{and} \qquad (4.20)$$

$$h_0 = h + \frac{1}{2}(u^2+v^2+w^2) \quad \text{or} \qquad (4.21)$$

h_0 can be written as:

$$h_0 = \frac{P}{\rho} + E \quad .$$

(4.22)

A further deduction can be made to give the total enthalpy of a fluid to be [64]:

$$\frac{\partial \rho h_0}{\partial t} = -\nabla \cdot (\rho h_0 \vec{u}) + \nabla \cdot (k \nabla T) + \frac{\partial P}{\partial t} + \left(\frac{\partial (u\tau_{xx})}{\partial x} + \frac{\partial (u\tau_{yx})}{\partial y} + \frac{\partial (u\tau_{zx})}{\partial z} \right)$$
$$+ \left(\frac{\partial (v\tau_{xy})}{\partial x} + \frac{\partial (v\tau_{yy})}{\partial y} + \frac{\partial (v\tau_{zy})}{\partial z} \right) + \left(\frac{\partial (w\tau_{xz})}{\partial x} + \frac{\partial (w\tau_{yz})}{\partial y} + \frac{\partial (w\tau_{zz})}{\partial z} \right) + S_h \quad .$$

(4.23)

Reviewing the equations for momentum and through substitution one derives the Navier-Stokes equations.

$$\rho \frac{du}{dt} = -(\frac{\partial P}{\partial x}) + \frac{\partial}{\partial x}\left[2\mu \frac{\partial u}{\partial x} + \lambda \nabla \cdot u \right] + \frac{\partial}{\partial y}\left[\mu \left(\frac{\partial u}{\partial y} + \frac{\partial v}{\partial x} \right) \right]$$
$$+ \frac{\partial}{\partial z}\left[\mu \left(\frac{\partial u}{\partial z} + \frac{\partial w}{\partial y} \right) \right] + S_x$$

(4.24)

$$\rho \frac{dv}{dt} = -(\frac{\partial P}{\partial y}) + \frac{\partial}{\partial x}\left[\mu \left(\frac{\partial u}{\partial y} + \frac{\partial v}{\partial x} \right) \right] + \frac{\partial}{\partial y}\left[2\mu \frac{\partial v}{\partial y} + \lambda \nabla \cdot u \right]$$
$$+ \frac{\partial}{\partial z}\left[\mu \left(\frac{\partial v}{\partial z} + \frac{\partial w}{\partial y} \right) \right] + S_y$$

(4.25)

$$\rho \frac{dw}{dt} = -(\frac{\partial P}{\partial z}) + \frac{\partial}{\partial x}\left[\mu \left(\frac{\partial u}{\partial z} + \frac{\partial w}{\partial x} \right) \right] + \frac{\partial}{\partial y}\left[\mu \left(\frac{\partial v}{\partial z} + \frac{\partial w}{\partial y} \right) \right]$$
$$+ \frac{\partial}{\partial z}\left[2\mu \frac{\partial w}{\partial z} + \lambda \nabla \cdot u \right] + S_z$$

(4.26)

Looking at the x-component and by equation manipulation, one arrives at the following:

$$\rho \frac{du}{dt} = -(\frac{\partial P}{\partial x}) + \frac{\partial}{\partial x}\left(\mu \frac{\partial u}{\partial x}\right) + \frac{\partial}{\partial y}\left(\mu \frac{\partial u}{\partial y}\right) + \frac{\partial}{\partial z}\left(\mu \frac{\partial u}{\partial z}\right)$$
$$+ \left[\frac{\partial}{\partial x}\left(\mu \frac{\partial u}{\partial x}\right) + \frac{\partial}{\partial y}\left(\mu \frac{\partial v}{\partial x}\right) + \frac{\partial}{\partial z}\left(\mu \frac{\partial w}{\partial x}\right)\right] + \frac{\partial}{\partial x}(\lambda \nabla \cdot u) + S_x \qquad (4.27)$$

which leads to a very useful form of the Navier-Stokes equations fundamental to the development of the finite volume method [64].

$$\rho \frac{du}{dt} = -(\frac{\partial P}{\partial x}) + \nabla \cdot (\mu \nabla u) + S_{M_x} \qquad (4.28)$$

For the purpose of this study, the stress tensor τ can be ignored due to the low velocity of laminar flow [46]. To summarise the above in terms of a general variable ϕ, which gives the conservative form of all fluid flow equations, including scalar quantities such as temperature one has [64]:

$$\overbrace{\frac{\partial(\rho \phi)}{\partial t}}^{Rate\, of\, increase\, of\, \phi\, of\, fluid\, element} + \overbrace{\nabla \cdot (\rho \phi u)}^{Net\, rate\, of\, flow\, of\, \phi\, out\, of\, fluid\, element} = \overbrace{\nabla \cdot (D_k \nabla \phi)}^{Rate\, of\, increase\, of\, \phi\, due\, diffusion}$$
$$\underbrace{+ S_\phi}_{Rate\, of\, increase\, of\, \phi\, due\, sources}$$
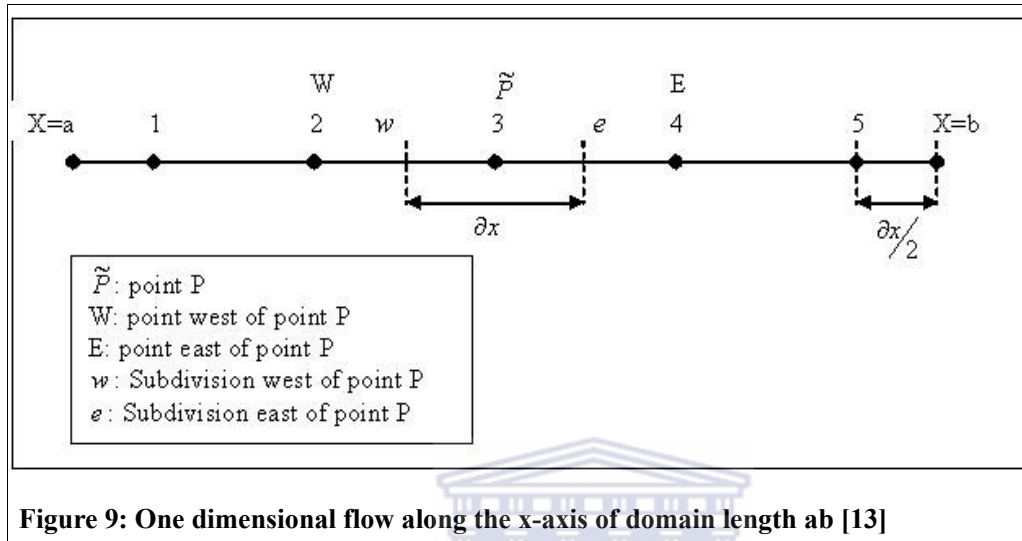
$$(4.29)$$

where D_k is the diffusion coefficient. As per the assumption that one first looks at the behaviour when the system operates under steady state conditions, it implies:

$$\frac{\partial \phi}{\partial t} = 0 \qquad . \qquad (4.30)$$

In order to gain an understanding of the problem one could, as is to follow, consider the one dimensional scenario where the velocity field is known. As illustrated in Figure 9, the first step in the implementation of the finite volume method is to divide the domain under

72

investigation into discrete control volumes. The second step is the discretisation of the above continuous equations, which leads to the following [64]:

$$\frac{d}{dx}D_k\frac{d\phi}{dx}=\frac{d}{dx}(\rho\phi u)+S_\phi \qquad (4.31)$$

Figure 9: One dimensional flow along the x-axis of domain length ab [13]

Looking at the particular example, a one dimensional length ab subdivided as per Figure 9, one has the formal integration over a control volume as:

$$\int_{\Delta V}\left(\frac{d}{dx}\right)\left(D_k\frac{d\phi}{dx}\right)dV=\int_{\Delta V}\left(\frac{d}{dx}\right)(\rho\phi u)dV+\int_{\Delta V}S_\phi dV \qquad (4.32)$$

The method of discretisation is deduced from the Taylor series which gives:

$$\phi(x+\Delta x)=\phi(x)+\left(\frac{\partial\phi}{\partial x}\right)_{\Delta x}\Delta x+\left(\frac{\partial^2\phi}{\partial x^2}\right)_{\Delta x}\frac{\Delta x^2}{2}+... \qquad (4.33)$$

which gives the change of ϕ in the x direction. Following this form, one has the value of ϕ at the point east , E of point $\tilde{P}$ to be the following:

$$\phi_E = \phi_{\tilde{P}} + \left(\frac{\partial \phi}{\partial x}\right)_{\tilde{P}} \Delta x + \left(\frac{\partial^2 \phi}{\partial x^2}\right)_{\tilde{P}} \frac{\Delta x^2}{2} + \dots \tag{4.34}$$

For the point west W of point $\tilde{P}$ one utilises the following Taylor series:

$$\phi(x - \Delta x) = \phi(x) - \left(\frac{\partial \phi}{\partial x}\right)_{\Delta x} \Delta x + \left(\frac{\partial^2 \phi}{\partial x^2}\right)_{\Delta x} \frac{\Delta x^2}{2} - \dots \quad \text{which gives} \tag{4.35}$$

$$\phi_W = \phi_{\tilde{P}} - \left(\frac{\partial \phi}{\partial x}\right)_{\tilde{P}} \Delta x + \left(\frac{\partial^2 \phi}{\partial x^2}\right)_{\tilde{P}} \frac{\Delta x^2}{2} - \dots \tag{4.36}$$

therefore one has for the above equation

$$\left(\frac{\partial \phi}{\partial x}\right)_{\tilde{P}} = \frac{\phi_E + \phi_{\tilde{P}}}{\Delta x} + O(\Delta x) \quad \text{and} \tag{4.37}$$

$$\left(\frac{\partial \phi}{\partial x}\right)_{\tilde{P}} = \left(\frac{\phi_{\tilde{P}} - \phi_W}{\Delta x}\right) + O(\Delta x) \tag{4.38}$$

where $O(\Delta x)$ stands for the truncated terms which in general for a finite difference scheme contains factors of Δx^n. Where the power n determines the rate at which the error tends to zero [64].

Therefore both of these equations are first order accurate. Subtracting the equations from each other allows one to evaluate the gradient at the mid-point $\tilde{P}$ which is second order accurate . This method is known as the central difference scheme and for point $\tilde{P}$ this is given as:

$$\left(\frac{\partial \phi}{\partial x}\right)_{\tilde{P}} = \left(\frac{\phi_E - \phi_W}{2\Delta x}\right) + O\left(\Delta x^2\right) \quad . \tag{4.39}$$

Applying this principle to the integrals above one arrives at the following:

$$\left(D_K A \frac{d\phi}{dx}\right)_e - \left(D_K A \frac{d\phi}{dx}\right)_w = \left(\rho A \phi u\right)_e - \left(\rho A \phi u\right)_w + \bar{S} \quad . \tag{4.40}$$

Flow should satisfy the continuity equation which states that with no external sources:

$$\frac{d\left(\rho u\right)}{dx} = 0 \tag{4.41}$$

which when discretised is:

$$\left(\rho A u\right)_e - \left(\rho A u\right)_w = 0 \tag{4.42}$$

From equation (4.39) one has the following:

$$\left(D_K A \frac{d\phi}{dx}\right)_e = D_{K_e} A_e \left(\frac{\phi_E - \phi_{\tilde{P}}}{2\left(\Delta x/2\right)}\right) \quad \text{and} \tag{4.43}$$

$$\left(D_K A \frac{d\phi}{dx}\right)_w = D_{K_w} A_w \left(\frac{\phi_{\tilde{P}} - \phi_W}{2\left(\Delta x/2\right)}\right) \tag{4.44}$$

For simplification we define two variables H and Γ, which represent the mass flux per unit area and diffusion conductance at cell faces.

$$H = \rho u \quad \text{and} \tag{4.45}$$

$$\Gamma = \frac{D_K}{\Delta x} \quad . \tag{4.46}$$

The area A is constant and therefore

$$A_e = A_w \quad .$$

(4.47)

Substituting these equations into equations (4.43) and (4.44) the results are as follows:

$$H_e \phi_e - H_w \phi_w = \Gamma_e (\phi_E - \phi_{\tilde{P}}) - \Gamma_w (\phi_{\tilde{P}} - \phi_W) + \bar{S} \quad .$$

(4.48)

From equation (4.42) one arrives at:

$$H_e - H_w = 0 \quad .$$

(4.49)

The central-differencing scheme uses linear interpolation for ϕ_e and ϕ_w such that

$$\phi_e = \frac{(\phi_{\tilde{P}} + \phi_E)}{2} \quad \text{and}$$

(4.50)

$$\phi_w = \frac{(\phi_W + \phi_{\tilde{P}})}{2} \quad \text{and therefore}$$

(4.51)

(4.52)

$$\frac{H_e}{2}(\phi_{\tilde{P}} + \phi_E) - \frac{H_w}{2}(\phi_W + \phi_{\tilde{P}}) = \Gamma_e (\phi_E - \phi_{\tilde{P}}) - \Gamma_w (\phi_{\tilde{P}} - \phi_W)$$

By rearranging the above where one solves for the variable ϕ at point $\tilde{P}$, $\phi_{\tilde{P}}$ as:

$$\left[\left(\Gamma_e + \frac{H_e}{2} \right) + \left(\Gamma_w - \frac{H_w}{2} \right) \right] \phi_{\tilde{P}} = \left(\Gamma_e - \frac{H_e}{2} \right) \phi_E + \left(\Gamma_w + \frac{H_w}{2} \right) \phi_W$$

(4.53)

If we let $a_E = \Gamma_e - \frac{H_e}{2}$ and

(4.54)

$$a_W = \Gamma_w + \frac{H_w}{2} \quad \text{one has:}$$

(4.55)

76

$$a_P \phi_P = a_E \phi_E + a_W \phi_W + \bar{S}, \quad \text{where} \tag{4.56}$$

$$a_P = a_E + a_W + H_e - H_w + S_P \tag{4.57}$$

and where S_P in this instance is equal to zero [64].

Another numerical scheme following a similar format is that of the upwind differencing. The point of difference however is that instead of the linear interpolation the central differencing scheme uses it makes the following conclusions:

- When fluid flow is in the positive direction $u_w > 0, u_e > 0$ which implies that H_w and H_e is greater than zero the scheme sets $\phi_w = \phi_W$ and $\phi_e = \phi_P$.

- When flow is in the negative direction i.e. $u_w < 0, u_e < 0$ which implies H_w H_e be less than zero the scheme sets $\phi_w = \phi_P$ and $\phi_e = \phi_E$ [6, 64].

To further illustrate the finite volume method the numerical method called the hybrid differencing scheme is illustrated below. Spalding introduced the scheme in 1972 and it is based on a combination of the two numerical methods namely the central differencing and the upwind differencing schemes mentioned above. As mentioned the central differencing scheme is accurate to the second order and is utilised by the hybrid differencing scheme for small Peclet numbers $(Pe < 2)$ it then in turn utilises the upwind differencing scheme for larger Peclet numbers. The Peclet number is a non-dimensional cell number which measures the relative strengths of convection and diffusion [64, 70]:

$$Pe = \frac{H}{\Gamma} = \frac{\rho u}{D_k / \Delta x} \tag{4.58}$$

The shorting coming of the central differencing scheme is its inability to determine flow direction, where in the event of the upwind differencing this is taken into account. The hybrid differencing scheme uses piecewise formulae based on the local Peclet number to evaluate the net flux through each control volume face. The Peclet number is evaluated at the face of the control volume [64]. Therefore in order to determine which numerical scheme to utilise, one has to firstly determine the Peclet number. Secondly, to make an informed decision on which numerical scheme to use one should take into account your assumptions and then thirdly, in order to produce physically realistic results a numerical scheme should have the following three fundamental properties [64]:

- Conservativeness – this is to ensure conservation of the property ϕ for the entire solution domain i.e. the flux of ϕ leaving a control volume across a certain face is equal to the flux of ϕ entering the adjacent control volume through the same face.

- Boundedness – Essentially this says that in the absence of sources the internal nodal values of property ϕ should be bounded by its boundary conditions.

- "Transportiveness" as defined in Versteeg [64] – illustrates the relationship between the magnitude of the Peclet number and the directionality of the flow.

The five most popular discretisation schemes are the Central Differencing, Upwind Differencing, Hybrid Differencing, Power Law and the QUICK scheme. The Central Differencing is not suitable for general purpose convection-diffusion problems as it lacks transportiveness and gives unrealistic solutions at large Peclet numbers [64]. Central-differencing schemes are known to produce unbounded solutions which can lead to stability problems for the numerical procedure [6, 68]. From Versteeg et al [64], the Upwind, Hybrid and Power law possess conservativeness, boundedness and transportiveness and are highly stable however suffer from false diffusion in multi-dimensional flows if the velocity vector is not parallel to one of the co-ordinates directions. Higher order schemes such as the QUICK
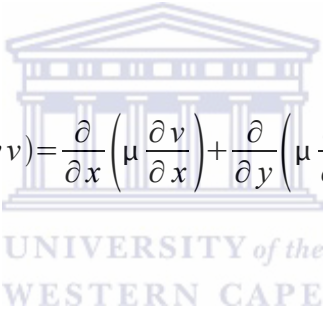
can minimise the false diffusion problem that occurs in the Upwind, Hybrid and Power law schemes; however it is less computationally stable [64].

To further our investigation one would have to incorporate the understanding of the convection of a scalar variable such as temperature, pollutant concentration etc. that depends on the magnitude and direction of the local velocity field. For this we revisit the momentum equations. For the three dimensional laminar steady flow we have [64]:

x-momentum equation:

$$\frac{\partial}{\partial x}(\rho u u) + \frac{\partial}{\partial y}(\rho v u) + \frac{\partial}{\partial z}(\rho w u) = \frac{\partial}{\partial x}\left(\mu \frac{\partial u}{\partial x}\right) + \frac{\partial}{\partial y}\left(\mu \frac{\partial u}{\partial y}\right) + \frac{\partial}{\partial z}\left(\mu \frac{\partial u}{\partial z}\right) - \frac{\partial p}{\partial x} + S_u$$

(4.59)

y-momentum equation:

$$\frac{\partial}{\partial x}(\rho u v) + \frac{\partial}{\partial y}(\rho v v) + \frac{\partial}{\partial z}(\rho w v) = \frac{\partial}{\partial x}\left(\mu \frac{\partial v}{\partial x}\right) + \frac{\partial}{\partial y}\left(\mu \frac{\partial v}{\partial y}\right) + \frac{\partial}{\partial z}\left(\mu \frac{\partial v}{\partial z}\right) - \frac{\partial p}{\partial y} + S_v$$

(4.60)

z-momentum equation:

$$\frac{\partial}{\partial x}(\rho u w) + \frac{\partial}{\partial y}(\rho v w) + \frac{\partial}{\partial z}(\rho w w) = \frac{\partial}{\partial x}\left(\mu \frac{\partial w}{\partial x}\right) + \frac{\partial}{\partial y}\left(\mu \frac{\partial w}{\partial y}\right) + \frac{\partial}{\partial z}\left(\mu \frac{\partial w}{\partial z}\right) - \frac{\partial p}{\partial z} + S_w$$

(4.61)

This can be rewritten and is illustrated in [46], where a factor ϵ is incorporated to consider the porosity of the electrodes and τ as previously mentioned is the viscous stress tensor [64, 46].

$$\frac{1}{\epsilon^2}\nabla \cdot (\rho \vec{u}\vec{u}) = -\nabla P + \nabla \cdot \tau + S_{\vec{u}}$$

(4.62)

The velocity field would then have to satisfy the continuity equation, which is given as follows:

$$\frac{\partial}{\partial x}(\rho u)+\frac{\partial}{\partial y}(\rho v)+\frac{\partial}{\partial w}(\rho z)=0 \quad .$$

(4.63)

For high temperature PEM fuel cells equation is stated as [45]:

$$\nabla\cdot(\rho \vec{u})=S_m$$

(4.64)

S_m takes into account the influence external sources .

As with the before-mentioned equations, the momentum equations contains non-linearities each of which are intricately coupled. The most complex matter at hand is solving the pressure gradient. For compressible flow, the continuity equation can be considered as transport equation for density and through the equation of state the pressure may be obtained [64]. The equation of state claims for a perfect gas that the following holds:

$$P=\rho R T \quad \text{and}$$

(4.65)

$$E_i=\tilde{C}_V T$$

(4.66)

For compressible fluids the equations of state provide the link between the energy equation and the mass and momentum conservations. The relation arises from the possibility of density variations as a result of pressure and temperature variations in the flow field [64].
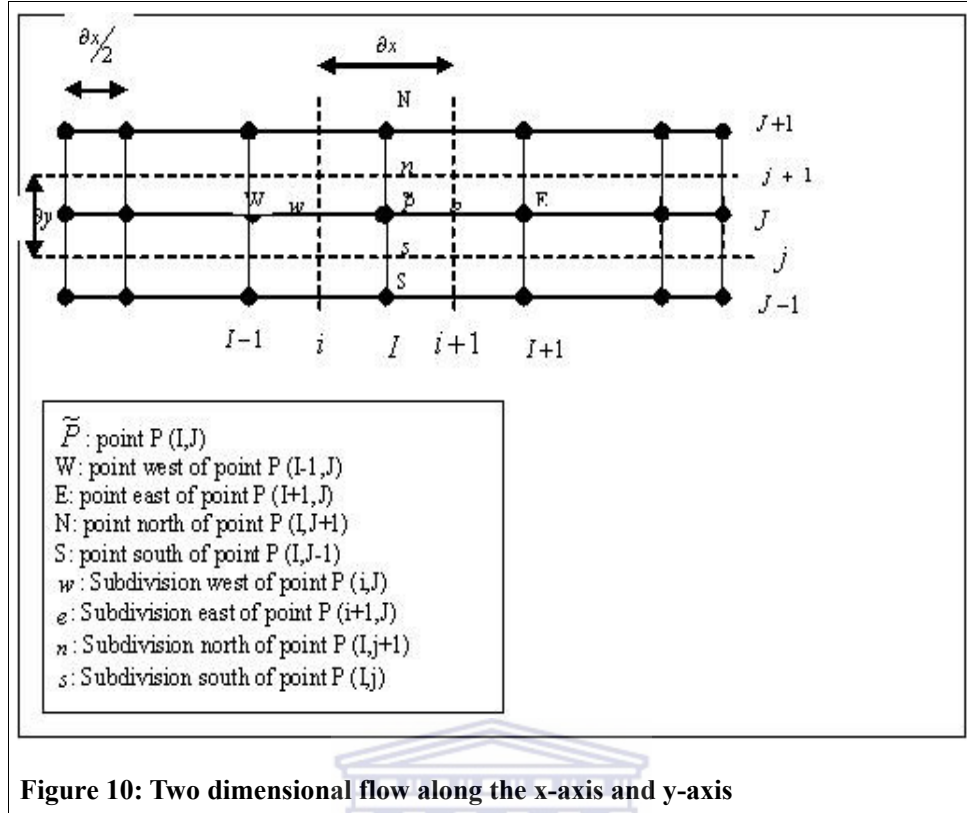
A method to solve problems associated with non-linearities and pressure- velocities linkages is through the application of a numerical method specifically catering for the pressure-velocity coupling. Two such methods are the SIMPLE, SIMPLER algorithms, which are iterative solution strategies.

SIMPLE is an acronym for Semi-Implicit Method for Pressure-Linked Equations and SIMPLER is the revised version thereof. These algorithms use the relationship between velocity and pressure corrections to enforce mass conservation and to obtain the pressure field [5]. Secondly, an approximate pressure field is used to derive the momentum equations. A pressure correction equation, deduced from the continuity equation is solved and then incorporated into amending the approximated velocity and pressure fields [64, 5].

As the algorithm iterates the initial approximated pressure and velocity field parameters are improved until convergence is obtained. By implementing a staggered grid [64], pressure and velocities are determined at different nodal points. In Figure 10 one notes that the velocity is determined at nodal points referred to as subdivisions w and e whereas pressure is determined at nodal points referred to in the diagram as W and E. This is primarily due to the fact that if velocities and pressures are both defined at the nodes of an ordinary control volumes a highly non-uniform pressure field can act as a uniform field in the discretised momentum equations [64]. The staggering of the velocity avoids the unrealistic behaviour of the discretised momentum equation for spatially oscillating pressures. Secondly, this arrangement determines velocities at exactly the locations where required for scalar transport – convection and diffusion – computations.

In the staggered grid arrangement the pressure gradient at point $\tilde{P}$ is given by the following [64]:

$$\frac{\partial P}{\partial x} = \frac{P_P - P_W}{\delta x_u} \tag{4.67}$$

Figure 10: Two dimensional flow along the x-axis and y-axis

It then follows that the discretised u-momentum equation is given as follows:

$$a_{i,J} u_{i,J} = \sum a_{nb} u_{nb} - \frac{P_{I,J} - P_{I-1,J}}{\delta x_u} \Delta V_u + \bar{S} \Delta V_u \qquad (4.68)$$

where ΔV_u is the volume of the cell and $\bar{S} \Delta V_u$ is the momentum source term. The pressure gradient is found by linear interpolation between the pressure nodes located at the boundaries of the cell u. $\sum a_{nb} u_{nb}$ is the notation used to specify the neighbouring cells, east of point $\tilde{P}$ is $(i+1,J)$, west of point $\tilde{P}$ is $(i-1,J)$, south by $(i,J-1)$ and north by $(i,J+1)$ [64]. The coefficients $a_{i,J}$ and a_{nb} can be calculated using any of the previously mentioned differencing schemes.

82

The values for the mass diffusive flux, H and diffusion conductance Γ can be obtained at each of the subdivision points north, n , south, s , east e or west, w as specified below [64]:

$$H_w = (\rho u)_w = \frac{H_{i,J} + H_{i-1,J}}{2} = \frac{1}{2}\left[\left(\frac{\rho_{I,J} + \rho_{I-1,J}}{2}\right)u_{i,J} + \left(\frac{\rho_{I-1,J} + \rho_{I-2,J}}{2}\right)u_{i-1,J}\right] \quad (4.69)$$
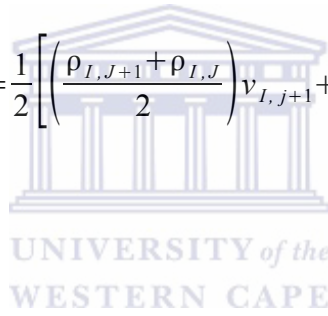
$$H_e = (\rho u)_e = \frac{H_{i+1,J} + H_{i,J}}{2} = \frac{1}{2}\left[\left(\frac{\rho_{I+1,J} + \rho_{I,J}}{2}\right)u_{i+1,J} + \left(\frac{\rho_{I,J} + \rho_{I-1,J}}{2}\right)u_{i,J}\right] \quad (4.70)$$

$$H_s = (\rho v)_s = \frac{H_{I,j} + H_{I-1,j}}{2} = \frac{1}{2}\left[\left(\frac{\rho_{I,J} + \rho_{I,J-1}}{2}\right)v_{I,j} + \left(\frac{\rho_{I-1,J} + \rho_{I-1,J-1}}{2}\right)v_{I-1,j}\right] \quad (4.71)$$

$$H_n = (\rho v)_n = \frac{H_{I,j+1} + H_{I-1,j+1}}{2} = \frac{1}{2}\left[\left(\frac{\rho_{I,J+1} + \rho_{I,J}}{2}\right)v_{I,j+1} + \left(\frac{\rho_{I-1,J+1} + \rho_{I-1,J}}{2}\right)v_{I-1,j+1}\right]$$

$$(4.72)$$

$$\Gamma_w = \frac{D_{k_{I-1,J}}}{x_i - x_{i-1}} \quad (4.73)$$

$$\Gamma_e = \frac{D_{k_{I,J}}}{x_{i+1} - x_i} \quad (4.74)$$

$$\Gamma_s = \frac{D_{k_{I-1,J}} + D_{k_{I,J}} + D_{k_{I-1,J-1}} + D_{k_{I,J-1}}}{4(y_J - y_{J-1})} \quad (4.75)$$

$$\Gamma_n = \frac{D_{k_{I-1,J+1}} + D_{k_{I,J+1}} + D_{k_{I-1,J}} + D_{k_{I,J}}}{4(y_{J+1} - y_J)} \quad (4.76)$$

To start the implementation of the SIMPLE algorithm a pressure field and velocity fields is approximated, $P^{'*'}, u_{nb}^{'*'}$ and $v_{nb}^{'*'}$. These values are incorporated into the following equation to solve $u_{i,J}^{'*'}$ and $v_{I,j}^{'*'}$ the velocity components [64, 5].

$$a_{i,J} u_{i,J}^{'*'} = \sum a_{nb} u_{nb}^{'*'} + \left(P_{I-1,J}^{'*'} - P_{I,J}^{'*'} \right) A_{i,J} + b_{i,J} \qquad (4.77)$$

where $b_{i,J} = \bar{S} \Delta V$ is the momentum source term and for $v_{I,j}^{'*'}$ $\qquad (4.78)$

$$a_{I,j} v_{I,j}^{'*'} = \sum a_{nb} v_{nb}^{'*'} + \left(P_{I,J-1}^{'*'} - P_{I,J}^{'*'} \right) A_{I,j} + b_{I,j} \qquad (4.79)$$

From Versteeg et al [64] one has that $A_{i,J}$ is the the respective face area of the control volume dependent on which combination i, j, I, J is specified. Further the pressure gradient can be determined through linear interpolation between the pressure nodes found at the control volume boundaries. The values found for $u_{i,J}^{'*'}$ and $v_{I,j}^{'*'}$ is then used to solve the following equation to determine the pressure correction, $\acute{P}$:

$$a_{I,J} (\acute{P})_{I,J} = a_{I-1,J} (\acute{P})_{I-1,J} + a_{I+1,J} (\acute{P})_{I+1,J} + a_{I,J-1} (\acute{P})_{I,J-1} + a_{I,J+1} (\acute{P})_{I,J+1} + (\acute{b})_{I,J}$$

$$(4.80)$$

The pressure correction is then used to determine the correct pressure and velocities [13, 72]:

$$P_{I,J} = P_{I,J}^{'*'} + (\acute{P})_{I,J} \qquad (4.81)$$

$$u_{i,J} = u_{i,J}^{'*'} + d_{i,J} \left((\acute{P})_{I-1,J} - (\acute{P})_{I,J} \right) \text{ and} \qquad (4.82)$$

$$v_{I,j} = v_{I,j}^{'*'} + d_{I,j} \left((\acute{P})_{I,J-1} - (\acute{P})_{I,J} \right) \qquad (4.83)$$

where $\quad d_{i,J} = \dfrac{A_{i,J}}{a_{i,J}}\quad$ and $\hspace{4cm}$ (4.84)

$$d_{I,j} = \frac{A_{I,j}}{a_{I,j}}$$ (4.85)

In determining the correct values for the pressure and velocities the respective $\quad \sum a_{nb} u_{nb}$ terms have been dropped which is the main approximation of the SIMPLE method [64]. These correct values and the initial guessed values for all other transported variables, ϕ is solved using the following equation:

$$a_{I,J}\phi_{I,J} = a_{I-1,J}\phi_{I-1,J} + a_{I+1,J}\phi_{I+1,J} + a_{I,J-1}\phi_{I,J-1} + a_{I,J+1}\phi_{I,J+1} + b\phi_{I,J}$$ (4.86)

The SIMPLE algorithm is an iterative process whereby the process continues until convergence is reached.
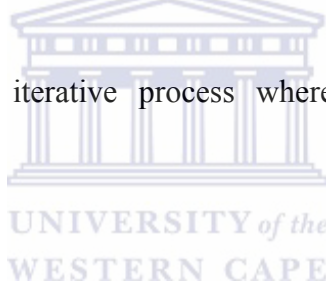
To model the fuel cell a commercial computational fluid dynamics (CFD) package called FLUENT is used. FLUENT is a parallel code which uses the above mentioned algorithms for the finite volume method and is iterative segregated implicit solver [46]. As an application, FLUENT already has a pre-existing PEM fuel cell package. In the PEM fuel cell model the transfer of current at the anode and cathode is by default the Tafel equation and as an option the Butler Volmer [3]. To ensure the model caters for the specific problem at hand, certain user defined functions (UDFs) needed to be changed. UDFs allow the user to customise the program to cater their problem specific [3]. The UDF functions are written in C code and found in an accompanying FLUENT file named pem_user.c [3, 25].

In order to model the PEM fuel cell thermally, as mentioned earlier in the chapter, the transport equation one evaluates is that of energy. As discussed prior to this chapter, the

conservation of energy for a high temperature PEM fuel according to Peng et al [46] and is given as:

$$\nabla \cdot (\vec{u}(\rho E + P)) = \nabla \cdot \left(\kappa^{eff} \nabla T - \sum h_k J_k + (\tau_{eff} \cdot \vec{u}) \right) + S_h \qquad (4.87)$$

where J_k is the flux of species k and defined by the following equation:

$$J_k = -\sum_{k=1} \rho D_k \nabla Y_k \qquad (4.88)$$

D_k is the diffusion coefficient and Y_k is the mass fraction of species k. τ_{eff} is the effective stress tensor, which from the assumption that the flow for the fuel cell is laminar can be ignored. κ^{eff} is defined as the thermal conductivity in a porous material consisting of the electrode solid matrix and gas. In FLUENT however, the gas diffusivity can be determined either by using what is known as the Dilute approximation or the Multicomponent method. With the dilute approximation method and the method undertaken we have:

$$D_k = \epsilon^{1.5}(1-s)^{r_s} D_k^0 \left(\frac{P_0}{P} \right)^{\gamma_p} \left(\frac{T}{T_0} \right)^{\gamma_t} \qquad (4.89)$$

where D_k^0 is the mass diffusivity of species k at reference temperature and pressure (P_0, T_0). s is defined as the volume fraction of liquid water or the water saturation. This, as part of the high temperature investigation is equated to zero. The values for the exponents (γ_p, γ_t) and the pore blockage exponent r_s is given as [3]:

$$P_0 = 101325 \, N/m^2$$
$$T_0 = 300K$$
$$\gamma_p = 1$$
$$\gamma_t = 1.5$$
$$r_s = 2.5$$

The full multicomponent diffusion method contains corrections that take into account the porous media tortuosity [4].

$$D_{eff}^{ij} = \epsilon^{1.5} D^{ij}$$

(4.90)

where D_{eff}^{ij} is the effective gas species diffusivity, ϵ is the porosity of the porous medium, and D^{ij} is the gas species mass diffusivity computed by the full multicomponent diffusion method and is given as:

$$D^{ij} = [D] = [A]^{-1} [B]$$

(4.91)

$$A_{ii} = -\left(\frac{X_i}{D_{i,N}} \frac{M_w}{M_{w,N}} + \frac{\sum_{j=1, j \neq i}^{N} X_j}{D_{ij}} \frac{M_w}{M_{w,i}} \right)$$

(4.92)

$$A_{ij} = X_i \left(\frac{1}{D_{ij}} \frac{M_w}{M_{w,j}} + \frac{1}{D_{i,N}} \frac{M_w}{M_{w,N}} \right)$$

(4.93)

$$B_{ii} = -\left(X_i \frac{M_w}{M_{w,N}} + (1 - X_i) \frac{M_w}{M_{w,i}} \right)$$

(4.94)

$$B_{ij} = X_i \left(\frac{M_w}{M_{w,j}} + \frac{M_w}{M_{w,N}} \right)$$

(4.95)

where $[A]$, $[B]$ and $[D]$ are $(N-1) \times (N-1)$ matrices, X is the mole fraction and M refers to the respective molecular weights [4].

The second, very significant change to the model that needs to be implemented is that of the ionic conductivity of the membrane. The membrane in the model by default is one that caters

for a low temperature PEM fuel cell which has a dependency on the water content. The equation hereof is given as:

$$\kappa_{mem} = \tilde{\beta} \left(0.514 \tilde{\zeta} - 0.326\right)^{\omega} e^{1268\left(\frac{1}{303} - \frac{1}{T}\right)} \tag{4.96}$$
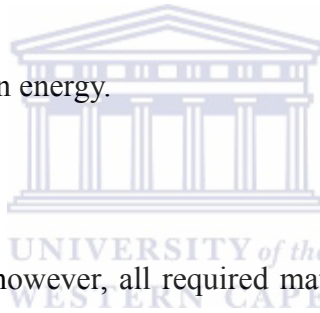
where $\tilde{\zeta}$ is the water content and $\tilde{\beta}$ and ω are model constants. For the following investigation the membrane conductivity equation modelled is [46]:

$$\kappa_{mem} = \kappa_0 \, e^{\left[\frac{-E_{A,\kappa}}{R}\left(\frac{1}{T} - \frac{1}{T_0}\right)\right]} \tag{4.97}$$

where from Peng et al [46],

$$\kappa_0 = 12.99 \, Sm^{-1} \quad \text{and} \tag{4.98}$$

$E_{A,\kappa}$ is defined as the activation energy.

At the time of the investigation however, all required material parameters were unavailable and therefore a decision was made to incorporate, unless specified in Peng et al, use the default material parameters available in FLUENT. This would also aid in doing somewhat of a comparative study. Therefore for the membrane conductivity the following equation is modelled:

$$\kappa_{mem} = \kappa_0 \, e^{\left[1268\left(\frac{1}{303} - \frac{1}{T}\right)\right]} \quad . \tag{4.99}$$

The water drag coefficient for high temperature membrane is low it is assumed to be negligible [3, 46]. The implication hereof is that one no longer needs to take into account the electro-osmotic water flux through the membrane [41].

The FLUENT module used in the computional section of this work caters for a low temperature fuel cell and therefore amendments to the module had to be incorporated. In order to do so, one implements these changes in a user defined function and for this particular application it is called pem_user_c. Here the osmotic drag coefficient for low temperature fuel cells is given as:

$$n_d = 2.5 \frac{\zeta}{22}$$
(4.100)

Where in place of equation (4.100) the below equation was implemented

$$n_d = 0 \quad .$$
(4.101)

The water content, ζ is defined is the FLUENT UDF as:

$$\zeta = 0.043 + 17.18a - 39.85a^2 + 36\,a^3\,(a<1)$$
(4.102)

$$\zeta = 14 + 1.4(a-1)(a>1)$$
(4.103)

where a is the water activity and is given as:

$$a = \frac{P_{WV}}{P_{sat}} + 2s$$
(4.104)

and as previously mentioned s is the volume fraction of liquid water or the water saturation

therefore a is reduced to:

$$a = \frac{P_{WV}}{P_{sat}}$$
(4.105)

P_{WV} is the water vapor pressure and is given as product of the vapor molar fraction,

x_{H_2O} and the local pressure, P [4].

89

$$P_{WV} = x_{H_2O} P .$$

(4.106)

P_{sat} the saturation pressure is found by the following equation:

$$\log_{10}(P_{sat}) = -2.1794 + 0.02953(T - 273.17) - 9.1837 \times 10^{-5}(T - 273.17)^2$$
$$+ 1.4454 \times 10^{-7}(T - 273.17)^3$$

(4.107)

Therefore the procedure to model the channel flow of a high temperature PEM fuel cell in FLUENT is [3]:

1. Creating and defining the geometry of the fuel cell channels in the package available from ANSYS.

2. Creating an appropriate mesh for the above mentioned geometry.

3. Importing the mesh file into FLUENT.

4. Defining fuel cell parameters, incorporating assumptions, setting up of the operating and boundary conditions and then to start calculations.

5. On successful completion, close all applications, incorporate the above mentioned changes into pem_user.c and rerun the calculations with the changes.

6. Process results.

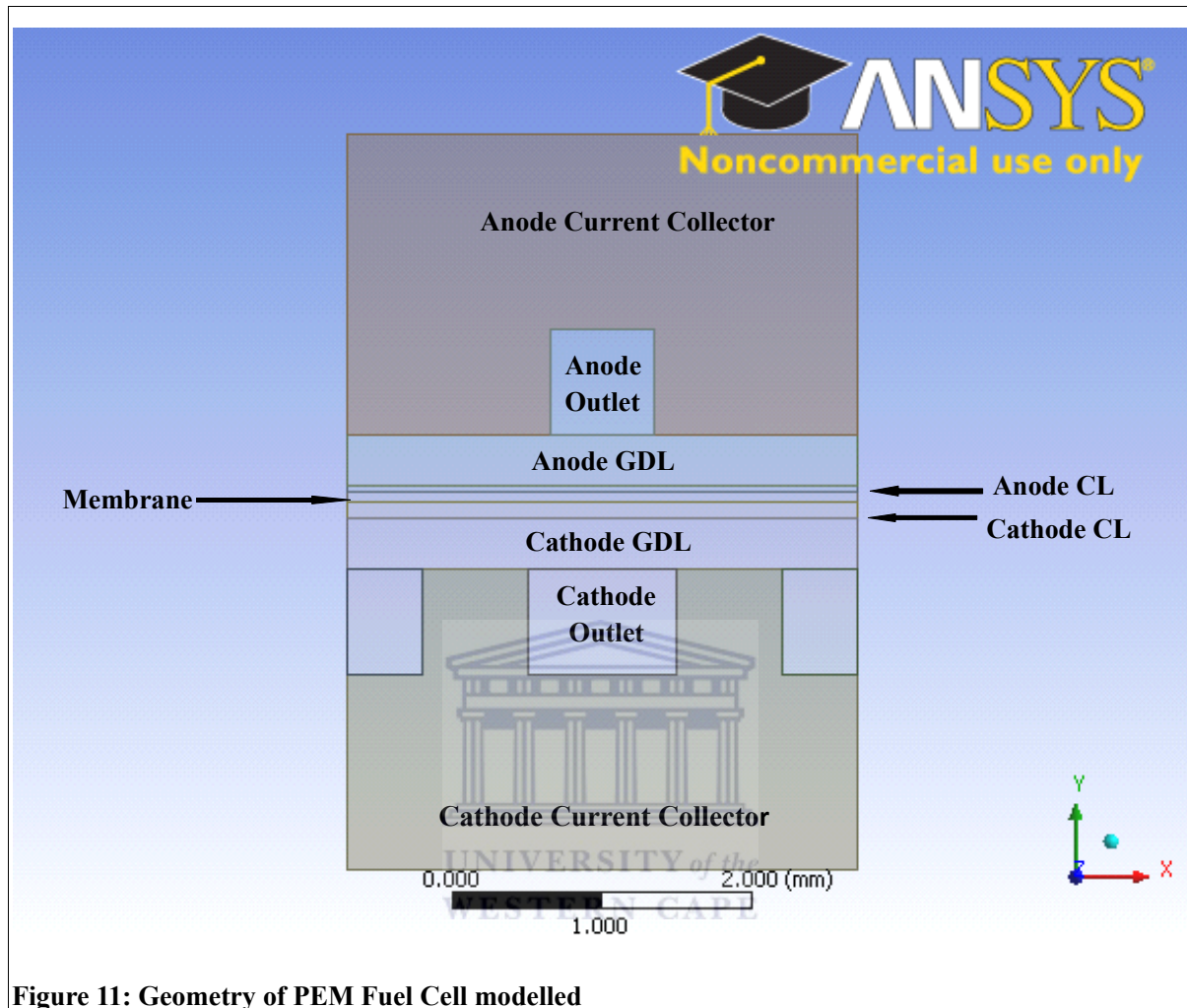# Chapter 5: Results and Discussion


Figure 11: Geometry of PEM Fuel Cell modelled

The first part of our investigation requires that the respective geometry be generated and be defined, which can be viewed in Figure 11.

The physical and geometric parameters is given in table 3.

Table 3: Geometrical Parameters [46]		
Parameters	Value	Unit
Cell Width	3.4	mm
Channel Length	235	mm
Channel Height	0.7	mm

Table 3: Geometrical Parameters [46]		
Anode Channel Width	0.7	mm
Cathode Channel Width	1	mm
Anode GDL Thickness	0.34	mm
Cathode GDL Thickness	0.34	mm
Anode Catalyst Thickness	0.04	mm
Cathode Catalyst Thickness	0.11	mm
Membrane Thickness	0.07	mm
Electrode Height	2	mm

The second step is creating the mesh/ grid on the geometry such that the can be calculated as specified in chapter 3. The mesh of the above geometry is given in Figure 12 and the quality of the mesh is given in table 4.
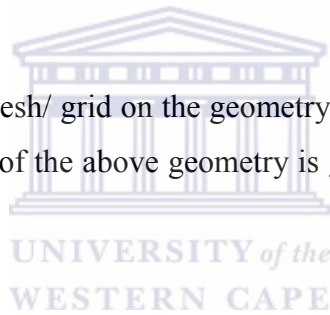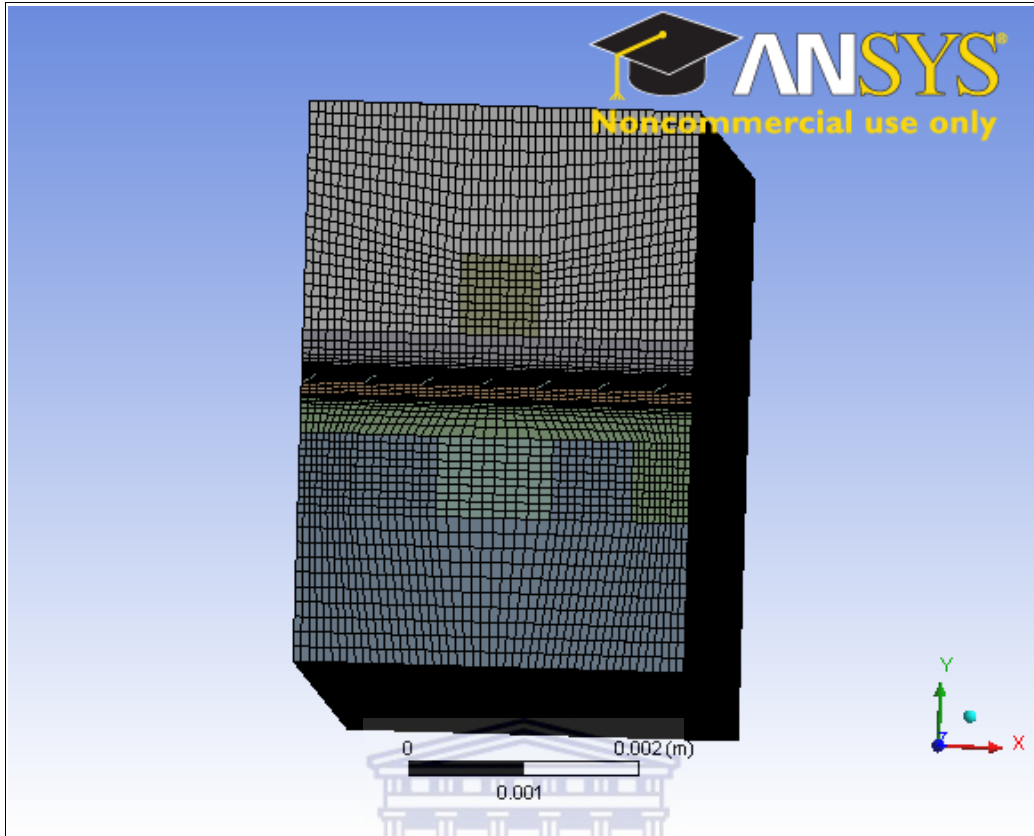
Figure 12: Mesh for PEM fuel cell channels Modelled

Table 4: Mesh Quality	
Number of Grid Points	227 103
Number of Elements	216 000
Maximum Cell Squish	0.82

By comparison to the number of mesh points as indicated in Peng et al [46] whose work is on the same geometrical parameters, 180 000 grid points was found to provide sufficient spatial resolution. Once the geometry and mesh has been created one exports it into FLUENT. On launching the FLUENT double precision and four processes was selected for processing options.

Within the Fuel Cell and Electrolysis Model, the model options selected was joule heating, reaction heating, electrochemistry sources and the Butler-Volmer rate. The joule heating option takes into account ohmic heating. In the study done by Peng et al [46] the ohmic heating is assumed to negligible in all areas other than the membrane. Motivation for this assumption is due to the high electric conductivity of these materials. Reaction heating takes into account heat generated from the electrochemical reactions. Including the electrochemistry sources ensures that the model takes into account the effects from the electrochemistry. For the calculation of the transfer currents the Butler-Volmer was selected.

In specifying the model parameters the values in table 5 was incorporated. The Open-Circuit Voltage is taken as 1.2V. The mass flow rates are values calculated using equations specified in the mass transfer section of chapter 1, where the current density incorporated in the calculations are those specified by Peng et al [46]. Values, unless referenced differently are taken as the parameter values available in FLUENT. As per Peng et al [46] the solutions are considered to have converged when the relative error in each field between two consecutive iterations was less than 1×10^{-6} .
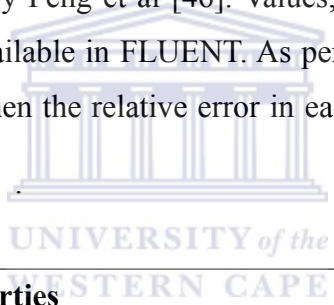
Table 5: Electrochemical properties		
	Anode	Cathode
Reference exchange current density Am^{-3}	1×10^8 [22]	170 [22]
Reference Concentration (kmol/m³)	1	1
Concentration Exponent	0.5	1
Exchange Coefficient	2	2
Porosity of GDL	0.8 [22]	0.8 [22]
Porosity of GCL	0.6 [22]	0.6 [22]

Table 5: Electrochemical properties		
GDL and GCL Hydraulic permeability	1.0×10^{-15}	1.0×10^{-15}

The value membrane ionic conductivity, κ_0 as mentioned in chapter 3 is $12.99\,S/m$. The material properties for the current investigation are taken to be default properties available in FLUENT and this is due to, as previously mentioned, that an entire set of parameter values was not available at the time of the investigation. The boundary conditions used in the investigation is given in table 6. The semi-colon separating values are with respect to the electric potentials, 0.4V, 0.6V and 0.8V.

Table 6: Boundary Conditions		
	Value	Unit
Anode Inlet		
Mass flow rate	3.21×10^{-7} ; 1.52×10^{-7} ; 2.35×10^{-8} using equation (1.107)	kg/s
Temperature	433 [46]	K
Direction specification method	Normal to Boundary	-
Mass fractions H_2;H_2O	1;0 [46]	-
Water Saturation	0 [3]	
Cathode Inlet		
Mass flow rate	1.39×10^{-5} ; 6.59×10^{-6} ; 1.02×10^{-6} using equation (1.109)	kg/s

Table 6: Boundary Conditions		
Temperature	433 [46]	K
Direction specification method	Normal to Boundary	-
Mass fractions O_2:H_2O	0.22;0 [46]	-
Water Saturation	0 [3]	
Anode and Cathode Outlets		
Pressure	1.1 [46]	atm
Temperature	433 [46]	K
Terminal Anode		
Temperature	433 [46]	K
Electric Potential	0 [46]	V
Terminal Cathode		
Temperature	433 [46]	K
Electric Potential (V_{cell})	0.4, 0.6,0.8 [46]	V

From the ANSYS PEM fuel cell tutorial for modelling a single channel [25], the recommendations for solution controls were kept. These include the multi-grid settings recommended, which are to change all parameters' multi-grid cycle to F-cycle with BCGSTAB, which stands for bi-conjugate gradient stabilized method, which is a stabilization method for the species and the two potential equations [3].

In Figure 13 the magnitude of average current density distribution in the membrane is displayed. Where the local current density I is determined by the following equation [46]:

$$I = -\kappa_{mem} \nabla \Phi_{mem}$$

(5.1)

where κ_{mem} and Φ_{mem} are as previously mentioned, the membranes' electrical conductivity and electronic phase potential respectively. The average current density, I_{avg} is the average of the local current density over the membrane and is determined as follows [46]:

$$I_{avg} = \frac{1}{A_{mem}} \int_{A_{mem}} I \cdot dA$$

(5.2)

where A_{mem} is the membrane area. In Figure 14 the molar concentration of oxygen in the cathode catalyst is displayed and in Figures 15 and 16 the local overpotential distribution at the anode catalyst, η_a and at the cathode catalyst, η_c respectively. For each of these scenarios $V_{cell} = 0.6V$.
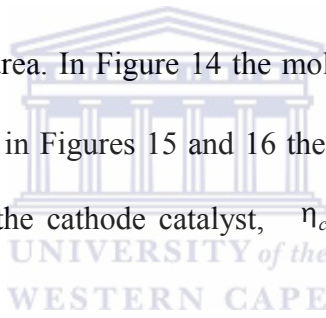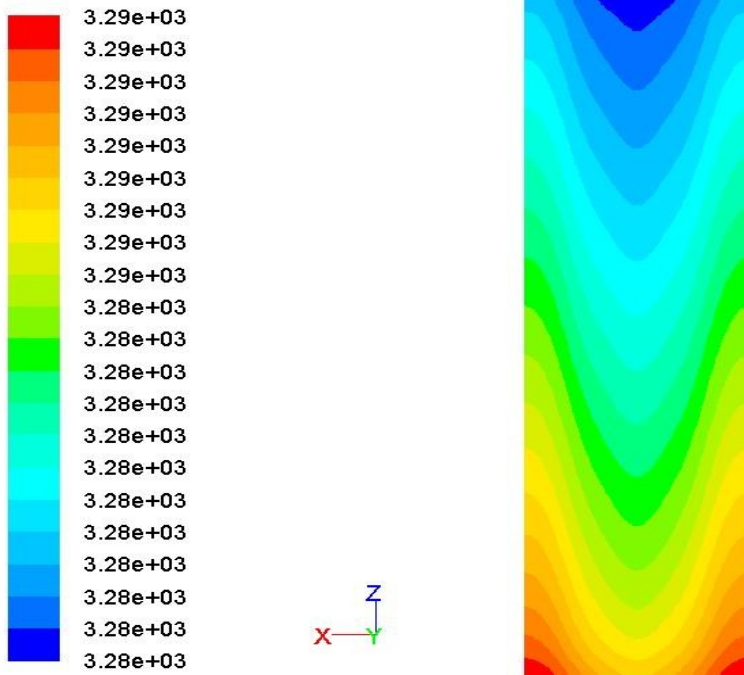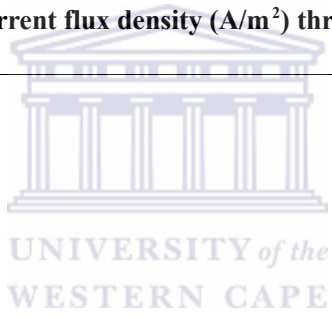
Figure 13: Magnitude of average current flux density (A/m^2) through Membrane y=1.185mm
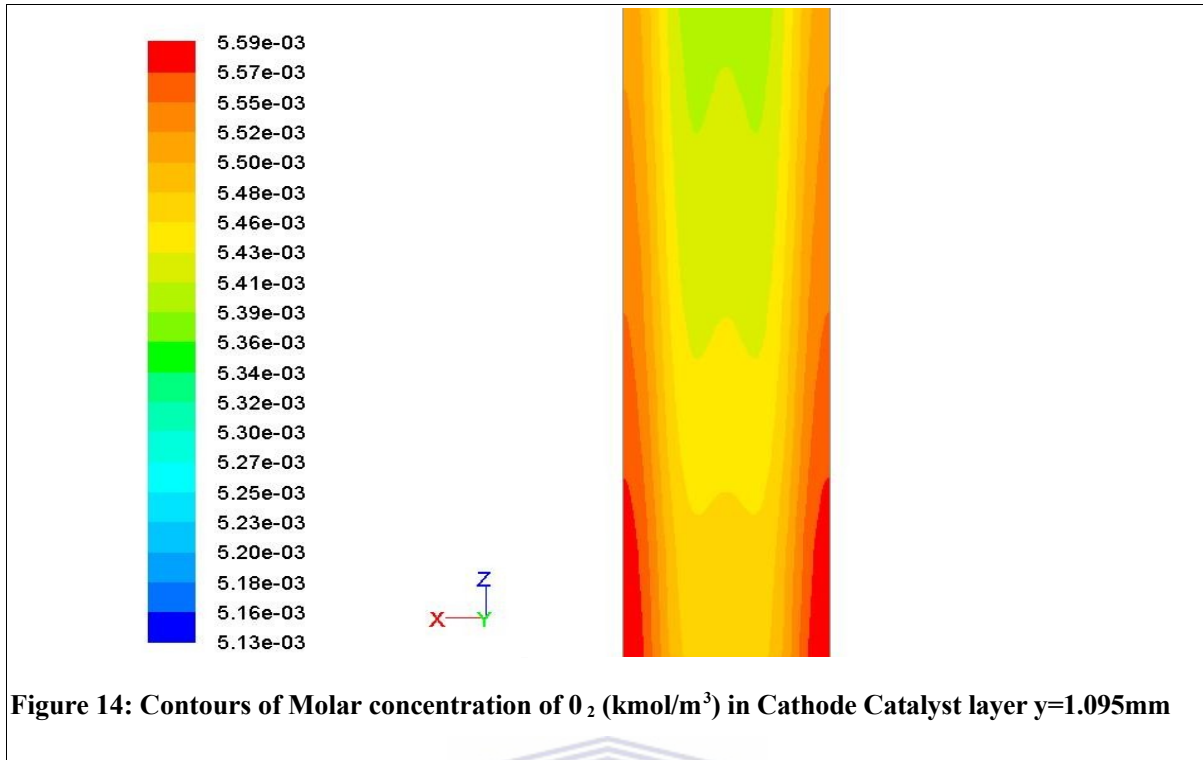
Figure 14: Contours of Molar concentration of 0 $_2$ (kmol/m³) in Cathode Catalyst layer y=1.095mm

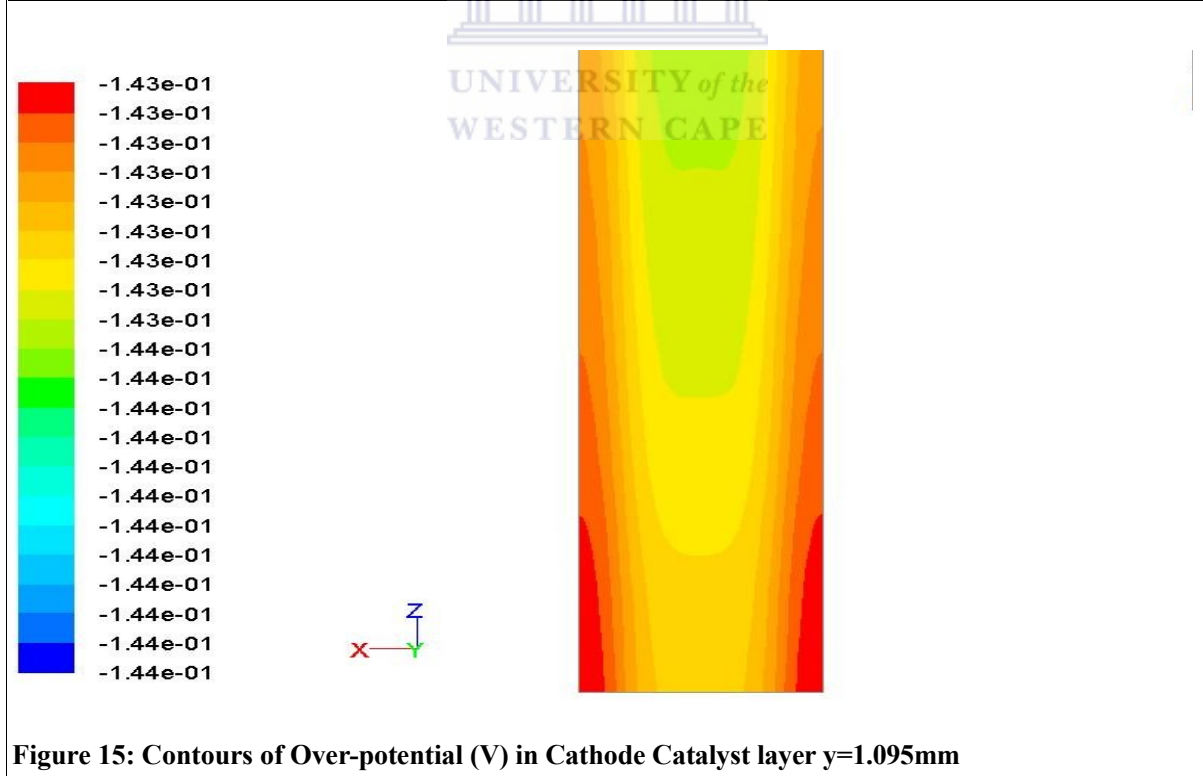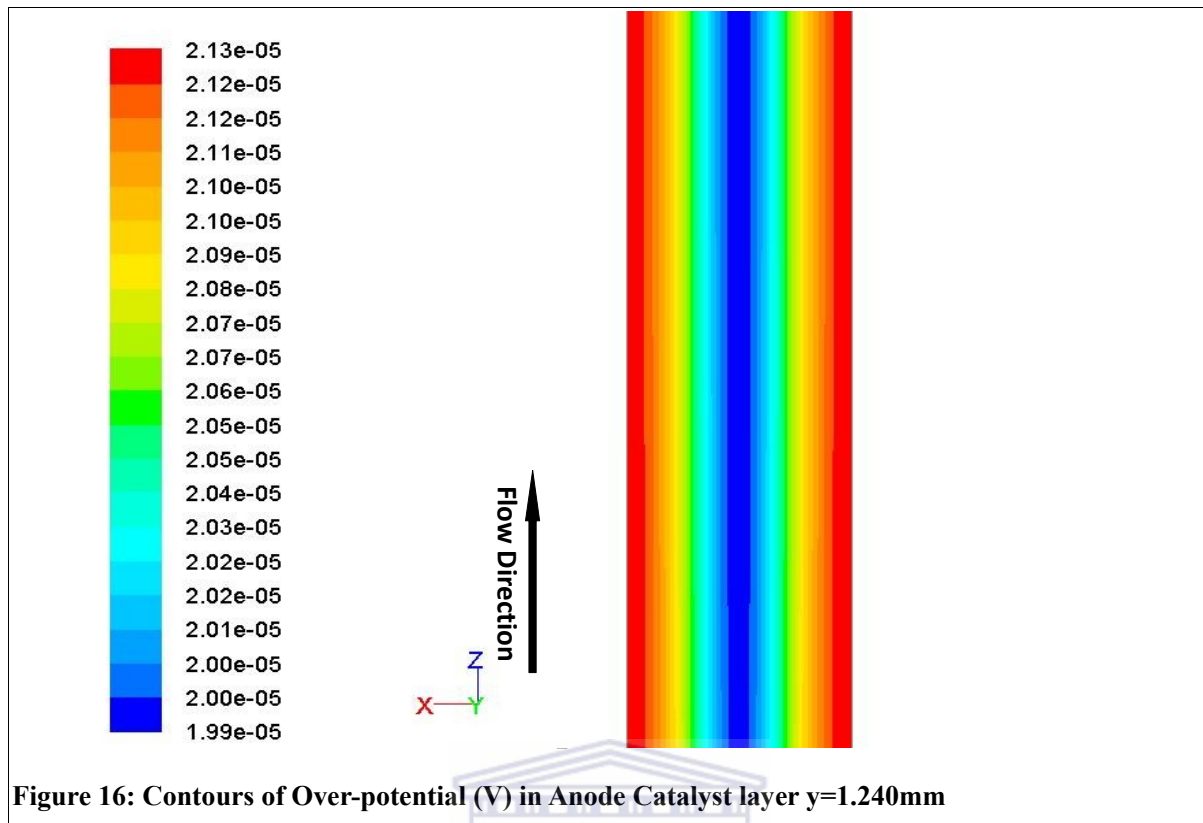**Figure 15: Contours of Over-potential (V) in Cathode Catalyst layer y=1.095mm**

Figure 16: Contours of Over-potential (V) in Anode Catalyst layer y=1.240mm

From Figure 14 one deduces that the concentration of oxygen is least in the areas where the anode and cathode gas channels coexist due to consumption and more specifically that the concentration of oxygen becomes less with the flow direction. The concentration decreases along the gas flow direction which is to be expected, for it decreases as the electrochemical reaction proceeds. This corresponds to the results in Peng et al [46] and therefore the average current density decreases along the flow direction. The local overpotential in Figures 15 and 16, illustrates that the plot for η_c corresponds with the results of Peng et al, as it decreases with flow direction and is of the same order of magnitude. From Peng et al [46] this results from the ohmic loss along the flow direction where a decrease in average current density also exists. For η_a the decrease along the flow direction, is not as apparent as that of the cathode overpotential but does exist, which coincides with distribution of average current density, however in comparison with the results of Peng et al, the values in this study are orders of magnitude lower.

concentration of oxygen becomes less with the flow direction. The concentration decreases along the gas flow direction which is to be expected, for it decreases as the electrochemical reaction proceeds. This corresponds to the results in Peng et al [46] and therefore the average current density decreases along the flow direction. The local overpotential in Figures 15 and 16, illustrates that the plot for η_c corresponds with the results of Peng et al, as it decreases with flow direction and is of the same order of magnitude. From Peng et al [46] this results from the ohmic loss along the flow direction where a decrease in average current density also exists. For η_a the decrease along the flow direction, is not as apparent as that of the cathode overpotential but does exist, which coincides with distribution of average current density, however in comparison with the results of Peng et al, the values in this study are orders of magnitude lower.

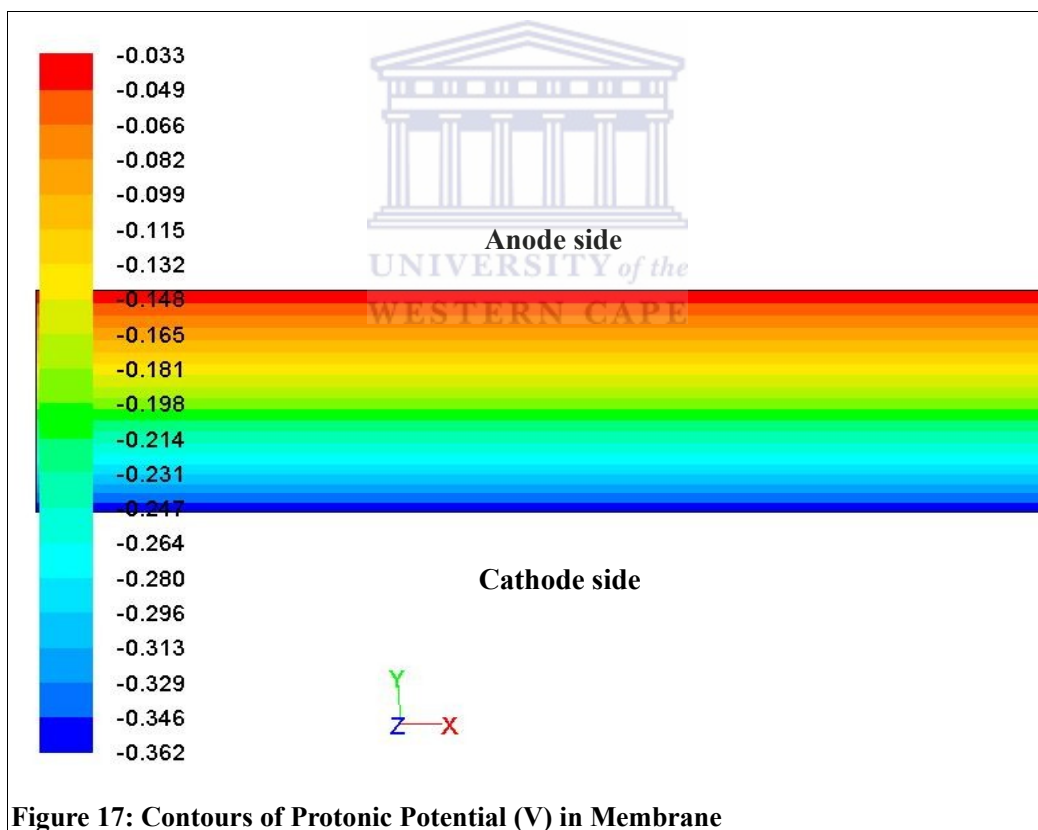**Figure 17: Contours of Protonic Potential (V) in Membrane**

Figure 17 illustrates the membrane phase potential. From Peng et al [46] the reason for gradients in y directions is due to the non-uniform local current production in the adjacent catalyst layers. In Figures 18 and 19 the contours of electric potential for the cathode and anode regions are illustrated respectively.

Figure 18: Contours of Electric Potential (V) in Cathode Current Collector and GDL
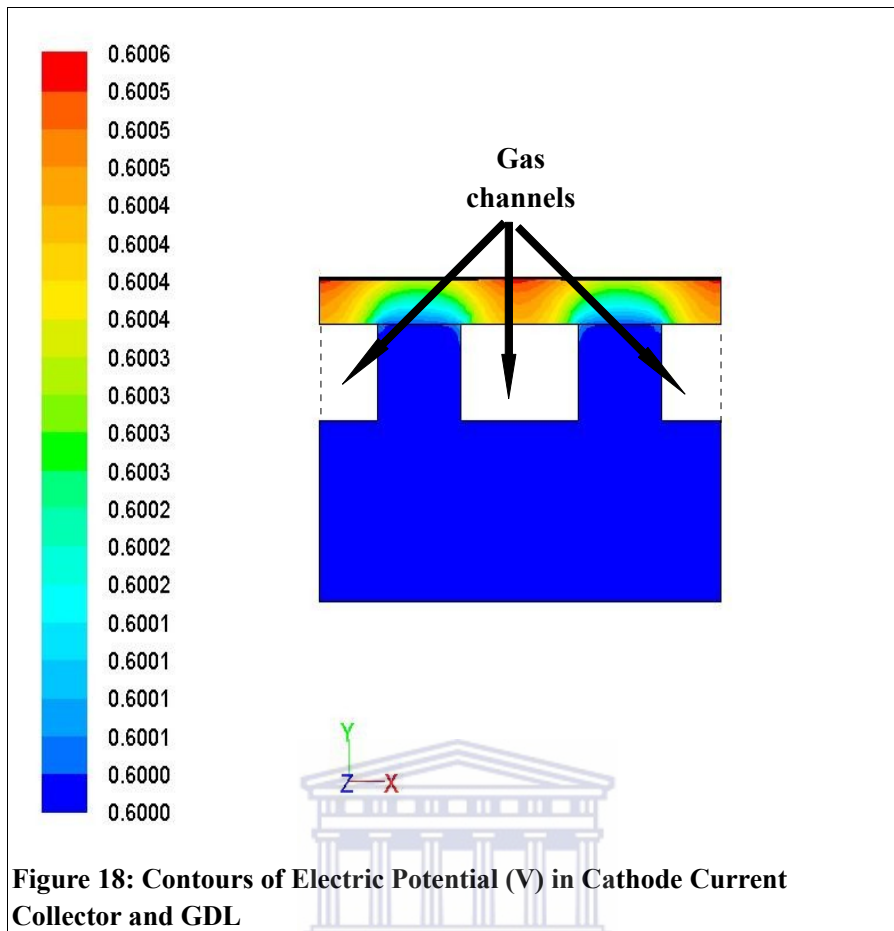
The results in Figure 18 corresponds to that of Peng, where the maxima occurs near the cathode catalyst and above the gas flow channels. In Figure 19, for anode side one has that the local minima occurs near the region of the catalyst and where the gas flow channels coexist. From Peng [46], this results in slower electrochemical reactions, with the implication of lower average current density.

Figure 19: Contours of Electric Potential (V) in Anode Current Collector and GDL
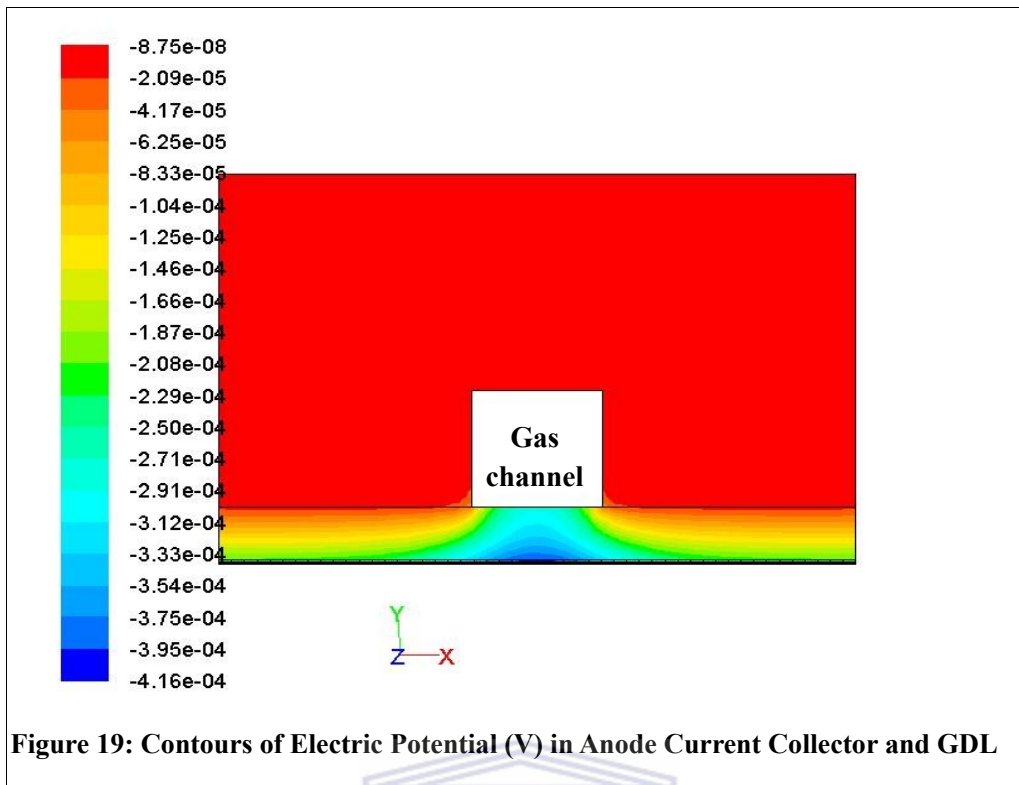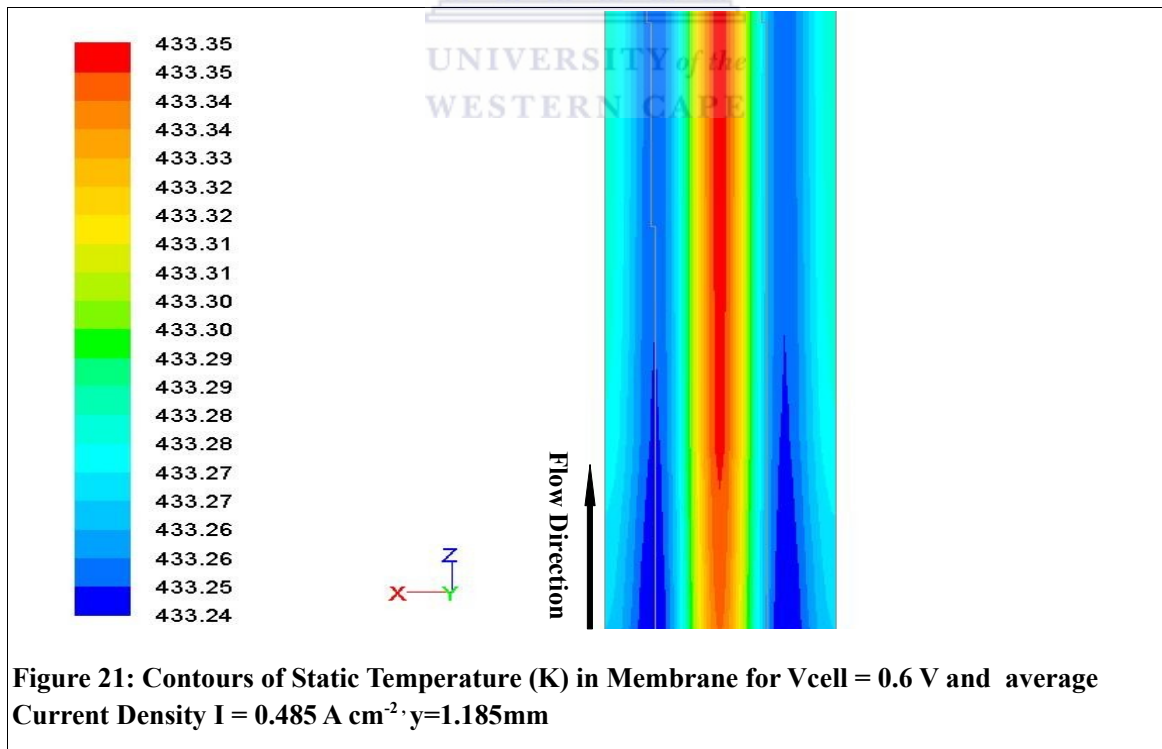
For the next part of the investigation and the aim of the investigation, we look at the temperature distribution in the channel. Figures 20, 21 and 22 shows the temperature distribution within the membrane at V_{cell} values of 0.4V and high average current density
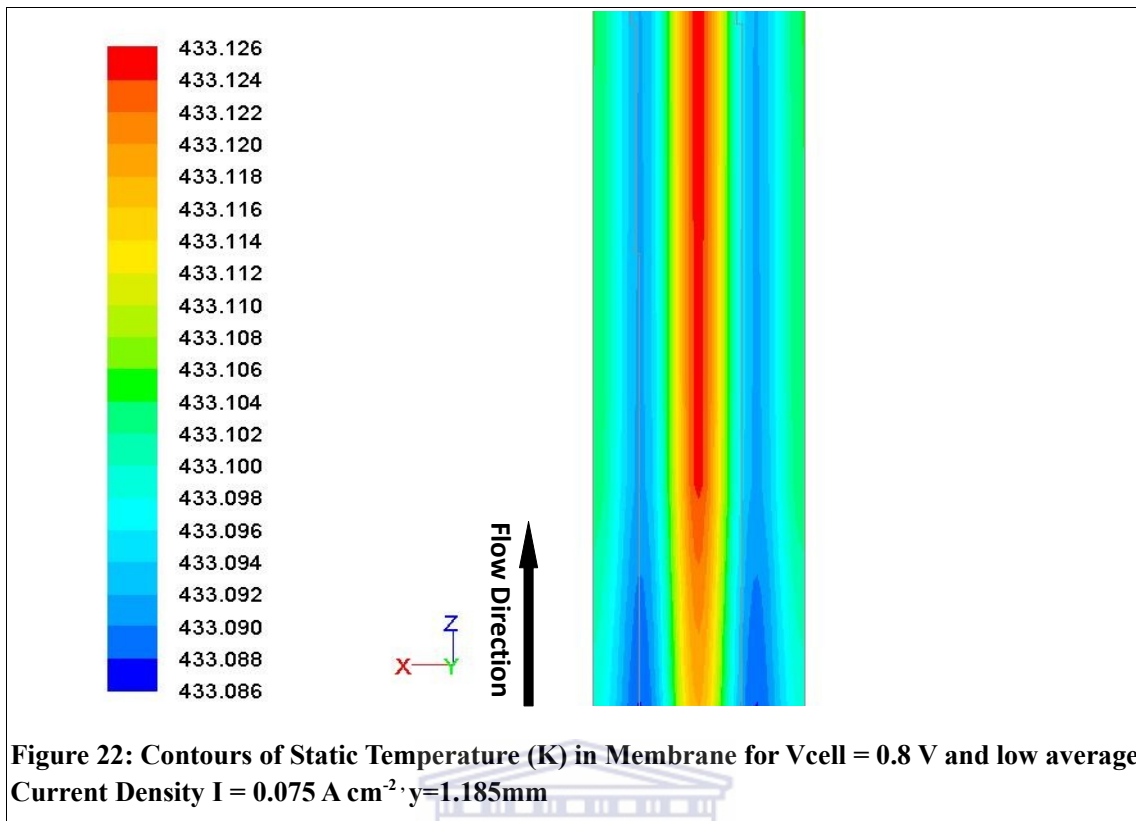
$I = 1.025 \, A \, cm^{-2}$, V_{cell} value of 0.6V and average current density $I = 0.485 \, A \, cm^{-2}$

and a V_{cell} value of 0.8V and low average current density $I = 0.075 \, Acm^{-2}$ respectively.

Figure 20: Contours of Static Temperature (K) in Membrane for V$_{cell}$ = 0.4 V and high average Current Density I = 1.025 A cm^{-2}, y=1.185mm
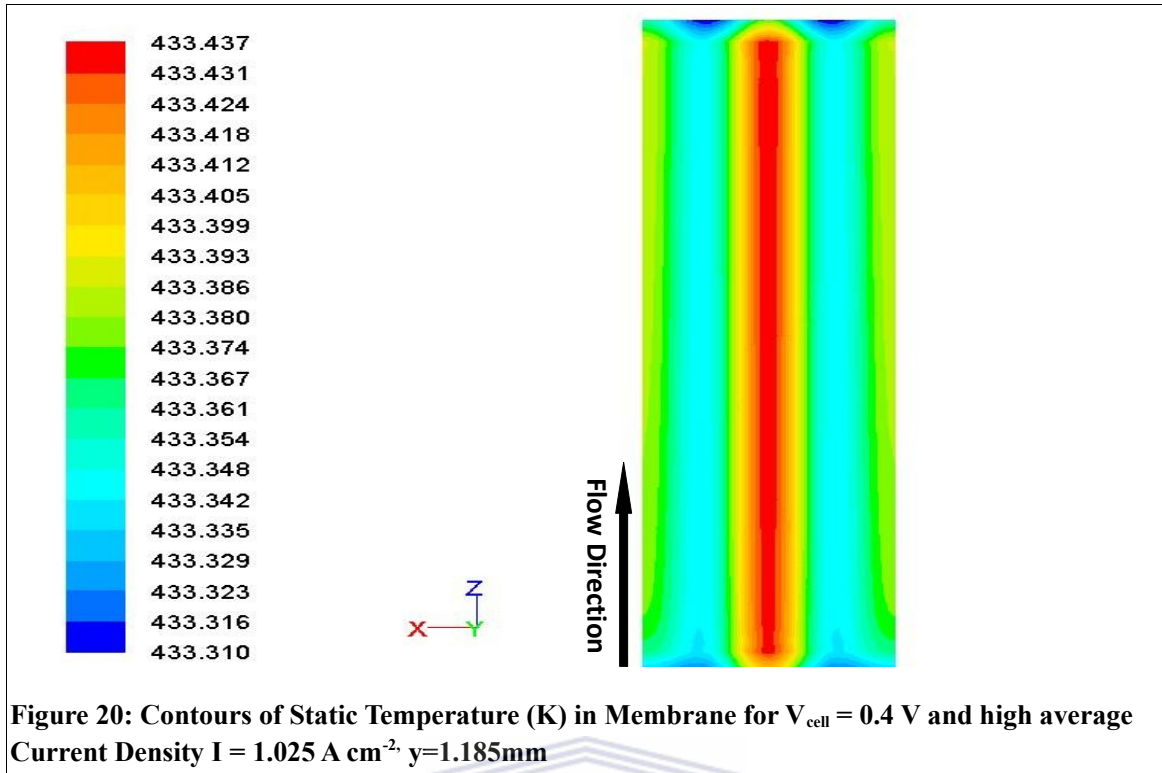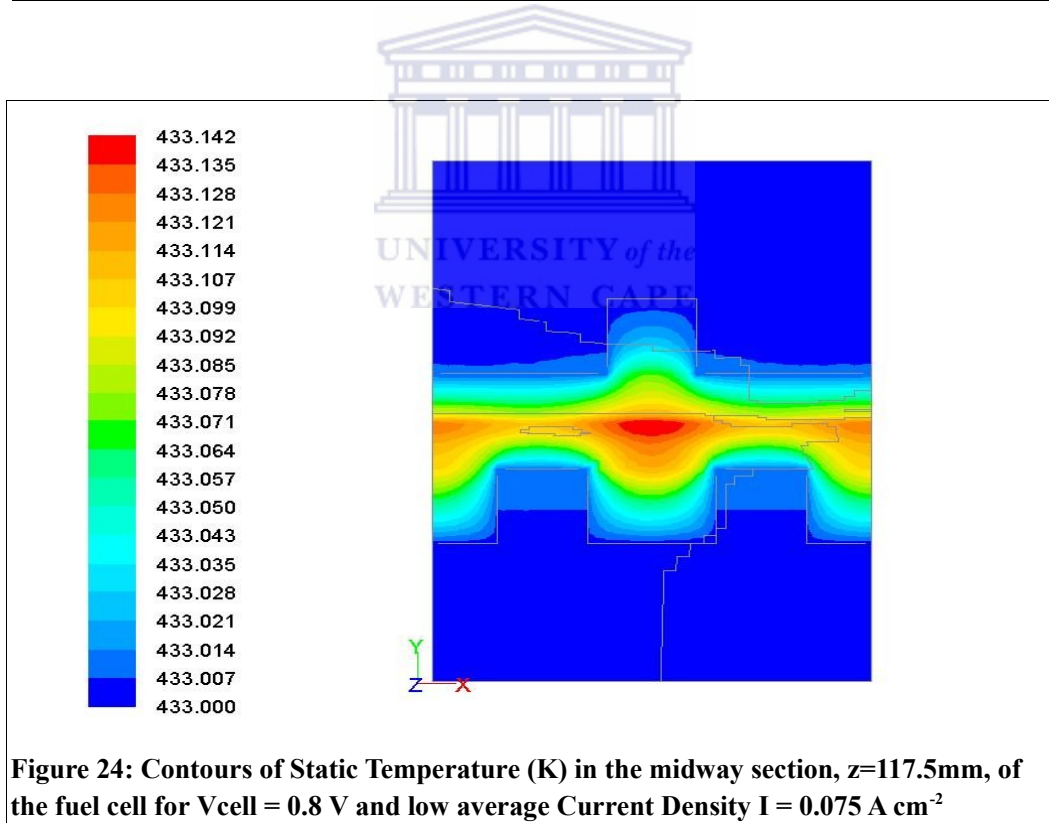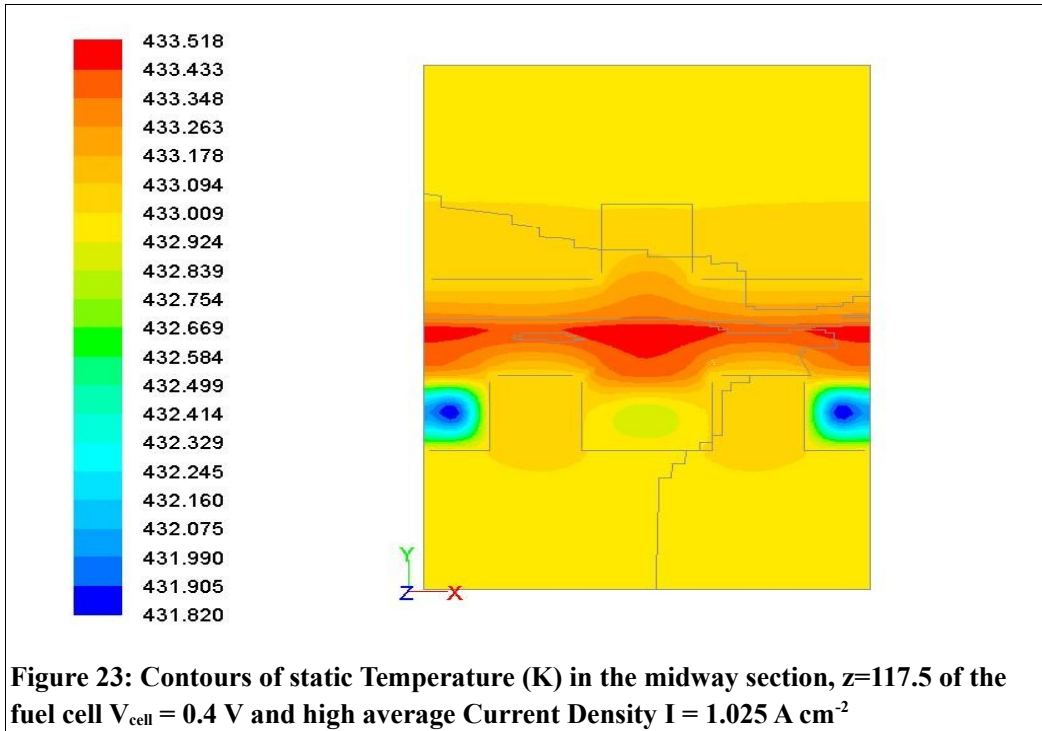
For the high average current density, Figure 20 one find that the temperature maxima occurs where the gas channels coincide.

Figure 21: Contours of Static Temperature (K) in Membrane for Vcell = 0.6 V and average Current Density I = 0.485 A cm^{-2}, y=1.185mm

Figure 22: Contours of Static Temperature (K) in Membrane for Vcell = 0.8 V and low average Current Density I = 0.075 A cm^{-2}, y=1.185mm

In the case of $V_{cell} = 0.6$ it is apparent that the temperature increases along the flow direction. For the low average current density state, $V_{cell} = 0.8$ Figure 22, the temperature difference between the inlet and outlet is small in comparison to when $V_{cell} = 0.6$, Figure 21. The temperature maximum occurs, in all cases, in the centre, where the gas channels coincide. In the following Figures, for each of the of the cases V_{cell} values of 0.4 and 0.8, the temperature distribution of the mid-way section of the fuel cell is displayed.

Figure 23: Contours of static Temperature (K) in the midway section, z=117.5 of the fuel cell V_{cell} = 0.4 V and high average Current Density I = 1.025 A cm⁻²

Figure 24: Contours of Static Temperature (K) in the midway section, z=117.5mm, of the fuel cell for Vcell = 0.8 V and low average Current Density I = 0.075 A cm⁻²

As with the membrane cross-section it is evident when comparing Figures 23 and 24 that the temperature variation increases with increasing average current density.

Chapter 6: Conclusion and Future Prospects

In this investigation a single-phase, high temperature PEM fuel cell model was studied and implemented in the framework of a CFD package, FLUENT. The complete set of conservation equations, mass, momentum, energy, species and charge are taken into account and solved numerically with a proper account of electrochemical kinetics. In modelling the fuel cell, all water produced was considered to be in vaporous form, given the temperature and pressure range in which the fuel operates. The transportation of water across the membrane is therefore ignored due to the low water electro-osmotic drag force [46].

The material properties of each layer of the fuel cell model is a combination of those presented in the work of Peng et al [46] , where high temperature PEM fuel cell operation is presented and pre-existing properties in FLUENT. In chapter 2, the challenges and advantages of high temperature operation is discussed and it is the hope to in future take better account hereof. The numerical method taken in account, discussed in chapter 3, is the SIMPLE algorithm.

In this investigation, straight-channels of a PEM fuel cell at an operating temperature $T = 433\mathrm{K}$ was studied numerically, evaluating the temperature distribution and cell performance and comparative study to the work of Peng et al [46] was done. From the results, two deductions are made corresponding to the work done by Peng et al [46], the current flux density decreases with flow direction whereas the of operating temperature increases, Figures 13 and 21, and the temperature variation across the fuel cell increases with the increasing of average current density.

Bibliography

[1] T. Akiki, W. Charon, M. Iltchev, G. Accary, R. Kouta, Influence of local porosity and local permeability on the performances of a polymer electrolyte membrane fuel cell, J. Power Sources. 195 (2010) 5258-5268.

[2] S.J. Andreasen, S.K. Kær, Modelling and evaluation of heating strategies for high temperature polymer electrolyte membrane fuel cell stacks, Int J Hydrogen Energy. 33 (2008) 4655-4664.

[3] ANSYS FLUENT, Fuel Cell Module Manual, 2010 (2009) 97.

[4] ANSYS FLUENT, Full Multicomponent Diffusion, 2010 (2006) 1.

[5] ANSYS FLUENT, Pressure- Velocity Coupling, 2010 (2006).

[6] ANSYS FLUENT, Spatial Discretization, 2010 (2006).

[7] F. Barbir, PEM Fuel Cells: Theory and Practice, Academic, Oxford, 2005.

[8] J.J. Baschuk, X. Li, Modeling of ion and water transport in the polymer electrolyte membrane of PEM fuel cells, Int J Hydrogen Energy. 35 (2010) 5095-5103.

[9] S. Basu, R. Shah, Introduction to fuel Cells, in: Anonymous Recent Trends in Fuel Cell Science and Technology, Springer, New York, 2007, pp. 1-9.

[10] R. Bouchet, S. Miller, M. Duclot, J.L. Souquet, A thermodynamic approach to proton conductivity in acid-doped polybenzimidazole, Solid State Ionics. 145 (2001) 69-78.

[11] R. Bouchet, E. Siebert, Proton conduction in acid doped polybenzimidazole, Solid State Ionics. 118 (1999) 287-299.

[12] D.F. Cheddie, N.D.H. Munroe, Semi-analytical proton exchange membrane fuel cell modeling, J. Power Sources. 183 (2008) 164-173.

[13] D.F. Cheddie, N.D.H. Munroe, A two-phase model of an intermediate temperature PEM fuel cell, Int J Hydrogen Energy. 32 (2007) 832-841.

[14] D.F. Cheddie, N.D.H. Munroe, Three dimensional modeling of high temperature PEM fuel cells, J. Power Sources. 160 (2006) 215-223.

[15] D. Cheddie, N. Munroe, Mathematical model of a PEMFC using a PBI membrane, Energy Conversion and Management. 47 (2006) 1490-1504.

[16] M. Coppo, N.P. Siegel, M.R.V. Spakovsky, On the influence of temperature on PEM fuel cell operation, J. Power Sources. 159 (2006) 560-569.

[17] D. Crow, Principles and Applications of Electrochemistry, Blackie Academic & Professional, London, 1994.

[18] E.L. Cussler, Diffusion: Mass Transfer in Fluid Systems, Cambridge University Press, New York, 1997.

[19] J.E. Dawes, N.S. Hanspal, O.A. Family, A. Turan, Three-dimensional CFD modelling of PEM fuel cells: An investigation into the effects of water flooding, Chemical Engineering Science. 64 (2009) 2781-2794.

[20] K. Dhathathreyan, N. Rajalakshmi, Polymer Electrolyte Membrane Fuel Cell, in: S. Basu (Ed.), Recent Trends in Fuel Cell Science and Technology, Anamaya Publishers, New Delhi, India, 2007, pp. 40-115.

[21] N. Djilali, Computational modelling of polymer electrolyte membrane (PEM) fuel cells: Challenges and opportunities, Energy. 32 (2007) 269-280.

[22] I. EG&G Technical Services, Fuel Cell Handbook, seventh ed., , Morgantown, West Virginia, 2004.

[23] P.M. Fisbane, S.G. Gasiorowicz, S.T. Thornton, PHYSICS FOR SCIENTISTS AND ENGINEERS WITH MODERN PHYSICS, THIRD ed., PEARSON PRENTICE HALL, UNITED STATES OF AMERICA, 2005.

[24] A.C. Fisher, Electrode Dynamics, Oxford University Press, Oxford; New York, 1996.

[25] Fluent Inc., Tutorial: Modeling a Single-Channel, Counter-Flow Polymer Electrolyte Membrane (PEM) Fuel Cell, 2010 (2007) 18.

[26] R. Fox, Introduction to Fluid Mechanics, Wiley, Hoboken, N.J., 2004.

[27] D. Giancoli, Physics: Principles with Applications, Prentice Hall, Upper Saddle River, N.J, 1998.

[28] M. Grujicic, K.M. Chittajallu, Design and optimization of polymer electrolyte membrane (PEM) fuel cells, Appl. Surf. Sci. 227 (2004) 56-72.

[29] S. Haji, Analytical modeling of PEM fuel cell i–V curve, Renewable Energy. 36 (2011) 451-458.

[30] M. Hatti, M. Tioursi, Dynamic neural network controller model of PEM fuel cell system, Int J Hydrogen Energy. 34 (2009) 5015-5021.

[31] J. Holman, Heat Transfer, 8th ed., McGraw-Hill, New York, 1997.

[32] E. Hontañón, M.J. Escudero, C. Bautista, P.L. García-Ybarra, L. Daza, Optimisation of flow-field in polymer electrolyte membrane fuel cells using computational fluid dynamics techniques, J. Power Sources. 86 (2000) 363-368.

[33] Houghton Mifflin Company, The American Heritage® Dictionary of the English Language, 4th ed., Houghton Mifflin Company, 2000.

[34] J.J. Hwang, S.J. Liu, Comparison of temperature distributions inside a PEM fuel cell with parallel and interdigitated gas distributors, J. Power Sources. 162 (2006) 1203-1212.

[35] V. Janardhanan, A detailed approach to model transport, heterogeneous chemistry and electrochemistry in solid-oxide fuel cells, (2007).

[36] J. Jang, W. Yan, H. Li, W. Tsai, Three-dimensional numerical study on cell performance and transport phenomena of PEM fuel cells with conventional flow fields, Int J Hydrogen Energy. 33 (2008) 156-164.

[37] D.H. Jeon, S. Greenway, S. Shimpalee, J.W. Van Zee, The effect of serpentine flow-field designs on PEM fuel cell performance, Int J Hydrogen Energy. 33 (2008) 1052-1066.

[38] H. Ju, H. Meng, C. Wang, A single-phase, non-isothermal model for PEM fuel cells, Int. J. Heat Mass Transfer. 48 (2005) 1303-1315.

[39] G. Karniadakis, Microflows and Nanoflows: Fundamentals and Simulation, Springer Science+Business Media, Inc., New York, NY, 2005.

[40] J. Koryta, Ions, Electrodes and Membranes, Wiley, Chichester, 1982.

[41] P. Lee, S. Han, S. Hwang, Three-Dimensional Transport Modeling for Proton Exchange Membrane (PEM) Fuel Cell with Micro Parallel Flow Field, Sensors. 8 (2008) 1475-1487.

[42] X. Li, I. Sabir, J. Park, A flow channel design procedure for PEM fuel cells with effective water removal, J. Power Sources. 163 (2007) 933-942.

[43] V. Marthur, J. Crawford, Fundamentals of Gas Diffusion Layers in PEM Fuel Cells, in: S. Basu (Ed.), Recent Trends in Fuel Cell Science and Technology, Anamaya Publishers, New Delhi, India, 2007, pp. 116-126.

[44] V.P. McConnell, High-temperature PEM fuel cells: Hotter, simpler, cheaper, Fuel Cells Bulletin. 2009 (2009) 12-16.

[45] V. Mehta, J.S. Cooper, Review and analysis of PEM fuel cell design and manufacturing, J. Power Sources. 114 (2003) 32-53.

[46] J. Peng, S.J. Lee, Numerical simulation of proton exchange membrane fuel cells at high operating temperature, J. Power Sources. 162 (2006) 1182-1191.

[47] B. Rismanchi, M.H. Akbari, Performance prediction of proton exchange membrane fuel cells using a three-dimensional model, Int J Hydrogen Energy. 33 (2008) 439-448.

[48] J. Russ, Fractal Surface, 1st ed., Plenum Press, New York, 1994.

[49] N. Selley, Experimental Approach to Electrochemistry, Edward Arnold, London, 1977.

[50] C. Siegel, Review of computational heat and mass transfer modeling in polymer-electrolyte-membrane (PEM) fuel cells, Energy. 33 (2008) 1331-1352.

[51] B.R. Sivertsen, N. Djilali, CFD-based modelling of proton exchange membrane fuel cells, J. Power Sources. 141 (2005) 65-78.

[52] C. Spiegel, Fuel Cell Thermodynamics, in: Anonymous PEM Fuel Cell Modeling and Simulation using Matlab, Academic Press, Burlington, 2008, pp. 15-48.

[53] C. Spiegel, Fuel Cell Mass Transport, in: Anonymous PEM Fuel Cell Modeling and Simulation using Matlab, Academic Press, Burlington, 2008, pp. 97-125.

[54] C. Spiegel, Fuel Cell Charge Transport, in: Anonymous PEM Fuel Cell Modeling and Simulation using Matlab, Academic Press, Burlington, 2008, pp. 77-96.

[55] C. Spiegel, Fuel Cell Electrochemistry, in: Anonymous PEM Fuel Cell Modeling and Simulation using Matlab, Academic Press, Burlington, 2008, pp. 49-76.

[56] C. Spiegel, An Introduction to Fuel Cells, in: Anonymous PEM Fuel Cell Modeling and Simulation using Matlab, Academic Press, Burlington, 2008, pp. 1-14.

[57] C. Spiegel, Modeling the Gas Diffusion Layers, in: Anonymous PEM Fuel Cell Modeling and Simulation using Matlab, Academic Press, Burlington, 2008, pp. 197-241.

[58] C. Spiegel, Modeling the Proton Exchange Structure, in: Anonymous PEM Fuel Cell Modeling and Simulation using Matlab, Academic Press, Burlington, 2008, pp. 167-195.

[59] C. Spiegel, Modeling the Catalyst Layers, in: Anonymous PEM Fuel Cell Modeling and Simulation using Matlab, Academic Press, Burlington, 2008, pp. 243-267.

[60] C. Spiegel, Modeling the Flow Field Plates, in: Anonymous PEM Fuel Cell Modeling and Simulation using Matlab, Academic Press, Burlington, 2008, pp. 269-298.

[61] C. Spiegel, Heat Transfer, in: Anonymous PEM Fuel Cell Modeling and Simulation using Matlab, Academic Press, Burlington, 2008, pp. 127-166.

[62] Sunderland J, Johnson K, Shape factors for heat conduction through bodies with isothermal or convective boundary conditions, 2010 5.

[63] H.R. Thirsk, A Guide to the Study of Electrode Kinetics, Academic Press, London, 1972.

[64] H.K. Versteeg, An Introduction to Computational Fluid Dynamics: The Finite Volume Method, Pearson Education Ltd, Harlow, England, 2007.

[65] X. Wang, X. Zhang, W. Yan, D. Lee, A. Su, Determination of the optimal active area for proton exchange membrane fuel cells with parallel, interdigitated or serpentine designs, Int J Hydrogen Energy. 34 (2009) 3823-3832.

[66] Y. Wang, K.S. Chen, J. Mishler, S.C. Cho, X.C. Adroher, A review of polymer electrolyte membrane fuel cells: Technology, applications, and needs on fundamental research, Appl. Energy. In Press, Corrected Proof.

[67] A. Weber, J. Newman, Modelling gas-phase transport in polymer-electrolyte fuel cells, The Electrochemical Society. 16 (2006) 61-66.

[68] J. Wendt, J.D. Anderson, Computational Fluid Dynamics, Springer, 2009.

[69] H. Young, Sears and Zemansky's University Physics, Addison-Wesley, San Francisco; Harlow, 2000.

[70] W. Yuan, Y. Tang, M. Pan, Z. Li, B. Tang, Model prediction of effects of operating parameters on proton exchange membrane fuel cell performance, Renewable Energy. 35 (2010) 656-666.

[71] J. Zhang, Y. Tang, C. Song, J. Zhang, Polybenzimidazole-membrane-based PEM fuel cell in the temperature range of 120–200°C, J. Power Sources. 172 (2007) 163-171.

[72] J. Zhang, Z. Xie, J. Zhang, Y. Tang, C. Song, T. Navessin, Z. Shi, D. Song, H. Wang, D.P. Wilkinson, Z. Liu, S. Holdcroft, High temperature PEM fuel cells, J. Power Sources. 160 (2006) 872-891.